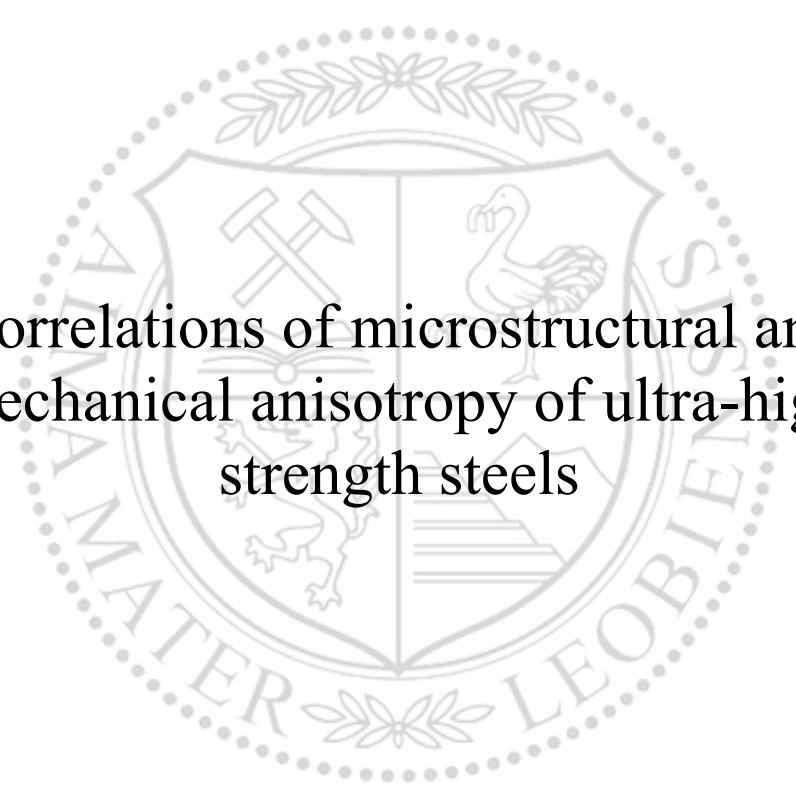




Chair of Design of Steels

Doctoral Thesis



Correlations of microstructural and  
mechanical anisotropy of ultra-high  
strength steels

Dipl.-Ing. Dr.mont. Raphael Esterl

July 2019

Conducted at

Chair of Design of Steels at the Department of Materials Science, Montanuniversität  
Leoben, 8700 Leoben, Austria

in the frame of

BMVIT Professorship for Industry

together with

voestalpine Stahl GmbH, 4020 Linz, Austria

## Affidavit

I declare on oath that I wrote this thesis independently, did not use other than the specified sources and aids, and did not otherwise use any unauthorized aids.

I declare that I have read, understood, and complied with the guidelines of the senate of the Montanuniversität Leoben for "Good Scientific Practice".

Furthermore, I declare that the electronic and printed version of the submitted thesis are identical, both, formally and with regard to content.

Leoben, June 2019

---

Raphael Esterl

*Gegen den Wind zu kreuzen bringt einen manchmal schneller zum Ziel, als mit dem Wind zu segeln.*

H. Lahm

## Danksagung

Der Erfolg meiner Dissertation ist vor allem jenen Menschen gewidmet, die mich in den letzten drei Jahren sowohl fachlich als auch persönlich begleitet haben.

An erster Stelle gebührt mein Dank meinem Betreuer, Prof. Ronald Schnitzer. Deine stets offene Tür, deine fachliche Kompetenz und deine motivierenden Schulterklopper haben die Arbeit mit meiner Dissertation wahrlich beflügelt. Es ehrt mich, der erste Dissertant unter deiner Stiftungsprofessur gewesen zu sein, wodurch ich auf den Vorzug kam, von dir persönlich betreut zu werden.

Nicht weniger Dank gilt meinem Ansprechpartner und Mentor bei der voestalpine Stahl, Markus Sonnleitner. Ich schätze unser äußerst freundschaftliches Verhältnis vom ersten Tag meiner Dissertation an und profitierte die letzten drei Jahre von deiner fachlichen Expertise. Als Betreuer hatte ich mit dir einen wahren Lottosechser, dein Input für meine Veröffentlichungen, deine Bereitstellung von Probenmaterial und unsere interessanten Gespräche bei unserem monatlichen Projektaustausch führten zu einer wirklich außergewöhnlichen Zusammenarbeit. Vielen Dank an dieser Stelle auch der voestalpine Stahl für den finanziellen Aufwand, den meine Arbeit samt Legierungsentwicklung und mechanischer Beprobung mit sich brachte.

Großer Dank gilt auch den Mitarbeitern des Department Metallkunde und Werkstoffprüfung und meinen Kollegen vom Lehrstuhl für Stahldesign. Voran meiner Kollegin, Sandra Ebner für die abwechslungsreichen Stunden im Büro und Gerhard Hawranek für die angenehmen Kaffeepausen und süditalienischen Vespaausfahrten.

Des Weiteren möchte ich meinen Freunden danken, die meine letzten 10 Jahre meiner Studentenzzeit in Österreich so mitgeprägt haben. Thomas, vielen Dank für deine Freundschaft und vor allem dein offenes Ohr, Birgit und Christoph, für eure fachliche und segeltechnische Begleitung, und dir lieber Dominik, unsere Telefonate und die Vorfreude auf den bevorstehenden Törn haben den Endspurt meiner Promotion wahrlich angekurbelt. In diesem Sinne: *always follow the sun!*

Und schließlich gilt besonderer Dank meiner gesamten Familie, die ohne Zweifel eine wichtige Rolle für meinen Erfolg im Studium und meiner Promotionslaufbahn einnahmen. Voran meinem Vater, Robert Esterl, der für mich nach wie vor das größte Vorbild ist und mir immer in allen Belangen zur Seite stand. Meine zahllosen Abenteuer zu See und auf meiner Vespa haben dir zu Recht viele Nerven gekostet. Und meiner Mutter, Gerda die sich dafür am Rosenkranz die Finger wund gebetet hat. Nach meinen zehn Jahren in Österreich freue ich mich nun auf die Heimkehr zu euch nach Bayern.

---

# Table of Contents

## Part A

	Abstract .....	1
	Kurzfassung .....	2
1	Introduction .....	4
2	State of the art .....	6
	2.1 Hot rolling of High-Strength Low Alloy (HSLA) low-carbon steels .....	6
	2.2 Alloying elements and their role in the production of UHS steels .....	8
	2.2.1 Titanium .....	10
	2.2.2 Niobium .....	10
	2.2.3 Vanadium .....	11
	2.2.4 Aluminum .....	11
	2.3 Anisotropy and crystallographic textures in hot rolled steel plates .....	12
	2.3.1 Inclusions .....	12
	2.3.2 Microstructural anisotropy and pancaking of the austenite grain .....	12
	2.3.3 Crystallographic texture .....	13
	2.4 Delaminations in Charpy notched impact specimens .....	14
	2.5 Relation of the current thesis to the state of the art .....	15
3	Summary of Publications .....	16
	3.1 List of publications .....	16
	3.1.1 Appended papers .....	16
	3.1.2 Conference presentation .....	17
	3.1.3 Supervised theses .....	17
	3.2 Summary of published contents .....	18
	3.2.1 Aim and scope of the investigations .....	18
	3.2.2 Visualization of the prior austenite grains .....	19
	3.2.3 Investigations on the recrystallization behavior .....	23
	3.2.4 Influence of the processing route on the hardenability .....	25
	3.2.5 Effect of Nb and V on the microstructure and the mechanical properties of direct quenched and tempered steels .....	27
	3.2.6 Investigations to separate the mechanical anisotropy and texture .....	28
4	Outlook and open questions .....	33
5	References .....	35

## Part B

- Paper I      Raphael Esterl, Markus Sonnleitner, Manfred Stadler, Günter Wölger, Ronald Schnitzer  
*Microstructural Characterization of Ultra-High Strength Martensitic Steels*  
Practical Metallography 55 (2018): 203 - 222
- Paper II      Raphael Esterl, Markus Sonnleitner, Ronald Schnitzer  
*Microstructural Analysis of the Recrystallization Behavior of Low Alloyed Steels*  
Steel research international 90 (2019) 3: 1800500
- Paper III      Raphael Esterl, Markus Sonnleitner, Ronald Schnitzer  
*Influence of Thermomechanical Treatment and Nb Micro-Alloying on the Hardenability of Ultra-High Strength Steels*  
Metallurgical and Materials Transactions A (2019)
- Paper IV      Raphael Esterl, Markus Sonnleitner, Boris Gschöpf, Ronald Schnitzer  
*Influence of V and Nb Micro-Alloying on Direct Quenched and Tempered Ultra-High Strength Steels*  
Steel research international (2019): 800640
- Paper V      Raphael Esterl, Markus Sonnleitner, Irmgard Weißensteiner, Karin Hartl, Ronald Schnitzer  
*Influence of quenching conditions on texture and mechanical properties of ultra-high strength steels*  
Submitted to Journal of Materials Science (2019)

## List of abbreviations and symbols

DQ	Direct quenching
DRX	Dynamic recrystallization
EBSD	Electron backscatter diffraction
FRT	Finish rolling temperature
HSLA	High strength low alloy
MAE	Micro-alloying elements
ODF	Orientation distribution function
PAG	Prior austenite grain
Q	Quenching
RQ	Re-austenitization and quenching
SEM	Scanning electron microscopy
SRX	Static recrystallization
T	Tempered
TMP	Thermomechanical processing
$T_{NR}$	Non-recrystallization temperature
UHSS	Ultra-high strength steels
UTS	Ultimate tensile strength
XRD	X-Ray diffraction
YS	Yield strength

# Part A



## Abstract

For the construction of mobile crane arms, ultra-high strength steels (UHSS) come to application to fulfil the requirements of an increased payload to weight ratio. Steels produced via thermomechanical processing and direct quenching (TM + DQ) provide several advantages over conventional quenching and tempering (Q+T) steels through the systematic combination of micro-alloying elements (MAE), process parameters and the subsequent quenching from the rolling heat. For a given carbon content, clear strength benefits can be reached by the advanced TM process route. Materials properties may be adjusted by an additional tempering heat treatment, which is accompanied by an asset in ductility. Nonetheless, the combination of MAE and low finish rolling temperatures (FRT) promotes certain properties that adversely affect the isotropy of the material. The microstructural anisotropy by the highly deformed austenite grain yields in an orientation dependence of the mechanical properties, which is expressed by differences between the longitudinal and transversal bendability and impact toughness.

In order to establish a correlation between the microstructure and the mechanical properties of UHS steels, the effect of the processing route and MAE on the condition of the prior austenite grain was studied. By this means, the goal of the present work was to characterize the underlying microstructural processes and reveal the reasons for the mechanical anisotropy.

A metallographic technique was developed to visualize the prior austenite grains and characterize their size and elongation. Double-hit deformations on a dilatometer were applied to study the influence of the MAE on the microstructural processes, which were visualized with this established metallographic method. Based on these observations, test alloys were developed to analyze the effect of MAE and process parameters on the mechanical properties. The investigations showed, that a decrease in the FRT lead to an augmented orientation dependence of the mechanical properties. However, a correlation between the pancaking and the mechanical anisotropy was not found, as a globular  $\gamma$  grain through re-austenitization exhibits similar anisotropy. Micro-alloying with Nb and V, both contribute to an increase of temper resistance, yet, the strengthening through V is accompanied by an embrittlement and significant decrease of the impact toughness. It was found further, that intensive annealing in the austenite region optimizes isotropy, however, certain microstructural features such as texture components are inherited so that a complete extinction of the mechanical anisotropy cannot be achieved. Overall, knowledge on the correlations of process route, micro-alloying elements and microstructure on the resulting mechanical properties of UHS steels could be acquired.

## Kurzfassung

Um den Anforderungen eines erhöhten Nutzlast- zu Eigengewichtsverhältnisses gerecht zu werden, kommen beim Bau von Mobilkranarmen ultrahochfeste (UHF) Stähle zum Einsatz. Thermomechanisch gewalzte und direktgehärtete (TM + DQ) Stähle bieten durch die systematische Kombination von Mikrolegierungselementen (MLE), Prozesssteuerung und das anschließende Direkthärten aus der Walzhitze wirtschaftliche Vorteile gegenüber herkömmlichen Vergütungsstählen. So können durch TM-Walzen bei gleichem Kohlenstoffgehalt deutlich höhere Festigkeitswerte erzielt werden und die gleichzeitige Kornfeinung erhöht zudem die Zähigkeit. Das Eigenschaftsprofil dieser Stähle wird durch eine Anlassbehandlung abgerundet. Die dadurch resultierende Anlasserweichung wird durch den oben genannten Festigkeitsvorteil kompensiert. Dennoch fördert diese Kombination aus MLE und den niedrigen Walzendtemperaturen (WET) eine Anisotropie der mechanischen Eigenschaften. Das im Walzprozess begründete Strecken des Austenitkorns hat zur Folge, dass sich die Längs- und Querwerte des Biege- und Kerbschlagbiegeversuch deutlich unterscheiden.

Um ein Verständnis der Mikrostruktur-Eigenschaftsbeziehungen von UHF Stählen zu erhalten, wurde der Einfluss von Prozessparametern und der MLE auf die zugrundeliegenden mikrostrukturellen Prozesse und die resultierende Austenitkornstruktur untersucht. Dadurch soll ein Zusammenhang mit der Anisotropie hergestellt werden.

Um die ehemaligen Austenitkörner sichtbar zu machen, wurde eine metallographische Methode entwickelt, die es schließlich ermöglicht, deren Größe und Streckung zu charakterisieren. Mittels Doppelschlagversuchen am Dilatometer wurde der Einfluss der MLE auf die Entwicklung der Mikrostruktur untersucht, die wiederum mit Hilfe der neu entwickelten metallographischen Methode dargestellt wurde. Darauf aufbauend wurden neue Legierungen konzipiert und am Warmwalzsimulator ausgewalzt, um schließlich den Einfluss der MLE und Prozessparameter auf die mechanischen Eigenschaften zu studieren. Diese Untersuchungen ergaben eine erhöhte Orientierungsabhängigkeit der mechanischen Eigenschaften mit abnehmender WET. Eine direkte Korrelation zwischen dem sogenannten *pancaking* und der mechanischen Anisotropie wurde jedoch nicht festgestellt. Ein reustenitisiertes, globulares Austenitgefüge wies ähnliche Anisotropie auf als ein TM gewalztes und direktgehärtetes. Nb und V tragen beide zur Anlassbeständigkeit bei, das Festigkeitsplus durch V wird jedoch von einer Anlassversprödung und somit einer Abnahme der Kerbschlagzähigkeit begleitet. Intensive Austenitisierungsglühungen verringern die Anisotropie, eine Texturererbung verhindert unter Umständen jedoch die vollständige Auslöschung der mechanischen Anisotropie.

Insgesamt konnten wichtige Erkenntnisse über die Zusammenhänge von Prozessparametern, Mikrolegierungselementen und der Mikrostruktur auf die resultierenden mechanischen Eigenschaften von UHS-Stählen gewonnen werden.

## 1 Introduction

In the past decades, the demand of a higher payload to weight ratio has dominated several sectors in material development. Moreover, the request of the automotive sector to reduce weight in order to decrease fuel consumption did forward steel research towards advanced (AHSS) and ultra-high-strength steels [1–8]. Further increase of material strength with sustaining its toughness allows the crane and truck industry to launch lifting systems with extended load capacity and higher action radii. For the production of mobile crane arm booms, ultra-high strength steels come to application to fulfil the requirements of an improved payload to weight ratio [1,9,10]. Thermomechanically processed and direct quenched steels have widely substituted UHS steels processed via the conventional quenching and tempering route. They offer economic benefits through the waiving of an additional heat treatment in the austenite regime and possess an immense strength profit through the subsequent quenching from the rolling heat after an systematic combination of micro-alloying and temperature control during hot rolling [1,9–12]. This profit results in the reduction of alloying elements such as carbon for achieving the same strength requirements as conventional Q+T steels, which optimizes the weldability significantly [13–16]. However, due to the characteristics of the processing route unfavorable mechanical properties emerge, which have not been fully investigated and entirely comprehended till now. Especially the mechanical anisotropy, which is expressed by differences between the longitudinal (L) and transversal (T) direction in the Charpy impact toughness and bendability is attributed to the high deformation of the austenite grain during the finishing rolling passes. Despite of the aforementioned disadvantages, steels produced via the conventional Q+T route possess a globular austenite grain, which is assumed to contribute to an optimized isotropy.

The focus of this thesis was to establish the microstructure-property relationships of UHS steels. It was investigated, if the TM processing route and the pancaking of the austenite grain is responsible for differences in the mechanical properties. These findings should propose possible manufacturing concepts and serve as basis for the development of new UHS steels. Besides the fulfilment of required mechanical properties, the developed approaches should be realizable at the hot strip mill with defined process limitations such as rolling temperatures and rolling forces. The easiest possibility of a further strength increase of structural steels would consist of an increase of the carbon content, which is implemented in the Q+T route. However, to ensure proficient weldability, hardenability and due to process limitations, this option should be avoided, as an increased carbon content significantly increases the susceptibility for cold

cracks. Consequently, the influence of MAE and their ability to provide the corresponding strength improvement for the emerging steel product should be established in order to provide an improved knowledge of process and alloying parameters on the properties of DQ UHS steels in an as-rolled and tempered condition.

The used methods ranged from light optical microscopy, scanning electron microscopy (SEM), electron backscatter diffraction (EBSD) and X-ray diffraction (XRD) to explain the observed mechanical characteristics of UHS steels on a microstructural basis. In addition, double-hit compressions on a deformation dilatometer Bähr 805 A/ D were used to demonstrate the different microstructural evolution conditional on the micro-alloying elements. In specific, two steels of interest were therefore envisaged in different process and alloying modifications. The first steel of concern is a TM rolled, direct quenched and tempered UHS steel with a Yield Strength (YS) of 1100 MPa and comes to application in the construction of mobile crane arms. The second steel of interest possesses with 0.17% the same carbon content, however, is neither temper resistant, nor alloyed with MAE. With a Brinell hardness of 500 HB it serves in the as-rolled condition as wear resistant plate for diverse applications in the transport industry, where abrasive bulk material is handled. Due to their different alloying concept, these steels exhibit different microstructures and therefore different mechanical properties. These steels therefore serve as predestined basis for studies concerning the microstructure-property relationship of UHS steels.

For the sake of simplicity, the two steels are labeled as *Steel A* for the not-tempered UHS steel grade and *Steel B* for the tempered and micro-alloyed steel grade.

In the following pages, this PhD thesis will highlight the current state of technology and summarize the most important findings of the attached publications.

## 2 State of the art

### 2.1 Hot rolling of high-strength, low alloy (HSLA) low-carbon steels

Until the early decades of the 20<sup>th</sup> century, the strength of hot-rolled steels was achieved by an increase of the carbon content up to 0.4% and additions of Mn up to 1.5% [4,17]. These steels consisted mainly of a ferrite-pearlite microstructure and reached yield stresses of 400 MPa, however not the essential toughness for modern applications [3,4,17]. The newly introduced fabrication technique welding, only allowed carbon contents of 0.2% due to the appearance of cold cracks, so that the knowledge of a strength improvement through grain refinement was essential [17]. Through process adaptations and advances in the metallurgical design by the application of micro-alloying elements, the resulting fine grained microstructure not only possessed higher strength, but also was prepared for weldability and showed high toughness even under reduced temperatures [4]. These high-strength, low alloy steels (HSLA), which were micro-alloyed with additions of Nb, V and Ti achieved their breakthrough with the massive application in the pipeline industry in the 70s, where they superseded the conventionally produced steels (Figure 1a) by the application of a so-called normalized rolling (Figure 1b) [4,5,18–22]. Figure 1 shows also schematically the relocation of the temperatures  $A_{c1}$ ,  $A_{c3}$  by additions of Mn, and the increase of the temperature, where below no  $\gamma$

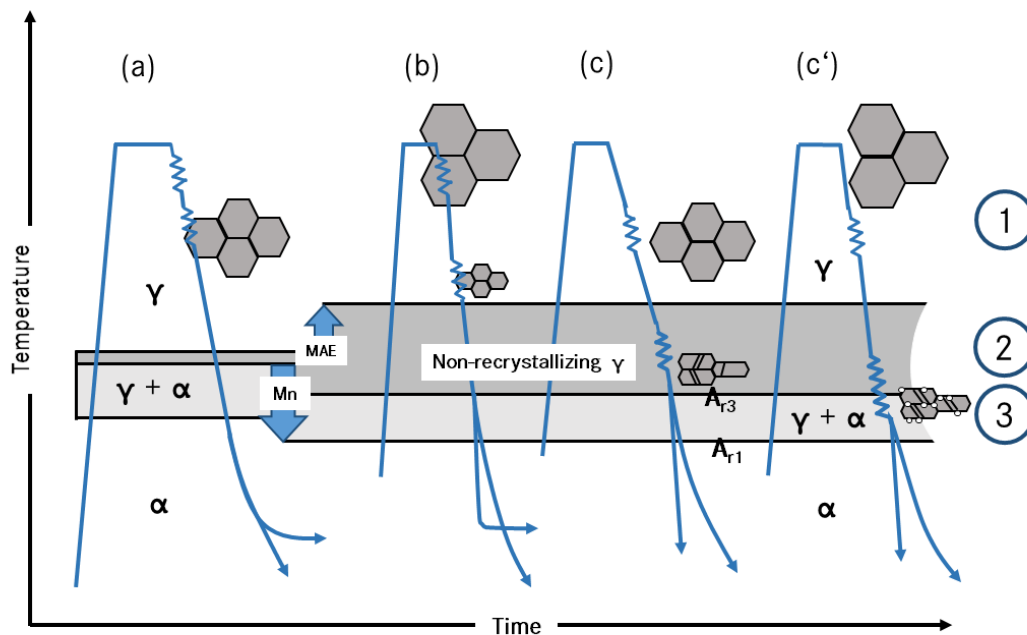


Figure 1: Schematic time-temperature schedule for different hot-rolling cycles and the corresponding microstructural evolution. a) Conventional rolling. b) Normalized rolling. The  $T_{NR}$  is elevated by the addition of MAE, Mn decreases  $A_{r1}$  and  $A_{r3}$ . Thermomechanical processing of a Nb-containing steel with an FRT in the c) non-recrystallizing austenite and in the c') two phase  $\gamma + \alpha$  region. Adapted from [4,17,23].

recrystallization takes place,  $T_{NR}$ , by additions of MAE [4,17,23]. Compared to the Al-grain refined steel, it was experienced, that Nb treated steels provided substantially higher strength in the as rolled condition, however a clear reduction in toughness was observed [8]. Despite of an improvement of the mechanical properties by a subsequent normalization, the strength benefits were forfeited [8]. An alternative route was required, which enables equal grain refinement and simultaneously compensates the drawbacks of cost and strength of the conventional normalizing. The resulting product, which firstly became known as controlled rolling (Figure 1c) and later established in term thermomechanical processing, consisted of an extremely low finish rolling temperature and involved both, advanced hot-rolling and in-line accelerated cooling from the rolling heat [8,24].

The microstructural evolution of thermomechanical processing is related to deformation in three stages, which are shown in Figure 1 [25,26]:

① Deformation in the recrystallization region: The coarse austenite grain is refined through a repeated sequence of deformation and recrystallization. The result is a fine-grained recrystallized microstructure.

② Deformation in the non-recrystallization region: The temperature in this region is too low for the recrystallization of the deformed austenite to be proceeded. The grains evoked from stage ① are formed in elongated, unrecrystallized austenite grains with deformation bands (Figure 1c). Subsequent cooling would result into the nucleation of ferrite on these deformation bands and thus the development of fine ferrite grains.

③ Deformation in gamma-alpha region: Deformation in this region generates further deformation bands on which proeutectoid ferrite can grow (Figure 1c'). Moreover, the deformed ferrite creates a substructure. During cooling, equiaxed alpha-grains evoke from unrecrystallized austenite and the deformed ferrite forms subgrains.

The main effort concerning the microstructural evolution in TMP consists in the formation of the deformation bands. These regions of high deformation density offer elevated potential for the nucleation of alpha grains in contrast to conventional rolling, where alpha grains exclusively nucleate at the gamma-grain boundaries. The deformation bands can be considered as grain boundaries concerning its tendency to ferrite nucleation and subsequently offer an additional nucleation spot to further increase the grain size. The second feature of one can profit during TMP is the formation of a subgrain structure, which occurs in the two-phase region. This effect correlates to the Hall - Petch law resulting in a strengthening effect with decreasing subgrain

size. A further effect, which takes influence on the microstructure is the rolling reduction itself, the rolling temperature and the sequence of reduction steps in the different deformation regions [11,25–27]. Lowering the rolling temperature in the two-phase region results in a decrease of tensile and yield strength. This effect is attributed to the grain refinement as consequence of a finer and accentuated-pancaked austenite grain. The higher the austenite grain boundary density is, the more nucleation spots for the ferrite transformation are introduced. Furthermore, the higher the amount of reduction is, the finer the resulting grain becomes – independent on the rolling schedule. Regarding the rolling in the two phase ( $\alpha+\gamma$ ) region, both phases are compressed. With increasing reduction,  $\gamma$  is more elongated and offers a finer  $\alpha$  grain [2,11,26]. However the dominating hardening mechanism consists of the subgrain hardening and the massive defect density leads to a stable dynamic recovery structure in  $\alpha$  grains [25,26]. In summary it can be quoted, that the main advantage in TMP over conventional hot rolling consist in the establishment of further nucleation spots for the formation of a fine grain structure. The development of a TMP processed steel and the adaption on its particular usage requires a sophisticated collaboration of alloying, rolling parameters and cooling factors. The interplays and their correlation are content in the subsequent chapters.

## 2.2 Alloying elements and their role in the production of UHS steels

The strength of UHS steels is the result of an interaction between temperature controlled rolling, selective use of MAE and transformation hardening [11,13,28,29]. Either hardening is performed after reheating the normalized steel to the  $\gamma$  region, which corresponds to a conventional Q+T route. Alternatively, quenching can be executed directly from the rolling heat after TM rolling as described in the previous chapter. Consequently, to reach the required strength, these two quenching routes are based on different concepts. Equal for both, however, is the use of carbon as the most common and most important alloying element [13]. Carbon has a strong strengthening potential. In martensitic steels, it promotes the tetragonal lattice distortion during the diffusion-less transformation and thus the emerge of a microstructure with a high dislocation intensity. The carbon content in UHS steels however is limited to 0.2% as contents above increase the risk of brittle fracture and cold cracking during welding [14,15,30]. Furthermore, carbon also elevates the flow stress, which particularly is reflected in the high forming forces during finish rolling of TMP [31,32]. Carbon contents of UHS vary concerning their achievable YS, and amount between 0.09% and 0.17% for YS between 960 and 1100 MPa for TM steels [1,9,33,34]. Q+T steels require higher carbon amounts for a given strength, so



that contents up to 0.21% are used. As solid-solution strengthener, Si follows with contents between 0.1 and 0.3%. Silicon comes to application as deoxidizer and retards the formation of perlite and bainite [3,7,12,13,29,35–37]. Mn belongs to the austenite-stabilizers and acts like Ni and Cu as solid solution strengthener. It is an important and effective element in increasing hardenability. Cu is used to increase weather-resistance and improves hardenability. Further it is observed, that Cu improves temper resistance through the formation of precipitates.

The micro-alloying elements play different roles during hot rolling. They act dissolved or in the form of finely dispersed (carbide-, nitride- or carbonitride-) precipitates on the grain refinement, recrystallization, recovery processes and the movement of dislocations [3,11,28,38,39]. In dissolved condition, they reduce the migration of the grain boundary through their increased solute drag and further are able to retard the  $\gamma$  to  $\alpha$  transformation. At a certain temperature, the alloying elements start to form precipitates and thereby hinder the recrystallization, which corresponds to a thermomechanical treatment. Their mode of action is dependent on their solubility product, and thus is a function of time, temperature and the chemical composition. Figure 2 expresses the influence of the common MAE on the grain size during heating. A plain C-Mn steel shows an augmented grain growth due to the lack of second phase particles. The grain growth characteristics of V, Al and Nb alloyed steels show indicated temperature limits of their abnormal grain growth, which are defined by the dissolving temperatures of their precipitates [39–41]. The characteristics of the common MAE are briefly summarized in the following, listed in the fundamental order of their sequence of precipitation.

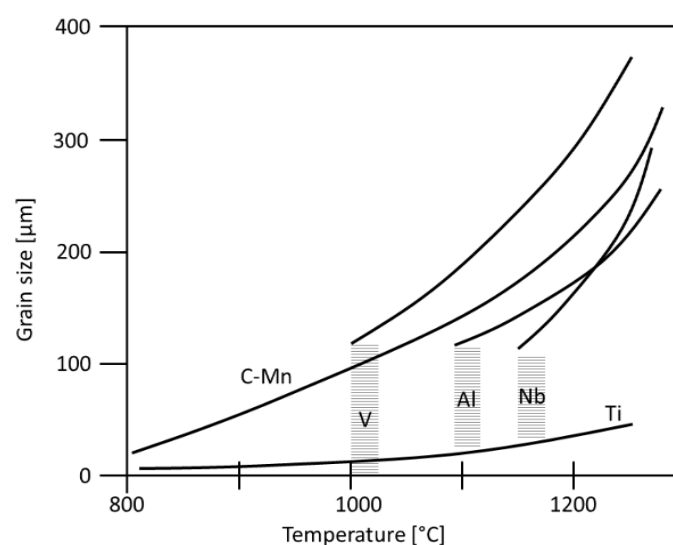


**Figure 2: Influence of the MAE on the austenite grain growth adapted from [39-41]. Ti possesses the highest dissolving temperature, followed by Nb at ~1150°C and V at ~1000°C. Al, commonly used as deoxidizer precipitates as AlN and acts as grain refiner in HSLA steels.**

### 2.2.1 Titanium

As displayed in Figure 2, Ti acts as the most effective grain pinner in micro-alloyed steels. TiN possesses the highest solubility product, so that for Ti-micro-alloyed steels dissolution temperatures of 1250°C are quite common to bring Ti back into solution and to ensure a homogenous distribution. This is necessary to avoid a heterogeneous grain growth through Ti which is unequally distributed or existent in too large precipitates [3,42,43]. Effective stoichiometric ratios have been reported with 3/4 Ti : 1 N, to provide a good distribution over the volume in order to act as efficient grain refiner [38,40–42]. TiC precipitates at lower temperatures compared to TiN. It also controls the austenite grain size during reheating, especially in welding [44].

### 2.2.2 Niobium

Niobium is the most prominent alloying element in elevating the  $T_{NR}$ , which is effective already at very low contents as depicted in Figure 3. The combination of the high stability of its carbonitrides (Nb(C,N)) and their deformation induced precipitation temperature in the mid to lower austenite region between 1000°C and 800°C [3,38,43] makes it the most effective MAE for delaying recrystallization and promoting a fine  $\alpha$  microstructure. These Nb(C,N) precipitate with usual diameter of 2 – 3 nm at the austenite grain boundaries, deformation bands and austenite-ferrite interphases, which leads to an considerable precipitation strengthening [3,8,38,43]. Additionally, Nb possess a significantly high solute drag, by its high atom radius compared to Fe so that, if dissolved, it also influences the diffusion-controlled processes of recrystallization [38,45–48]. However, its role as grain boundary “pinner“ is by far stronger than in retarding recrystallization by its solute drag. Furthermore, Nb acts in retarding the  $\gamma$  to  $\alpha$

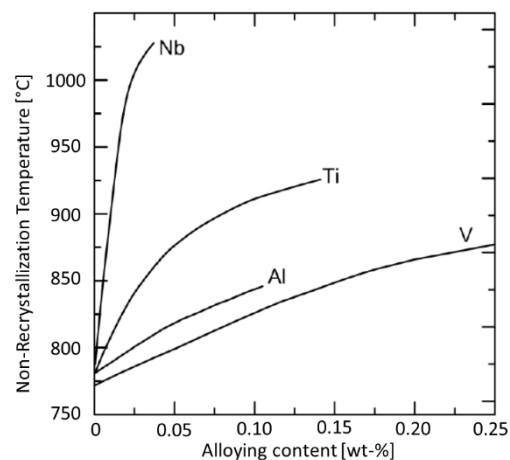


**Figure 3: Effect of MAE on  $T_{NR}$ . Nb already effects at relatively low alloying contents of <0.05% and increases  $T_{NR}$  significantly. The influence of Ti and Al is less pronounced, as well as V only acts at high solute contents. Adapted from [39-40]**

transformation in dissolved condition and promotes the formation of non-equilibrium transformed microstructures such as bainite and martensite [12,38,49]. Dissolved Nb precipitates during tempering and additionally provides a significant strength contribution [50].

### 2.2.3 Vanadium

Vanadium precipitates during cooling only at very low temperatures (below 800° C), thereby it plays only a subordinate role as recrystallization retarding element in the TM rolling process. It possesses a high solubility in the austenite, which – by exclusive use of V as MAE – cannot inhibit the grain growth effectively. Consequently, Ti is commonly added to V micro-alloyed steels in order to prevent excessive grain growth at elevated temperatures [51]. Due to its low solute drag, V rather promotes the recrystallization prior to the  $\gamma$  to  $\alpha$  transformation temperatures, which makes it interesting during recrystallization-controlled rolling as by this means, it stimulates the static recrystallization process between the rolling passes [52]. In the context of Nb micro-alloying it has been shown, that the transformed microstructure is smaller when it emerges from a unrecrystallized and pancaked austenite grain [53]. However, for V steels was observed, that the transformed microstructure is independent on the shape of the PAG, as recrystallized austenite grains produce the same  $\alpha$  grain size as unrecrystallized  $\gamma$  grains [51,54,55]. As a result V micro-alloyed steels possess a by far uniform austenite grain, which is assumed to result in isotropic mechanical properties [52]. Tempering of V-containing steels show secondary hardening by precipitates of VC and  $V_4C_3$  which results in a increase in hardness [56], however it was also observed that these precipitates contribute to a significant embrittlement [50].

### 2.2.4 Aluminum

Al is no classic MAE, yet a prominent alloying element acting as grain refiner, so that it is worth listing. Aluminum is a low-cost material that surpasses the properties of Si in its role as deoxidation element [3]. At rolling temperatures below 1100° C it precipitates with atmospheric nitrogen to AlN and pins the austenite grains. Consequently, it fulfils actually two functions in steel production and is established in the processing of fine-grained structural steels. Al belongs to the  $\alpha$  formers and raises the  $A_{r3}$  temperature [3,11,57]. Regarding its recrystallization texture, aluminum nitrides endorse a preferential development of {111} texture components [8]. Due to its affinity to Nitrogen, a competition between Aluminum and Vanadium for the available N is predestined, which should be considered [58].

## 2.3 Anisotropy and crystallographic textures in hot rolled steel plates

Several research groups have dedicated numerous publications to the characterization and minimization of the anisotropy of hot rolled steels [27,34,59–69]. This subject is of major interest for both, the steel manufacturer and the processor of the steel product. Correlations of process parameters and the anisotropy have been described, however, a clear depiction of this issue does not exist until now. In specific three sources can be described which cause differences of the mechanical properties in longitudinal and transversal direction [59] and are described in the following.

### 2.3.1 Inclusions

Inclusions, such as manganese sulphides, silicates, alumina and combinations of oxides are the contribution of the steelmaking route to the anisotropy of hot rolled steels [59]. Inclusions occur during the initial solidification and further related chemical segregations. During rolling these phases, especially manganese sulphides and silicates elongate towards the rolling direction or fracture in the form of stringers [59,70,71]. The result are non-uniform mechanical properties between different testing directions in terms of fracture mode and toughness, tensile elongation and bending properties [59,70,72]. Nonmetallic inclusions affect the accumulation of stresses on adjacent cementite particles, which are more brittle than the matrix. MnS inclusions loose cohesion with the surrounding matrix, the stress concentration around the created hole results in the emerge of voids or cleavages [59,73]. A decrease in the rolling reduction [69,74], a reduction of sulphides concentration or the control of the shape and size of these nonmetallic particles [59,71,73,75] are capable to reduce the resulting anisotropy. A full extinction however is not possible, even if the concentration of sulphides is reduced below 0.01wt.-%[76].

### 2.3.2 Microstructural anisotropy and pancaking of the austenite grain

The microstructural anisotropy is characterized for example by alternating planar patches of different microstructural constituents, e.g. layers of ferrite and perlite. This arrangement is also known as banding [59,76] and contributes to the orientation dependence of properties. These layers arise by the segregation of solutes during the cooling of the material. Elements such as manganese, silicon, phosphorus and sulphur are partitioned and then solidify, resulting in a composition gradient. The subsequent deformation causes the expansion of these regions. During the following  $\gamma$  to  $\alpha$  transformation, these planar shaped layers provoke the formation of alternating phases, by different affinity to nucleation [59]. In steels, which are alloyed with

austenite stabilizers to obtain a bainitic or martensitic microstructure, areas in which a depletion of these elements took place can decompose into ferrite with the result of an inhomogeneous microstructure [59,77]. In micro-alloyed steels, composition gradients can also lead to areas of reduced recrystallization-retarding elements and thus regions, where premature recrystallization took place, whereas other regions are highly pancaked. These areas contribute to the unfavorable orientation dependence of properties. In this context, also the pancaking of austenite grains during TM rolling involves detrimental properties, which manifests itself in mechanical anisotropy. During the deformation in the non-recrystallizing austenite unfavorable textures are promoted, which are described in the following chapter. Furthermore, during pancaking, the through segregations weakened boundaries fracture in the form of delamination cracks [78,79]. Since the austenite grains experience stronger deformation towards the rolling direction rather than to the transversal direction, longitudinal specimens naturally have a lower notch impact than transverse samples due to the described delamination cracking.

### 2.3.3 Crystallographic texture

The main causes of the mechanical anisotropy are defined by the aforementioned factors, so that the crystallographic texture often plays a subordinate role [59]. Several researchers have even observed, that crystallography has little or no role in the orientation dependence of the mechanical properties [59,80,81] and rather elongated sulphides [82] or an uneven distribution of carbide-enriched microstructural components possess the major influence [83,84]. Nevertheless, often one of the above-described factors coincides with an unfavorable texture and results in these differences of the mechanical properties between the longitudinal and transversal direction. A clear delineation is rarely possible, however, several texture components are of interest as they are associated to knowingly engender a certain orientation dependent material behavior. For hot rolled material, relevant components can be found in a ODF map in a direction of  $\Phi_2 = 45^\circ$  [85,86]. The  $\{001\}\langle 110 \rangle$ , which originates from the recrystallized austenite cube texture and the  $[113]\langle 110 \rangle$  texture, both located upon the  $\alpha$  fiber are known to reduce ductility and simultaneously trigger significant anisotropy and shear fracture [85–87]. Furthermore, the  $\{001\}\langle 110 \rangle$  has been found to have a detrimental effect on the occurrence of delaminations [85]. In opposite to that, the  $\{332\}\langle 113 \rangle$  texture, which is located, upon the  $\varepsilon$  fiber, the same as the  $\{554\}\langle 225 \rangle$ , rank as the most beneficial among the transformation textures in hot rolled steels as they both improve ductility [85–87]. The

influence of their occurrence and factors which contribute to the formation of certain textures are described elsewhere [85].

Consequently, the orientation dependence of the mechanical properties can be traced back to the described factors. However, a clear differentiation and quantification of a certain factor to its effect on the anisotropy is not possible. For example, a highly pancaked austenite grain influences both, texture and inclusion structure and inclusions itself favor the formation of certain textures. A consequence of the described factors is the formation of delamination cracks, which are described in the following chapter.

## 2.4 Delaminations in Charpy notched impact specimens

The fracture appearance of Charpy notched impact specimens of TM-processed steels is often characterized by delamination cracks, also known as fissures, splits or separations [88]. These delaminations, which typically appear aligned parallel to the rolling plane [88] have been reported and intensively studied in the 70s and 80s as TM rolling became increasingly popular, especially in the production of pipelines [11,20,28,78,79,89–100]. For the formation of delaminations, two conditions must be fulfilled, (1) the austenite grain is deformed and pancaked through a previous TM process route and (2) the steel experienced a temper treatment. As-rolled DQ samples generally do not exhibit this phenomenon. Furthermore, after normalization these delaminations vanish [88,101,102].

As described in the previous chapter, the mechanical anisotropy is a consequence of crystallographic texture, intergranular fracture along grain boundaries through a segregation of dissolved elements such as P, Sb, Sn and aligned particles and inclusions [61,67,103]. Consequently, delaminations of Charpy impact specimen are the result of these effects. The primary reason for delaminations cracks is the combination of highly pancaked austenite grains, which are aligned parallel to the rolling direction and thus susceptible for grain-boundary segregation [58,59] with the appearance of {001} cleavage planes along the grain boundaries [85,104]. These delaminations change the profile of the ductile-brittle transition temperature [102]. On the one hand, they serve by the absorption of the fraction energy through “delamination toughening” [106–111] by triggering the ductile fracture, which in consequence increases the impact energy [67,105]. On the other hand, in the ductile region they reduce the impact toughness through cleavage fracture parallel to the rolling sheet [105,112]. This occurrence of delaminations is hardly avoidable for TM rolled, high strength steels, especially when subjected to annealing heat treatments. However, adjustments in the rolling process are

capable to reduce the intensity of unfavorable textures, such as the aforementioned  $\{001\}\langle 110 \rangle$ , which consequently can alleviate the effects of a cleavage fracture behavior [85,103–105].

## 2.5 Relation of the current thesis to the state of the art

The current thesis builds up on the knowledge of UHS steels, the influence of common micro-alloying elements on the microstructure and their beneficial effects on the mechanical properties. The thesis should span the bow between the present knowledge of TM processed steels and the quantitative description of the underlying microstructural processes. The emphasis thereby shall be on the characterization of the microstructure and the depiction of the influencing parameters. In concrete, how micro-alloying elements influence the recrystallization and if the observations from laboratory scale investigations can be transmitted to the industrial scale in the hot strip mill. A further focus lays on the mechanical isotropy, which is dependent on several factors as described above, however, possesses no quantifiable and distinguishable dimension. Hence, the effect of various alloying elements on microstructure, mechanical properties and especially their connection to the mechanical anisotropy should be clarified and be discussed.

## 3 Summary of Publications

### 3.1 List of Publications

#### 3.1.1 Appended Papers

All appended papers can be found in part B of this thesis.

Paper I:

Esterl R, Sonnleitner M, Stadler M, Wölger G, Schnitzer R (2018)

*Microstructural Characterization of Ultra-High Strength Martensitic Steels*

Practical Metallography 55 (2018) 4: 203 - 222

DOI: 10.3139/ 147.110491

Paper II:

Esterl R, Sonnleitner M, Schnitzer R (2018)

*Microstructural Analysis of the Recrystallization Behavior of Low Alloyed Steels*

Steel research international 90 (2019) 3: 382 - 391

DOI: 10.1002/ srin.201800500

Paper III:

Esterl R, Sonnleitner M, Schnitzer R (2019)

*Influences of Thermomechanical Processing and Nb Micro-Alloying on the hardenability of Ultra-High-Strength Steels*

Metallurgical and Materials Transactions A (2019)

DOI: 10.1007/ s11661-019-05235-8

Paper IV:

Esterl R, Sonnleitner M, Gschöpf B, Schnitzer R (2019)

*Influence of V and Nb Micro-Alloying on Direct Quenched and Tempered Ultra-High Strength Steels*

Steel research international (2019): 800640

DOI:10.1002/ srin.201800640

Paper V:

Esterl R, Sonnleitner M, Weißensteiner I, Hartl K, Schnitzer R (2019)

*Texture analysis after different quenching sequence to separate the mechanical anisotropy of UHS steels*

Submitted to Journal of Materials Science



Contributions of the author: The author of this thesis is responsible for planning, conception and writing of all papers. The steel samples for the metallographic analysis were provided by voestalpine Stahl GmbH. Furthermore, the rolling of the test alloys was performed at the voestalpine in Linz, as well as the measurement of the mechanical properties. All microstructural investigations (experiments and data evaluation) were carried out and interpreted by the author himself or executed in form of a supervised thesis. Following results were produced externally:

Paper I: The Confocal Laser Scanning Microscopy was performed at the Chair of Ferrous Metallurgy at the Montanuniversität Leoben.

Paper V: The quantification of the ODF maps was executed at the Christian Doppler Laboratory for Advanced Aluminum Alloys at the Montanuniversität Leoben.

### 3.1.2 Conference presentation

Esterl R, Sonnleitner M, Spindler H, Schnitzer R (2017): *Characterization of the recrystallization behavior of hot rolled steels*. EUROMAT, Thessaloniki, Greece.

### 3.1.3 Supervised theses

Hartl K (2018) Texturentwicklung bei Wärmebehandlungen von ultrahochfesten Stählen. Bachelor thesis, Montanuniversität Leoben.

Gschöpf B (2018) Mikrostrukturelle Analyse von ultrahochfestem Warmband. Bachelor thesis, Montanuniversität Leoben.

Hinterleitner J (2018) Entwicklung einer Auswertemethodik zur Analyse von mechanischen Kennwerten thermomechanisch gewalzter ultrahochfester Stähle. Bachelor thesis, Montanuniversität Leoben.

Jabr A (2019) Bruchaufreissungen in Kerbschlagproben thermomechanisch gewalztem ultrahochfesten Warmbands. Bachelor thesis, Montanuniversität Leoben.

## 3.2 Summary of published contents

### 3.2.1 Aim and scope of the investigations

The aim of this thesis was to establish the microstructure-property relationship of UHS steels. Due to the fact, that during TM rolling, the finish rolling is accomplished below  $T_{NR}$ , the austenite grain experiences a pancaking towards the rolling direction. This elongation of the  $\gamma$  grain is assumed to influence the isotropy of the mechanical properties negatively. Thus, the first investigations comprised the visualization and quantification of the microstructure of martensitic UHS steels. For these examinations, light optical microscopy was used. The properties of the emerging product are dependent on the underlying microstructural development. Thus, the subsequent investigations concentrated on the description of the recrystallization processes, such as dynamic and static recrystallization. To study these recrystallization processes, the suitability of laboratory scale deformation units needed to be established. Therefore, a deformation dilatometer Bähr 805 A/ D came to application to display and describe the influence of MAE and the process route in terms of their impact on the microstructure. The crucial issue of the present thesis is the optimization of the mechanical properties, in specific, the isotropy of TM rolled steels. In contrast to that, material, which is air-cooled after rolling and then quenched and tempered shows clear advantages. The key to solve this questions consisted of two different approaches. In a first method, four industrially available TM processed UHS steel grades were characterized in terms of their mechanical properties and the peculiarities of their microstructure in the as-rolled (TM-rolled) condition and after six different normalization and quenching treatments. Therefore, three temper resistant steel grades (*Steel B* and modifications thereof) and a wear resistant steel grade (*Steel A*) were mechanically tested in different heat treatment conditions. The second key to treat the central issue was the production and processing of 15 different test alloys. Based on intensive reviews of the existing literature and the knowledge and experience of the processing-property relationship following conditions were defined:

- A carbon content of 0.17% defines sufficient strength ( $YS > 1100$  MPa) in the direct quenched condition and still offers excellent weldability.
- The process parameters need to be applicable at the hot mill simulation unit and compatible with the hot strip mill. Two different FRT should be performed.
- The influence of MAE on the mechanical properties and their behavior after re-austenitization as well as their behavior after tempering should be established.

The available UHS steel grades, *Steel A* and *Steel B* were therefore adapted with regard to different MAE and rolled in a hot mill simulation unit. Six different conditions of the test alloys were investigated, in concrete terms, two different FRTs in the as-rolled and tempered condition and compared to RQ and RQ+T. The mechanical and microstructural investigations should clarify the influence of the MAE and process parameters as basis for the development of new UHS steels.

The investigations performed should answer the following questions:

- Which methods are well-suited for the visualization and characterization of the microstructure prior to the martensitic transformation? This technique should be easy-to applicable, reproducible and describe the PAG structure with regard to their size, distribution and aspect ratio.
- Is it possible to study recrystallization processes on a laboratory-scale? Are peculiarities, measured with a deformation dilatometer, visible in the microstructure? Does this method finally allow the reconstruction of a hot-rolling scenario on the dilatometer and a subsequent study of the microstructural evolution?
- Does the processing route influence the hardenability of UHS steels? Although,  $M_S$  and  $M_F$  are determined by the chemical composition, the condition of the  $\gamma$  grain or precipitated/ dissolved elements influence the diffusion-less and non-equilibrium transformations. Is it consequently possible, that for a given chemical composition the hardenability is alterable by different productions routes?
- What is the role of the processing route on the properties of UHS steels? How do MAE, in specific Nb and V, influence the mechanical properties in the as-rolled condition? In which expand are strength and toughness changed through a subsequent tempering?
- Are the differences of mechanical properties in longitudinal and transversal direction dependent on the microstructure and what is the role of the used MAE? Is the mechanical anisotropy inherited or can an intensive heat treatment in the austenite region delete this property?

These questions are discussed in the following pages with respect to the published papers enclosed to this thesis.

### 3.2.2 Visualization of the prior austenite grains

The first assignment of the present thesis was to establish a technique for an efficient, economic and reproducible characterization of the microstructure of TM processed UHS steels.

This task is inevitable to connect the microstructure with the mechanical properties of the actual industrially produced TM+DQ steel products, *Steel A* and *Steel B*. And further, this issue is of major interest in order to transfer the mechanical properties of the subsequently developed test alloys down to the characteristics of its microstructure. Due to the fact, that the size of the PAGs defines the dimensions of the transformed  $\alpha$  or  $\alpha'$  microstructure [113–115] and so the strength and toughness of the emerging steel product, the access to the prior  $\gamma$  grain is fundamental. Moreover, the PAG contains certain features, which are inherited to the transformed microstructure and manifest themselves in an anisotropy of the mechanical properties [59,60,63].

Due to the fact, that the microstructure of direct quenched steels mainly consists of martensite and bainite, the austenite grain cannot be accessed conveniently. Also literature often depicts the process to access PAGs of martensitic steels as demanding procedure [116,117]. In Paper I, several techniques are presented to reveal the PAG structure of different martensitic UHS steels.

A standard technique to reveal the actual transformed ferritic/ bainitic/ martensitic microstructure consists of a etching with Nital. In some cases, this etchant can be sufficient to mark the PAG as displayed in Figure 4a. Regarding the highly-pancaked austenite grain of a TM steel in Figure 4b, the blocks, which emerge from the former  $\gamma$  grain boundaries provide information about the position of the PAG. For a pure qualitative analysis of the PAG size and structure, this Nital etchant can be satisfactory, however it is not suitable for an accurate quantification.

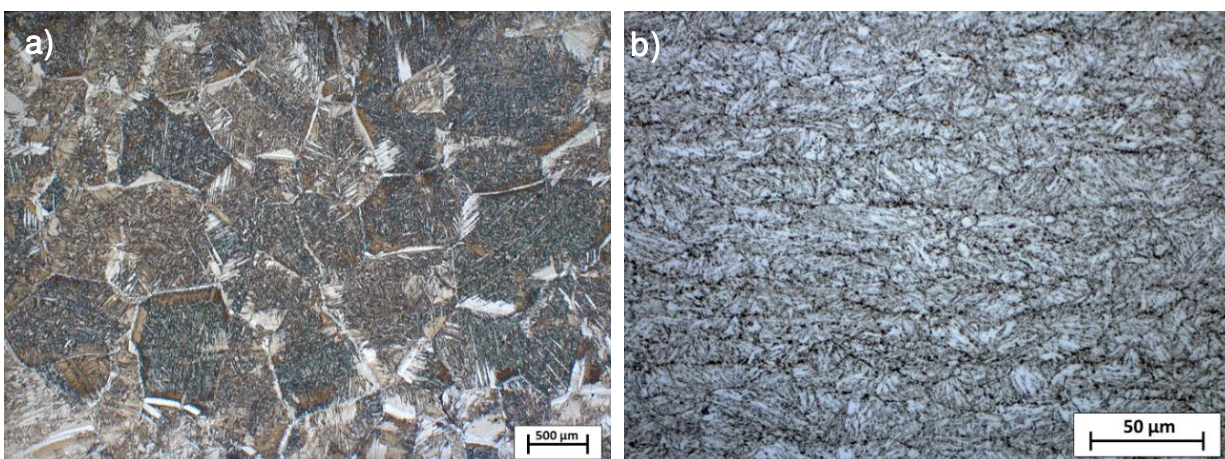


**Figure 4:** In some cases, a Nital etchant is sufficient to reveal the PAG boundaries, exemplarily depicted for a plain carbon structural steel (a). Due to the fact, that the laths and blocks are oriented towards the highly-pancaked austenite grain, their boundaries can be assumed as displayed for a TMP UHS steel in (b). For a quantification of the PAG structure, however, this etchant is not suitable.

The main method of choice consists of a picric acid etchant. Based on the composition proposed by Bechêt and Beaujard in 1955 [118], this etchant was modified by different wetting agents and varying additions of HCl [117,119–121]. The resulting successful composition consists of picric acid and *Sodium dodecyl sulfate* as wetting agent, which is cold filtered and then, depending on the alloying content of the investigated material, mixed with 1 -3 drops of HCl [36]. If the etching attack does not produce the desired results, it is recommended to heat the etchant in a water bath to 70°C and then to repeat the etching, taking a much shorter etching time (<1min). A clear improvement of the etching result can be accomplished, if the samples experience a temper treatment at 600°C for 15 min. Figure 5 shows the successful application of the developed etchant on a micro-alloyed UHS steel (*Steel B*) processes with an FRT of a) 900°C and b) 850°C. With decreasing reduction below  $T_{NR}$ , the pancaking increases. After re-austenitization (Figure 5c) the PAGs appear in a globular shape.

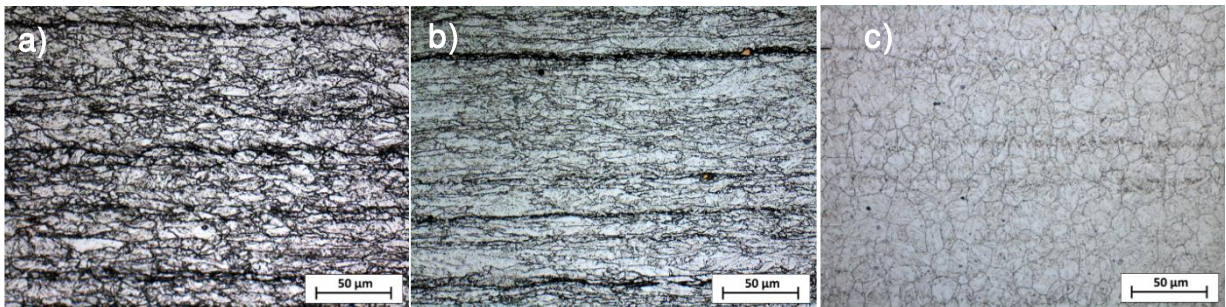


**Figure 5: Successful application of the developed etchant to reveal PAGs of a martensitic steel (*Steel B*). a) After a finish rolling at 900°C, the pancaking of the  $\gamma$ -grains of the micro-alloyed UHS steel is already present, yet still globular grains appear. b) The same steel processed with a FRT of 850°C, the pancaking is significantly increased. c) After re-austenitization, the grains appear in a globular shape.**

Further techniques were investigated to visualize the PAGs. In specific, an automated reconstruction via EBSD data on basis of the theoretical transformed groupoid structure formed by the origin grain (ARPGE) proposed by Cayron [122–125]. It represents a reliable alternative to metallographic techniques as investigated by several researchers, who prove its adequacy in the reconstruction of the PAG structure of martensitic steels [126] and welding structures [127–129]. This technique was successfully applied as demonstrated in Figure 6a-c. This technique additionally allows both, a quantification of the martensitic grains and of the reconstructed prior austenite grains. However, this technique requires a time consuming sample preparation and an intense EBSD scanning of at least 4 h and consequently fails as suitable method for the reproductive characterization of a large number of PAGs. Nevertheless, this technique shall play an important role in the characterization of the microstructure of the test alloys, which will be discussed in a subsequent chapter (Paper III and V).

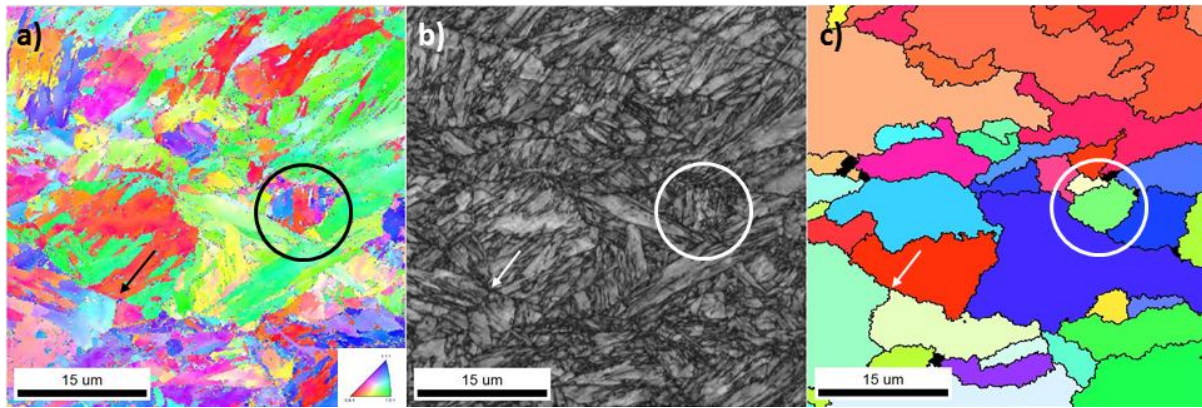


**Figure 6: EBSD map with selected grain zones: a) Image quality map with inverse pole figure map, b) correlating black/ white image quality map with dark shaded phase boundaries and c) unique color coded map of reconstructed PAGs with ARGPE.**

The effectiveness of an etchant is shown when the images enable a quantification of the highlighted microstructure and the effort of a manual post-processing is minimal. In combination with the image analysis software “Olympus Stream” and “MIPAR” [130], the grains were quantified in terms of equivalent grain size and the corresponding aspect ratio after application of the established etchant. Subsequently a grain size distribution was performed as depicted in Figure 7 for three different positions: near the surface of the strip, 1.5 mm and 3 mm below the strip of the TM-processed UHS steel, which was finish-rolled at a temperature of a) 850 °C and b) 900 °C.

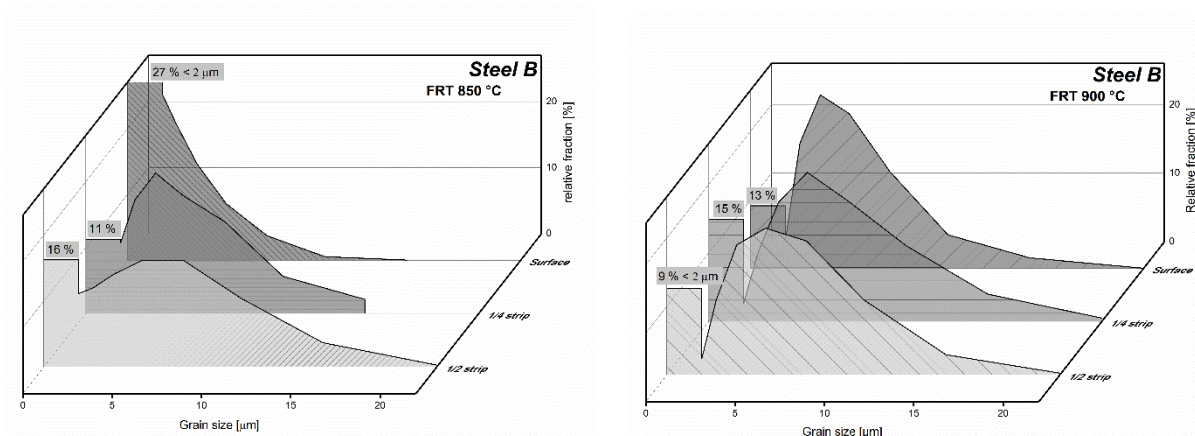


**Figure 7: Grain size analysis of *Steel B* according to ASTM E 112 – 12 at a FRT of 850 °C (a) and a FRT of 900 °C (b) at three different positions (surface, ¼ of strip thickness and center thickness).**

The established etchant consequently enables in combination with an image analysis software conclusions concerning the recrystallization behavior in the austenite region dependent on temperature and the degree of deformation. This may serve as basis for studies on the recrystallization behavior of TM-processed steels in order to highlight the influences on the microstructure with varying deformation parameters, which was performed in Paper II.

### 3.2.3 Investigations on the recrystallization behavior

Microstructural processes in a hot-rolling mill consist of static, dynamic and metadynamic recrystallization, recovery and complex combinations thereof [48,131–141]. To portray these microstructural processes on a laboratory-scale, Paper II describes diverse possibilities to characterize firstly the recrystallization behavior of differently alloyed steels and thus the influence of several MAE by means of flow stress curves recorded with a Deformation Dilatometer Bähr 805 A/ D [142]. The chemical composition of the six steels investigated is listed in Table 1.

*Table 1: Chemical composition of the steels investigated [wt-%]. Steel C is a modification of the tempered TM-Steel B and is investigated in detail in chapter 3.2.*

Steel	Description	C	Mn	Cr	Ni	Mo	Cu	V	Ti	Nb	B
1	S275JR	0.15	1.1	0.02	<0.01	0.01	0.01	<0.01	<0.01	<0.01	<0.001
2	16MnCr5	0.15	1.2	1.20	<0.01	0.01	0.01	<0.01	<0.01	<0.01	<0.001
3	S355 + Nb	0.15	1.1	0.02	<0.01	0.01	0.03	<0.01	<0.01	0.01	<0.001
A	hardenable steel	0.17	2.3	0.30	<0.01	0.01	0.08	<0.01	0.02	<0.01	0.002
B	hardenable steel +MAE	0.17	1.4	0.70	1.0	0.50	0.45	0.05	0.02	0.04	<0.001
C	hardenable steel +MAE	0.09	1.8	1.00	0.50	0.20	0.01	0.10	0.02	<0.01	<0.001

To study the SRX, which would correspond to the recrystallization between the rolling passes, double-hit deformations are the method of choice. Furthermore, with this method, the determination of the  $T_{NR}$  is possible [39,134–145]. For the quantitative description of dynamic recrystallization, flow stress curves with varying temperature and strain rate are performed to calculate the activation energy  $E_A$  for the onset of DRX [137,146–151]. The static recrystallization is associated with a softening and follows the Johnson - Mehl - Avrami kinetics. This softening is displayed in Figure 8 for the six steels investigated and can be divided in mainly two groups. Steel 1 (S275JR) and 2 (16MnCr5), as well the hardenable *Steel A* show an accelerated softening due to the lack of recrystallization retarding elements. Steel 2 (S355+Nb), *Steel B* and *Steel C* possess a delayed SRX. Although *Steel A*, which accordingly belongs to the UHS steels, alloyed with a significant amount of  $\gamma$  stabilizers, recrystallizes like a plain carbon steel. Moreover, the S335+Nb steel, ranks in the group of UHS steels concerning its retarded recrystallization, which can be related to the augmented effect of Nb.

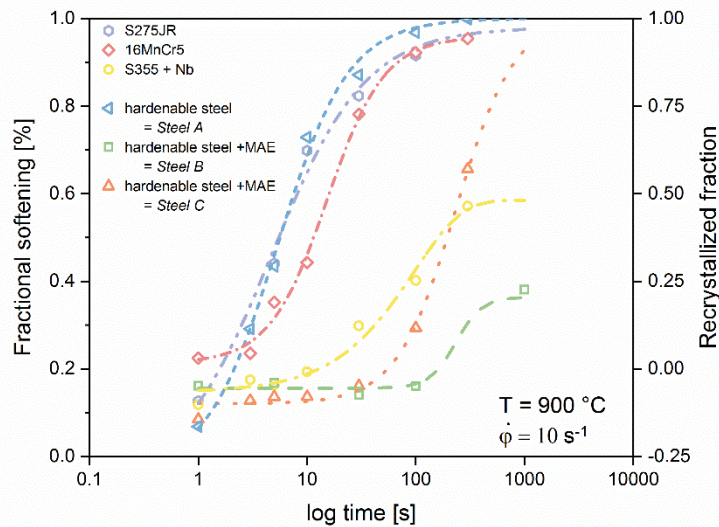


**Figure 8: Classification of six low C-steels with varying alloying content relating to their SRX behavior following the Johnson-Mehl-Avrami recrystallization kinetics. Two groups can be differentiated: On the left side, steels with a rather fast softening behavior, on the right side, steels in which the recrystallization is decelerated.**

In order to investigate the microstructural evolution of *Steel A* and *Steel B*, which rank in the same strength grade, but show a different recrystallization behavior, the above-described developed etching agent was used to show their different grain evolution. A deformation sequence with increasing cumulative strains, simulating a hot rolling scenario was performed to show, how both steels react on the imposed deformation. Figure 9a shows, that *Steel A* recrystallizes between the deformation passes, developing a uniform globular grain size (Figure 9b), whereas *Steel B* possesses increasing flow stresses after each pass due to the usage of Nb. According to Figure 9c, the grain sizes decrease after each pass, yet a significant amount of bigger (pancaked) grains remains.



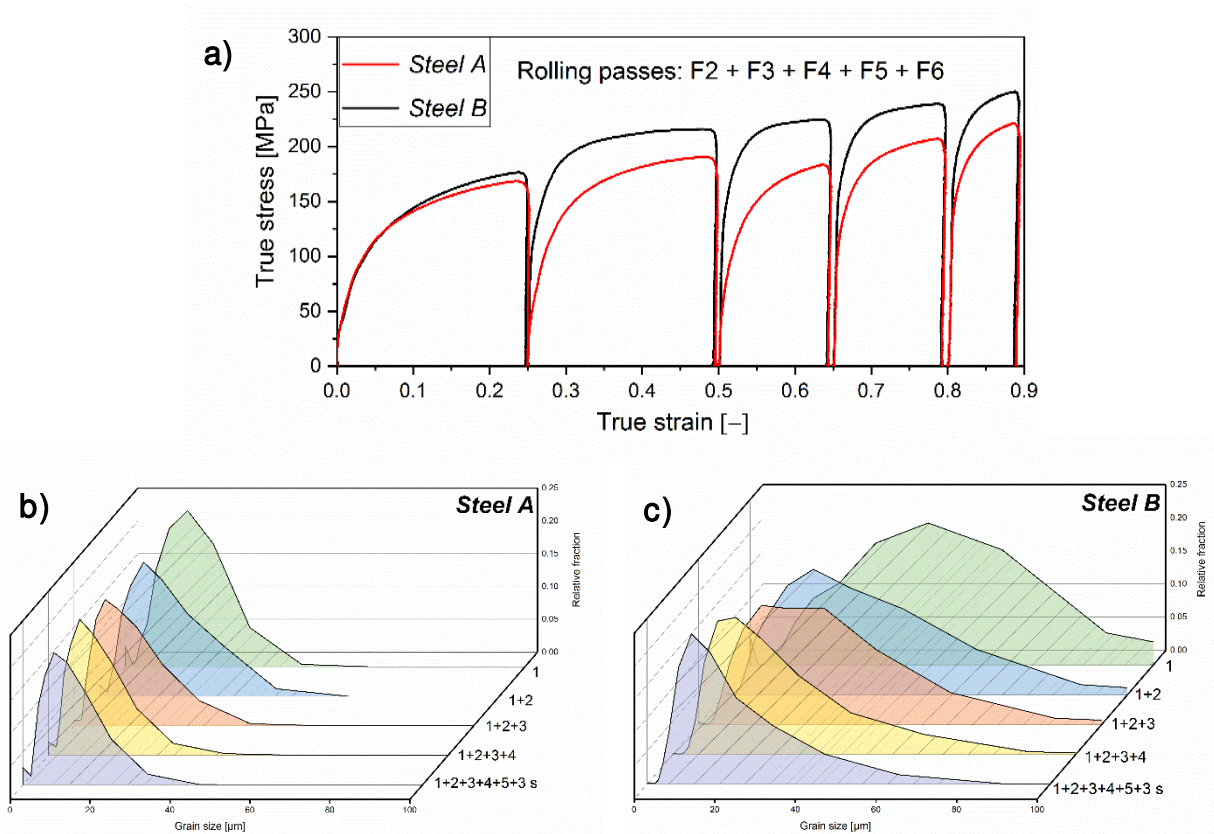


**Figure 9: Sequenced deformation performed on two UHS steels. a) Flow stress curves of *Steel A* and *Steel B*. Despite of their same strength level, concerning their softening they behave differently: *Steel A* shows a softening between the passes, whereas *Steel B* shows increasing flow stresses. Grain size distribution of *Steel A* (b) and *Steel B* (c) after the different rolling passes.**

### 3.2.4 Influence of the processing route on the hardenability

In Paper II, it was shown, that two investigated steels, *Steel A* and *Steel B*, both with a carbon content of 0.17%, rank in a similar strength level although their alloying concept and consequently their microstructural evolution differ considerably. Due to the lack of Nb, *Steel A* exhibits a fine uniform grain after each rolling pass, whereas the grains of *Steel B* are significantly bigger and possess an elongated (pancaked) shape. If the hypothesis is confirmed, that a recrystallized austenite grain is able to reduce the mechanical isotropy, the use of MAE, which promote the pancaking, need to be reconsidered. Consequently, the loss of hardness through the dispense of MAE needs to be compensated. To guarantee the required strength and hardenability for the defined carbon content, the compensation is accomplished by the increase of elements which retard the  $\gamma$  to  $\alpha$  transformation and increase hardenability. This issue was investigated in Paper III, in which the influence of the processing route on the critical cooling rate was explored. Three steels were object of this research: *Steel A* and *Steel B*, whose composition is given in Table 1, and a variant of *Steel A* with 0.04%Nb. Different cooling rates

were applied after deformation corresponding to two different rolling cycles with varying finish rolling temperatures (FRT). The obtained hardness values were compared to those received through conventional quenching after austenitization.

The investigations, depicted in Figure 10, showed, that the samples processed via TMP obtained significantly higher hardness values compared to the RQ route. Moreover, the hardness increased with decreasing FRT. Further, it was observed, that, that Nb leads to an expedited formation of bainite and ferrite, which was observed for the samples of *Steel A* +Nb subjected to re-austenitization and quenching. For the lower cooling rates, the hardness of the RQ specimen decreases considerably due to the increased PAG size [152]. In a dissolved condition Nb rather retards the  $\gamma$  to  $\alpha$  transformation as it was experienced by the TM processing of *Steel B*. Further it was observed, that finer grains additionally promote an accelerated martensite transformation. Increasing the reduction in the non-recrystallizing austenite regime elevates the  $M_s$  temperature. This effect dominates over an accelerated formation of martensite due to smaller austenitic grain sizes.

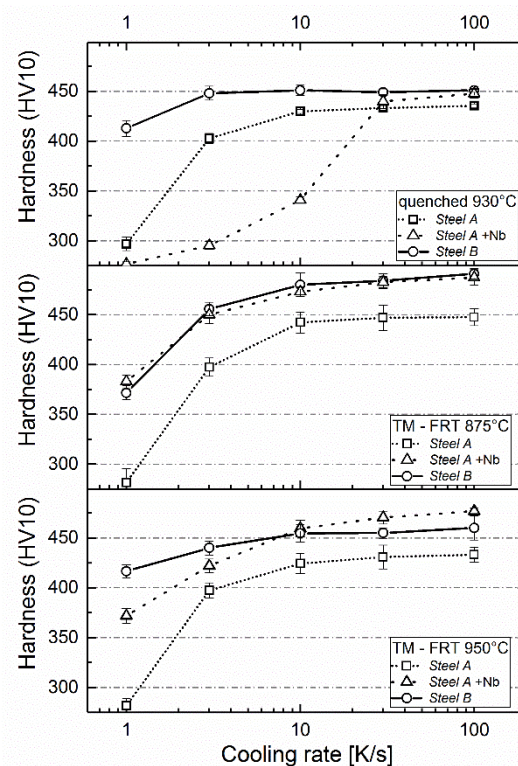


**Figure 10: Effect of FRT on the hardenability of *Steel A*, *Steel A* +Nb and *Steel B* compared to quenching after previous austenitization for 5 min at 930°C. A decreased FRT delivers higher hardness values for all steels. However, *Steel B* exhibits a significant hardness decrease at low cooling rates compared to the higher FRT and the Q-route. Top graph: Nb retards the hardenability on the undeformed and simple quenched samples. Middle graph: with increasing Nb content, higher hardness values are achieved at a FRT of 875°C. Bottom graph: Nb influencing the final hardness and retarding the  $\gamma$  to  $\alpha$  transformation at low cooling rates at a FRT of 950°C.**

### 3.2.5 Effect of Nb and V on the microstructure and the mechanical properties of direct quenched and tempered steels

Paper IV dealt with the role of Nb and V micro-alloying and compares the influence of the process routes, especially the influence of the finish rolling temperature during TMP on the mechanical anisotropy [50]. With special emphasis on the orientation dependence, the mechanical properties obtained by a TM process route were compared to those achieved through a RQ process route. For these investigations, test alloys based on the concept of *Steel A*, which was examined in the previous Papers I - III, were produced and rolled on a hot-mill simulator. The chemical composition is listed in Table 2. Base alloy 1 (\*) corresponds to the composition of *Steel A*, which was alloyed with varying amounts of Nb. Base alloy 2 is a variant of *Steel A* which was alloyed with 0.7%Cr in order to increase temper resistance and enhance hardenability [2,4,6,8]. To base alloy 2, varying amounts of V were added to investigate the influence of V in retarding recrystallization and its role during tempering.

*Table 2: Chemical composition of the test alloys, based on Steel A (\*Base alloy1) and modified with Nb, V and Cr [wt-%]*

Base alloy	Variation	C	Si	Mn	Al	Cr	Cu	V	Nb	Ti	B
1	(*)	0.167	0.20	2.38	0.049	0.280	0.089	0.005	<0.002	0.021	0.0025
	Nb+	0.173	0.19	2.36	0.043	0.280	0.079	0.005	0.021	0.020	0.0024
	Nb++	0.175	0.20	2.37	0.041	0.280	0.089	0.005	0.040	0.020	0.0026
2		0.169	0.20	2.30	0.057	0.710	0.078	0.005	<0.002	0.021	0.0024
	V+	0.170	0.21	2.30	0.053	0.700	0.078	0.097	<0.002	0.021	0.0026
	V++	0.179	0.22	2.29	0.049	0.700	0.081	0.194	0.002	0.021	0.0026

Paper IV combines the gained knowledge of the (1) metallographic analysis, (2) the quantification of the DRX behavior via the Zener-Hollomon parameter and the activation energy and (3) the characterization of the mechanical properties in terms of their anisotropy. On the one hand, several observations reported in literature could be confirmed, however a lot of details were completely unknown. Metallographic investigations on the PAG structure confirmed the impact of Nb on the pancaking of the  $\gamma$  grain, which resulted in a strong strength contribution in combination with a low FRT (0.04%Nb: +50 MPa). Unattended till now, however, was the even more pronounced impact of Nb on the strength after tempering, which can be seen in Figure 11. An addition of 0.04%Nb to the base alloy 1 result in an increase of 130 MPa in strength after tempering compared to the Nb-free variant. The effect of V on the strength improvement after TM rolling is very small, however, after tempering, an addition of 0.2%V increases the strength compared to the V-free variant by an amount of 200 MPa. This increase

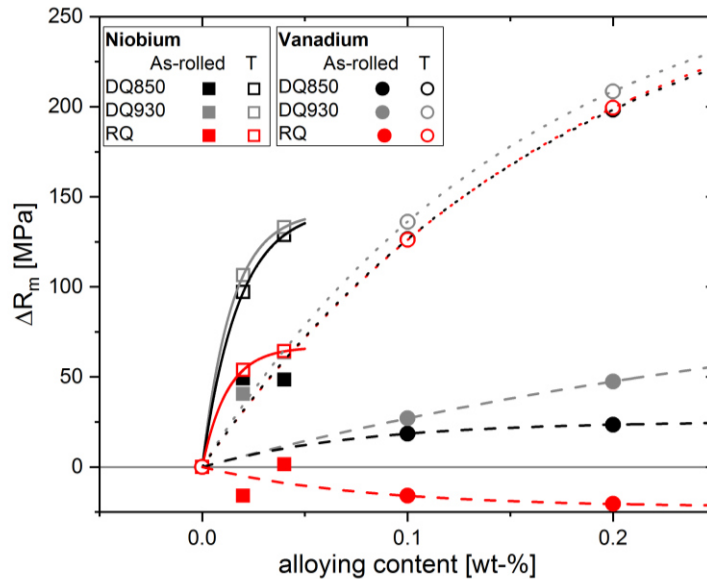


**Figure 11: Strength contribution of Nb and V. The effect of V for strength improvement during TM rolling is very small (dashed lines), and even negative if re-austenitized. However, during tempering it significantly increases the UTS by 200 MPa (dotted lines). Nb has no effect as strengthener after re-austenitization and Q, however, delivers a plus of >50MPa after tempering. During TM processing (DQ850, DQ930), little amounts of Nb already contribute to a strengthening. After tempering, again the effect is even more pronounced**

in strength, however is accompanied by a decrease of the Charpy impact toughness through the embrittling effect of precipitation hardening. In order to compare the TM processed steels with regard to their mechanical anisotropy to those, which were subjected a conventional hardening, all test alloys were additionally tested after re-austenitization prior to quenching. The metallographic analysis delivered an equiaxed austenite grain, however, the mechanical anisotropy was not improved. It was observed, that a higher FRT in TM rolling resulted in a decreased pancaking and improved mechanical anisotropy, yet, the globularization of the  $\gamma$  grains through re-austenitization even deteriorated the isotropy. Nevertheless, the question remains, what else is responsible for this anisotropy. Furthermore, why does the reduced pancaking through a higher FRT results in an improvement of this anisotropy, whereas a full equiaxed grain does not. Consequently, there is an accumulation of properties in hot-rolled materials that are active even after austenitization. In order to further investigate this issue, Paper V addresses the question of whether this inheritance is dependent on the MAE composition and whether it is possible to extinguish it by varying heat treatments.

### 3.2.6 Investigations to separate the mechanical anisotropy and texture

According to the acquired knowledge, presented in Paper IV, the globular  $\gamma$  grain of a re-austenitized UHS steel does not result in the extinction of the mechanical anisotropy. The

aforementioned causes, which can contribute to a mechanical anisotropy of hot rolled steels (chapter 2.4) - and are concurrently not related to the metallurgical process route - are consequently reduced to a single reason. Paper V clarifies the issue, if the mechanical anisotropy can be connected to a remaining texture, which is inherited to the microstructure after re-austenitization. Furthermore, the question seeks clarification if it is possible to extinguish both anisotropy and/ or texture through intensive heat treatments and normalization in the austenite region. These investigations were performed on four different industrially available UHS steels with varying alloying contents. In specific, three micro-alloyed and temper resistant steels, *Steel B* and variations thereof (subsequently named as *Steel C* and *D*) and additionally *Steel A* were investigated. The two variations of *Steel B* possess a decreased carbon content of 0.09%, the chemical composition of *Steel C* is given in Table 1, *Steel D* has lower additions of Cr and Ni. *Steel A* and *Steel B*, both have a carbon content of 0.17%. As mentioned in Paper III, *Steel A* is alloyed with elevated additions of Si and Mn to enable a through-hardening [153]. The temper resistance of *Steel B* is given by elevated amounts of Cr, Ni, Mo and Cu [13,153,154]. *Steel B* possesses also 0.04% Nb in order to facilitate for a TM process route by increasing  $T_{NR}$ . The steels were investigated in the as-rolled condition and compared to re-austenitization and quenching, for which three different austenitization procedures were performed. The conventional re-austenitization and quenching consists of an austenitization at a temperature of 930° C for 5 min followed by water quenching. In the second route (NRQ), quenching is performed after a normalization treatment and an extended austenitization time of 30 min. In the third route (HRQ), quenching was executed after a higher austenitization temperature of 1050° C.

Regarding the microstructure, analyzed by means of EBSD techniques, a clear pancaking of the *Steel B* and *Steel C* towards the rolling direction is observed after TM + DQ (Figure 12b + c). The inverse pole figure map of *Steel B* clearly highlights the impact of Nb on the grain refinement, both, in DQ condition but as well after RQ (Figure 12e). The martensitic microstructure of *Steel A* originates from globular PAGs, which are clearly visible in Figure 12a and are obviously larger compared to *Steel B*. During re-austenitization, the PAGs of all steels investigated form a globular shape, which can be seen in Figure 12 d - f. The grains of *Steel C* coarsen as well by RQ due to the lack of Nb as grain “pinner”.

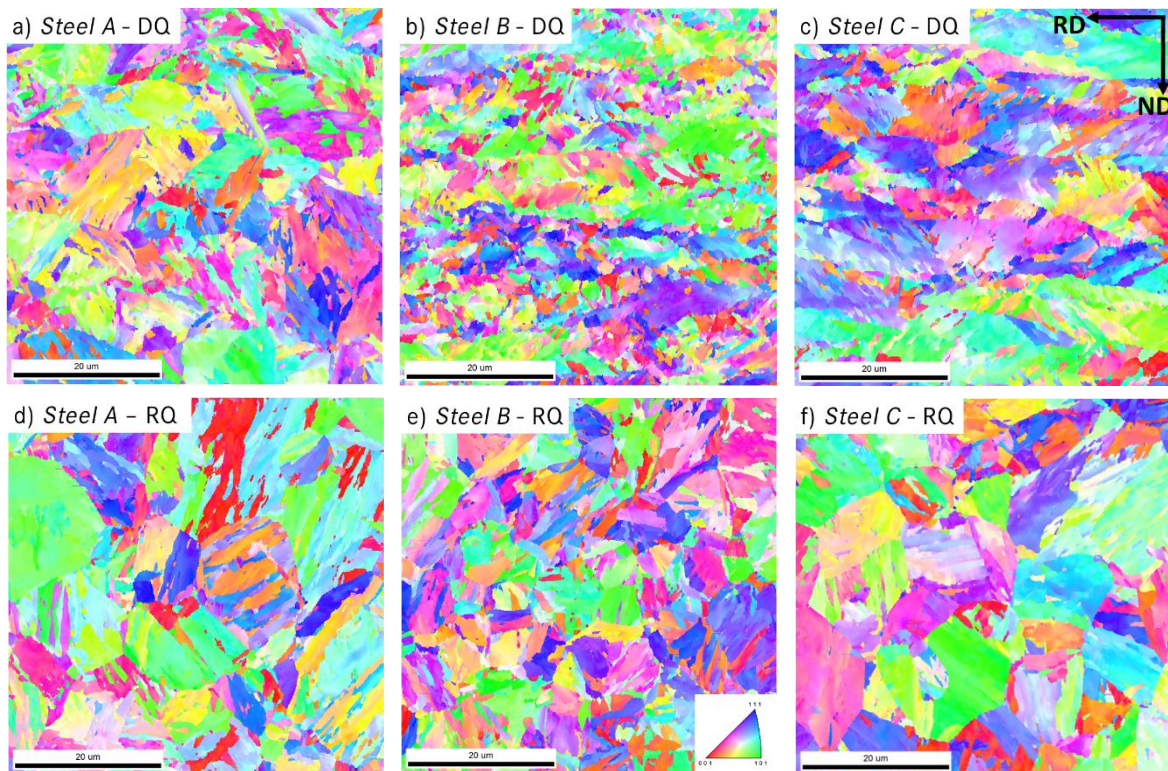


**Fig. 12: EBSD inverse pole figures for the transversal direction in the as-rolled condition for a) *Steel A*, b) *Steel B* and c) *Steel C*. The MAE in *Steel B* (b) and *Steel C* (c) promote a pancaking towards the rolling direction, the PAGs are clearly visible as elongated grains. *Steel B* (b) exhibits the finest microstructure (martensitic block and laths). *Steel A* (a) possesses globular PAGs. d-f) Although, after re-austenitization and quenching (RQ) the PAGs increase and globularize for d) *Steel A* and f) *Steel C*, *Steel B* (e) still maintains the finest microstructure.**

It was observed as well, that by hardening after a prior re-austenitization the UTS decreases significantly. According to Figure 13a, the heat treatment in the  $\gamma$  region has a negative effect on the Charpy impact toughness of *Steel C* and *Steel D*, especially if a normalization is performed prior to quenching. The impact toughness of *Steel B* is slightly improved. At first glance, the anisotropy of *Steel C* and *Steel D* appears to be improved, however, regarding the absolute  $A_v$  values it becomes apparent, that the toughness decreases into the brittle fracture region. Also the innately low anisotropy of *Steel A* can be traced back to the generally low level of impact toughness. Regarding *Steel B*, no influence of the heat treatment on the anisotropy can be observed. The different behavior of the impact toughness after re-austenitization is explained by the different microstructural evolution of the steels. EBSD images highlighted, that the grains of *Steel A*, *Steel C* and *Steel D* significantly coarsen during re-austenitization, whereas *Steel B* maintains – through the grain pinning of Nb precipitates – a very small grain size. Figure 13b describes the volume portions of the relevant texture components, which were analyzed by means of XRD measurements and calculated with MTEX [155] based on the obtained pole figures. All steels investigated contain a decisive fraction of the  $\{001\}\langle 110\rangle$

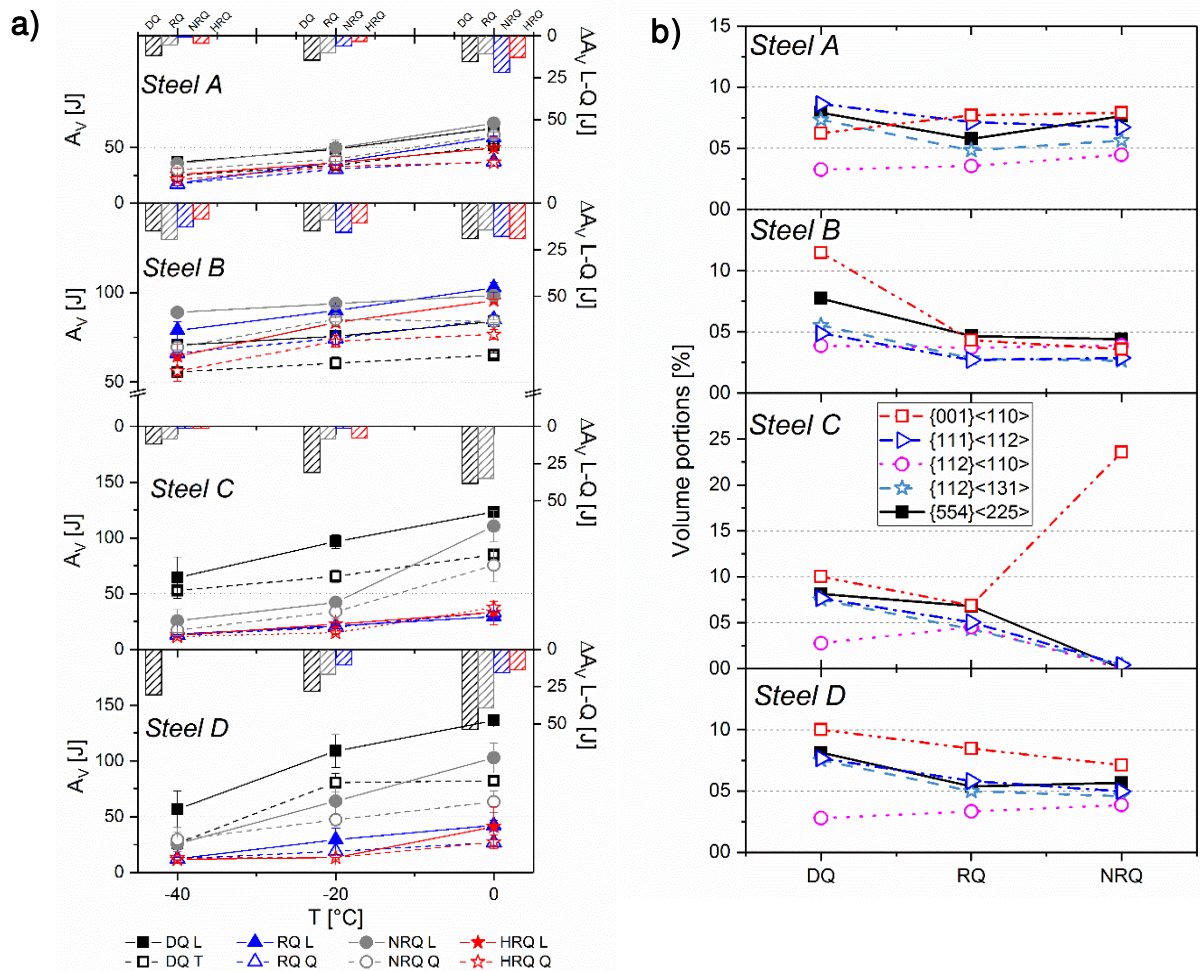


Figure 13a: Charpy impact toughness between  $-40^\circ\text{C}$  and  $0^\circ\text{C}$  and the corresponding differences between the longitudinal and transversal direction. *Steel C* and *D* deteriorate through re-austenitization and even more after normalization and quenching. *Steel A* does not show pronounced influence of the hardening treatment due to generally lower impact toughness. The impact toughness values of *Steel B*, which are already very high are little improved through both RQ and NRQ. The L-T anisotropy of *Steel C* and *D* seems to benefit from re-austenitization, whereas *Steel B* does not show any reaction not even by high austenitization temperatures.

Figure 13b: Effect of the different hardening procedures on the texture components of the investigated steels calculated through MTEX based on the obtained pole figures. Decreasing textures can be observed during re-austenitization of *Steel A* and *Steel B*. *Steel C* shows an augmented  $\{001\}\langle 110\rangle$  texture after normalization, *Steel B* exhibits texture remnants, however the proportions change after re-austenitization

component. This orientation arises from the recrystallized austenite cube texture [85,156] and thus is sparsely present in *Steel B* which is alloyed with strong recrystallization retarding elements (Nb) preventing a recrystallization prior to transformation. The  $\{001\}\langle 110\rangle$  texture is unfavorable for impact toughness, provokes delamination and crack propagation [85,104], which can be observed in the  $A_V/T$  diagram in Figure 13b. With an increase of the  $\{001\}\langle 110\rangle$  component, the impact toughness decreases diametrical and falls to values below 50 J already at a temperature of  $0^\circ\text{C}$ . The relatively high proportions of the  $\{001\}$  in-sheet plane component in the DQ condition of *Steel A*, *C* and *D* might explain differences between L and T. This is

confirmed by the fact, that a reduction of the  $\{001\}\langle 110 \rangle$  partitions reduce the impact toughness anisotropy after RQ (Figure 13a). However, the question remains, why an almost levelled-out texture distribution as it exists in *Steel A* after re-austenitization (Figure 13b) still possesses small but present differences between L and T. And in opposite to that, *Steel B*, which exhibits a significant amount of defined texture components even after HRQ exhibits excellent Charpy impact values in each condition (DQ and RQ) with a relatively small anisotropy. Consequently, a clear link between a remaining anisotropy and prevailing textures thus cannot be made with certainty. However, the present investigations confirm, that the FRT not only plays a major role during TMP but rather influences the mechanical properties through the inheritance of microstructural characteristics. Although, the usage of MAE and the reduction of the FRT provokes through a highly deformed  $\gamma$  grain a mechanical anisotropy, this does not mean simultaneously, that the microstructural cancellations of these peculiarities are the key to a mechanical isotropy.



## 4 Outlook and open questions

The aim of the thesis was to provide deeper insight into the microstructure-property relationship of hot rolled UHS steels. The obtained knowledge should serve as basis for the development of steels with improved mechanical properties and an improved mechanical isotropy. It was verified, that an increased reduction in the non-recrystallization regime results in an augmented mechanical anisotropy. However, a correlation between the degree of pancaking and the differences between the mechanical properties in L and T direction has been disproved. Despite of a globular austenite grain after RQ, it occurs, that the mechanical anisotropy in the Charpy impact test is present in the same extent as after DQ, in which the aspect ratio achieves values above 3. This fact is in contradiction to the phenomenon, that an elevated FRT which is associated with a reduced pancaking reduces the mechanical isotropy. Further it was observed, that tempering decreases the mechanical anisotropy too, although the size and structure of the PAG remains untouched at the corresponding temperature of 600° C. Although, it has been described, that several peculiarities, such as a preferential texture are inherited after re-austenitization, it was observed, that the corresponding mechanical anisotropy often behaves diametrically to its microstructural characteristics: A remaining texture with constant volume portions observed in samples of *Steel B* lead to a inalterable anisotropy in the Charpy impact toughness, whereas the *Steel A* shows the same anisotropy despite of an elimination of its texture components. And further, normalized and quenched samples of *Steel C* exhibit a strong austenite cube texture and in opposite do not possess any anomalies in its mechanical anisotropy [157].

Although, several factors influencing the mechanical anisotropy have been illuminated and specific correlations could be established, the remaining anisotropy have not been understood entirely. Consequently, this open questions leave room for certain assumptions. In specific: why does a temper treatment reduce the differences of the mechanical properties between L and T, although no crystallographic rearrangement (recrystallization) takes place? The relatively high amount of carbide forming elements stabilizes the laths and lath boundaries so that the reduction in the dislocation density merely is accompanied by the emerge of lath-shaped ferritic grains, whose packets are aligned in the same direction as the lath in the original martensite [29]. The laths and packets of a TM rolled material are mainly oriented in 45° towards the rolling direction as they origin from its pancaked  $\gamma$  grain, but no rearrangement occurs during tempering. The only assumption is, that through tempering the Fe<sub>3</sub>C particles arrange in a specific orientation which reduce the mechanical anisotropy. This hypothesis could be clarified

by TEM investigations. Nevertheless, this thesis should be regarded with reservation as it was observed, that the apparent improvement of the anisotropy often is accompanied by the deterioration of the absolute values. The initial differences between L and T are reduced, however, there was no improvement regarding the relative difference values.

Subsequently, several factors play a role in the existence of mechanical anisotropy. A significant influence is the shape and orientation of non-metallic inclusions [75,158–160], which, however, were not the objective of this thesis. Nevertheless, to further understand and especially quantify the mechanical anisotropy, the characterization of these inclusions and its role concerning the different mechanical behavior between L and T is a topic worth investigating.

Nevertheless, within the scope of this thesis, a new steel grade “alform1300x-treme” was established and already finds application in the first mobile cranes. This strength level is a milestone in the development of TM processed structural steels, with regard to the defined carbon content.

---

## 5 References

1. Klein, M., Rauch, R., Spindler, H., and Stiaszny, P. (2012) Ultra High Strength Steels Produced by Thermomechanical Hot Rolling–Advanced Properties and Applications. *BHM Berg- Hüttenmänn. Monatshefte*, 157 (3), 108–112.
2. Babcock, W.R., and Wilcox (1995) A review of Steels: Metallurgy and Applications by D.T.Llewellyn. *Mater. Manuf. Process.*, 10 (2), 330–331.
3. Gladman, T. (1997) *The physical metallurgy of microalloyed steels*, Institute of Materials, London, England, UK.
4. Krauss, G. (2005) *Steels: Processing, Structure, and Performance*, ASM International, Ohio, USA.
5. DeArdo, A.J., Hua, M.J., Cho, K.G., and Garcia, C.I. (2009) On strength of microalloyed steels: an interpretive review. *Mater. Sci. Technol.*, 25 (9), 1074–1082.
6. Totten, G.E. (2006) *Steel heat treatment: metallurgy and technologies*, CRC Press, Portland, Oregon, USA.
7. Bargel, H.J., and Schulze, G. (1987) *Werkstoffkunde*, Springer-Verlag, Berlin, Heidelberg, Germany.
8. Llewellyn, D.T., and Hudd, R.C. (1998) *Steels: metallurgy and applications*, Butterworth-Heinemann, Oxford, England; Woburn, MA, USA.
9. Klein, M., Spindler, H., Luger, A., Rauch, R., Stiaszny, P., and Eigelsberger, M. (2005) Thermomechanically Hot Rolled High and Ultra High Strength Steel Grades – Processing, Properties and Application. *Mater. Sci. Forum*, 500–501, 543–550.
10. Sonnleitner, M., Klein, M., Spindler, H., Stiaszny, P., and Spiradek-Hahn, K. (2008) Exceeding the limits of TM-rolled hot strip steel by transformation hardening on the runout table. *3rd Int. Conf. Thermomechanical Process. Steels*, 1–11. Padua, Italy
11. Tamura, I. (ed.) (1988) *Thermomechanical processing of high-strength low-alloy steels*, Butterworths, London, UK.
12. Hensger, K.E., and Bernštejn, M.L. (1984) *Thermomechanische Veredlung von Stahl*, VEB Deutscher Verlag für Grundstoffindustrie, Leipzig, DDR.
13. Gottstein, G. (2007) *Physikalische Grundlagen der Materialkunde*, Springer-Verlag, Berlin, Germany.
14. Grong, O., and Matlock, D.K. (1986) Microstructural development in mild and low-alloy steel weld metals. *Int. Met. Rev.*, 31 (1), 27–48.
15. Schnitzer, R., Zügner, D., Haslberger, P., Ernst, W., and Kozeschnik, E. (2017) Influence of alloying elements on the mechanical properties of high-strength weld metal. *Sci. Technol. Weld. Join.*, 22 (6), 536–543.
16. Abson, D.J., and Pargeter, R.J. (1986) Factors influencing as-deposited strength, microstructure, and toughness of manual metal arc welds suitable for C-Mn steel fabrications. *Int. Met. Rev.*, 31 (1), 141–196.
17. Bhadeshia, H., and Honeycombe, R. (2017) Chapter 10 - Thermomechanical Treatment of Steels, in *Steels: Microstructure and Properties (Fourth Edition)* (eds. Bhadeshia, H., and Honeycombe, R.), Butterworth-Heinemann, Oxford, UK, pp. 271–301.
18. Kozasu, I. (1992) Processing - Thermomechanical Controlled Processing, Pickering F.B., Ed., in *Constitution and Properties of Steels*, vol. 7, VCH, Weinheim, Germany, pp. 183–217.
19. Cohen, M., and Hansen, S.S. (1979) Microstructural control in microalloyed steels, in *MiCon 78: Optimization of Processing, Properties, and Service Performance Through Microstructural Control*, ASTM International.
20. Bramfitt, B.L., and Marder, A.R. (1973) Processing and Properties of Low Carbon Steel. JM Gray, Ed. *Met Soc AIME*, 191–224.

21. DeArdo, A.J. (2001) Metallurgical basis for thermomechanical processing of microalloyed steels. *Ironmak. Steelmak.*, 28 (2), 138–144.
22. DeArdo, A.J. (1998) Microalloyed strip steels for the 21st century. *Mater. Sci. Forum*, 284, 15–26.
23. Stroetmann, R. (2017) Nachhaltigkeit und ressourceneffizienter Einsatz höherfester Stähle, Vortrag: iforum Nachhaltigkeit: Lösungen für ressourceneffizientes Planen und Bauen, TU Dresden, Dresden, Germany.
24. Vanderbeck, R.W. (1958) Controlled Low-Temperature Hot Rolling as Practiced in Europe. *Weld. J.*, 37 (3), 114–116.
25. Tanaka, T. (1981) Controlled rolling of steel plate and strip. *Int. Met. Rev.*, 26 (1), 185–212.
26. Bakkaloğlu, A. (2002) Effect of processing parameters on the microstructure and properties of an Nb microalloyed steel. *Mater. Lett.*, 56 (3), 263–272.
27. Kaijalainen, A.J., Liimatainen, M., Kesti, V., Heikkala, J., Liimatainen, T., and Porter, D.A. (2016) Influence of Composition and Hot Rolling on the Subsurface Microstructure and Bendability of Ultrahigh-Strength Strip. *Metall. Mater. Trans. A*, 47 (8), 4175–4188.
28. Morrison, W.B. (2009) Microalloy steels – the beginning. *Mater. Sci. Technol.*, 25 (9), 1066–1073.
29. Bhadeshia, H., and Honeycombe, R. (2017) Chapter 9 - Tempering of Martensite, in *Steels: Microstructure and Properties*, Butterworth-Heinemann, Oxford, UK, pp. 237–270.
30. Graville, B. (1976) Cold cracking in welds in HSLA steels. *Weld. HSLA Microalloyed Struct. Steel ASM*, 85–101.
31. Maekawa, K., Shirakashi, T., and Usui, E. (1983) Flow stress of low carbon steel at high temperature and strain rate (Part 2) - flow stress under variable temperature and variable strain rate. *Bull. Jpn. Soc. Precis. Eng.*, 17, 167–172.
32. Hatta, N., Kokado, J., Kikuchi, S., and Takuda, H. (1985) Modelling on flow stress of plain carbon steel at elevated temperatures. *Steel Res. Int.*, 56 (11), 575–582.
33. Kaijalainen, A., Pallaspuuro, S., and Porter, D.A. (2014) Tempering of Direct Quenched Low-Alloy Ultra-High-Strength Steel, Part I – Microstructure. *Adv. Mater. Res.*, 922, 316–321.
34. Pallaspuuro, S., Kaijalainen, A., Limnell, T., and Porter, D.A. (2014) Tempering of Direct Quenched Low-Alloy Ultra-High-Strength Steel, Part II – Mechanical Properties. *Adv. Mater. Res.*, 922, 580–585.
35. ASM International, Handbook Committee (1991) *ASM handbook: Heat treating*, ASM International, Materials Park, Ohio, USA.
36. Sakuma, Y., Matsumura, O., and Takechi, H. (1991) Mechanical properties and retained austenite in intercritically heat-treated bainite-transformed steel and their variation with Si and Mn additions. *Metall. Trans. A*, 22 (2), 489–498.
37. Liu, S.K., and Zhang, J. (1990) The influence of the Si and Mn concentrations on the kinetics of the bainite transformation in Fe-C-Si-Mn alloys. *Metall. Trans. A*, 21 (6), 1517–1525.
38. Nussbaum, G. (2002) Strukturbildungsprozesse und Struktur/ Eigenschafts-Relationen in mikrolegierten Schmiedestählen nach thermomechanischer Behandlung mit variierenden Abkühlkonzepten, PhD Thesis, RWTH Aachen, Aachen, Germany.
39. Homsher, C.N. (2013) Determination of the Non-recrystallization Temperature (TNR) in Multiple Microalloyed Steels, PhD Thesis, Colorado School of Mines, Colorado, USA.
40. Cuddy, L.J. (1981) The effect of microalloy concentration on the recrystallization of austenite during hot deformation. *Thermomechanical Process. Microalloyed Austenite*, 129–140. Warrendale, PA, USA
41. Cuddy, L.J., and Raley, J.C. (1983) Austenite grain coarsening in microalloyed steels. *Metall. Trans. A*, 14 (10), 1989–1995.

42. Adrian, H., and Pickering, F.B. (1991) Effect of titanium additions on austenite grain growth kinetics of medium carbon V–Nb steels containing 0.008–0.018%N. *Mater. Sci. Technol.*, 7 (2), 176–182.
43. Gladman, T. (1999) Precipitation hardening in metals. *Mater. Sci. Technol.*, 15 (1), 30–36.
44. Haslberger, P., Holly, S., Ernst, W., and Schnitzer, R. (2018) Precipitates in microalloyed ultra-high strength weld metal studied by atom probe tomography. *Weld. World*, 62 (4), 713–719.
45. Speer, J.G., and Hansen, S.S. (1989) Austenite recrystallization and carbonitride precipitation in niobium microalloyed steels. *Metall. Trans. A*, 20 (1), 25–38.
46. Dutta, B., and Sellars, C.M. (1987) Effect of composition and process variables on Nb (C, N) precipitation in niobium microalloyed austenite. *Mater. Sci. Technol.*, 3 (3), 197–206.
47. Dutta, B., and Sellars, C.M. (1986) Strengthening of austenite by niobium during hot rolling of Microalloyed steel. *Mater. Sci. Technol.*, 2 (2), 146–153.
48. Palmiere, E.J, Garcia, C.I., and DeArdo, A.J (1992) Static Recrystallization and Precipitation During the Hot Deformation of Austenite. *Process. Microstruct. Prop. Microalloyed Mod. High Strength Low Alloy Steels*, 113–143.
49. Esterl, R., Sonnleitner, M., and Schnitzer, R. (2019) Influence of Thermomechanical Treatment and Nb Micro-Alloying on the Hardenability of Ultra-High Strength Steels. in prod. *Metall. Mater. Trans. A*.
50. Esterl, R., Sonnleitner, M., Gschöpf, B., and Schnitzer, R. (2019) Influence of V and Nb Micro-Alloying on Direct Quenched and Tempered Ultra-High Strength Steels. in prod. *Steel Res. Int.*
51. Lagneborg, R., Siwecki, T., Zajac, S., and Hutchinson, B. (1999) The role of vanadium in microalloyed steels. *Scand JMet.*, 28 (5), 186–241.
52. Glodowski, R.J (2005) A review of vanadium microalloying in hot rolled steel sheet products. *Appl. Technol. Vanadium Flat-Roll. Steels – Vanitec Symp. Suzhou China*, 43–51.
53. Kozasu, I., Ouchi, C., Sampei, T., and Okita, T. (1977) Hot rolling as a high-temperature thermo-mechanical process. *Proc Conf Microalloying 75 1977 120-125*, 120–135.
54. Lagneborg, R., Roberts, W., Sandberg, A., and Siwecki, T. (1981) Influence of processing route and nitrogen content on microstructure development and precipitation hardening in V microalloyed HSLA-steels. *Proc Conf Thermomechanical Process. Microalloyed Austenite*, 163 – 194. Pittsburgh, PA, USA
55. Siwecki, T., Hutchinson, B., and Zajac, S. (1995) Recrystallization controlled rolling of HSLA steels. *Proc. Int. Conf.*, 197–211.
56. Gündüz, S., and Cochrane, R.C. (2005) Influence of cooling rate and tempering on precipitation and hardness of vanadium microalloyed steel. *Mater. Des.*, 26 (6), 486–492.
57. Shams, N. (1985) Austenite grain coarsening in low–carbon manganese steels containing niobium and aluminium. *Mater. Sci. Technol.*, 1 (11), 950–953.
58. Matlock, D.K., and Speer, J.G. (2009) Microalloying concepts and application in long products. *Mater. Sci. Technol.*, 25 (9), 1118–1125.
59. Jo, M.S., Suh, D.W., and Bhadeshia, H.K.D.H. (2013) Mechanical Anisotropy in Steels for Pipelines. *ISIJInt.*, 53 (8), 1305–1314.
60. Imai, T., Nishida, Y., and Kogiso, S. (1982) Anisotropy of the charpy impact value of carbon steels and corrective heat treatment. *J Mech. Work. Technol.*, 7 (2), 147–161.
61. Jo, M.S., Suh, D. –W., Bae, J.H., Sanchez Mouriño, N., Petrov, R., Kestens, L.A.I., and Bhadeshia, H.K.D.H. (2012) Experiments to separate the effect of texture on anisotropy of pipeline steel. *Mater. Sci. Eng. A*, 556, 601–606.
62. Zong, C., Zhu, G., and Mao, W. (2013) Effect of crystallographic texture on the anisotropy of Charpy impact behavior in pipeline steel. *Mater. Sci. Eng. A*, 563, 1–7.

63. Kaijalainen, A.J., Suikkanen, P., Karjalainen, L.P., and Jonas, J.J. (2014) Effect of Austenite Pancaking on the Microstructure, Texture, and Bendability of an Ultrahigh-Strength Strip Steel. *Metall. Mater. Trans. A*, 45 (3), 1273–1283.
64. Kaijalainen, A., Vähäkuopus, N., Somani, M., Mehtonen, S., Porter, D., and Kömi, J. (2017) The Effects of Finish Rolling Temperature and Niobium Microalloying on the Microstructure and Properties of a Direct Quenched High-Strength Steel. *Arch. Metall. Mater.*, 62 (2), 619–626.
65. Kaijalainen, A.J., Suikkanen, P.P., Linnell, T.J., Karjalainen, L.P., Kömi, J.I., and Porter, D.A. (2013) Effect of austenite grain structure on the strength and toughness of direct-quenched martensite. *J Alloys Compd.*, 577, 642–648.
66. Kaijalainen, A.J., Suikkanen, P.P., Karjalainen, L.P., and Porter, D.A. (2016) Influence of subsurface microstructure on the bendability of ultrahigh-strength strip steel. *Mater. Sci. Eng. A*, 654, 151–160.
67. Jo, M.S., Suh, D.-W., Bae, J.H., and Bhadeshia, H.K.D.H. (2012) Role of delamination and crystallography on anisotropy of Charpy toughness in API-X80 steel. *Mater. Sci. Eng. A*, 546, 314–322.
68. Odesskii, P.D. (1969) Anisotropy of the mechanical properties of high-strength steels for metal structures. *Met. Sci. Heat Treat.*, 11 (5), 357–361.
69. Tomita, Y. (1993) Improved fracture toughness of ultrahigh strength steel through control of non-metallic inclusions. *J Mater. Sci.*, 28 (4), 853–859.
70. Baker, T.J., and Charles, J. (1972) Deformation of MnS inclusions in steel. *J Iron Steel Inst*, 210 (9), 680–690.
71. Baker, T.J., and Charles, J. (1973) Type II Manganese Sulphides--Their Deformation and Effect on Steel Fracture. *J Iron Steel Inst.*, 211 (3), 187–192.
72. Hodge, J.M., Frazier, R.H., and Boulger, F.W. (1959) The effects of sulfur on the notch toughness of heat-treated steels. *Trans. Am. Inst. Min. Metall. Eng.*, 215 (5), 745–753.
73. Baker, T.J., Kavishe, F.P.L., and Wilson, J. (1986) Effect of non-metallic inclusions on cleavage fracture. *Mater. Sci. Technol.*, 2 (6), 576–582.
74. Tomita, Y. (1990) Fracture toughness of calcium-modified ultrahigh-strength 4340 steel. *Metall. Trans. A*, 21 (10), 2739–2746.
75. Thornton, P.A. (1971) The influence of nonmetallic inclusions on the mechanical properties of steel: A review. *J Mater. Sci.*, 6 (4), 347–356.
76. Matrosov, Yu.I., and Polyakov, I.E. (1976) Viscosity and plasticity rise and reduction of anisotropy of low-alloy steel properties. *Stal'*, (2), 162–167.
77. Jarczok, C.F., Girardi, D.J., and Rowland, E.S. (1956) On banding in steel. *Trans ASM*, 48, 279–305.
78. Almond, E.A. (1970) Delamination in banded steels. *Metall. Trans.*, 1 (7), 2038–2041.
79. Bourell, D.L. (1983) Cleavage delamination in impact tested warm-rolled steel. *Metall. Trans. A*, 14 (12), 2487–2496.
80. Mintz, B., Morrison, W.B., Morris, P.P., and Davies, G.J. (1976) The influence of texture on the tensile and impact properties of controlled steels, in *Texture and Properties of Materials*, edit. by Davies G.J., The Metal Society, London, UK, pp. 224–234.
81. Pyshmintsev, I., Gervasyev, A., Petrov, R., Carretero Olalla, V., and A.I. Kestens, L. (2011) Crystallographic Texture as a Factor Enabling Ductile Fracture Arrest in High Strength Pipeline Steel. *Mater. Sci. Forum*, 702–703, 770–773.
82. Fegredo, D.M., Faucher, B., and Shehata, M.T. (1985) Influence of inclusion content, texture and microstructure on the toughness anisotropy of low carbon steels, in *Strength of Metals and Alloys*, vol. 2, Pergamon Press, Oxford, UK, pp. 1127–1132.

- 
83. Petrov, R.H., García, O.L., Mulders, J.J.L., Reis, A.C.C., Bae, J.H., Kestens, L., and Houbaert, Y. (2007) Three Dimensional Microstructure–Microtexture Characterization of Pipeline Steel. *Mater. Sci. Forum*, 550, 625–630.
  84. Petrov, R.H., García, O.L., Mourino, N.S., Kestens, L.A.I., Bae, J.H., and Kang, K.B. (2007) Microstructure-texture related toughness anisotropy of API-X80 pipeline steel characterized by means of 3D-EBSD technique. *Mater. Sci. Forum*, (558–559), 1429–1434.
  85. Ray, R.K., Jonas, J.J., Butrón-Guillén, M.P., and Savoie, J. (1994) Transformation Textures in Steels. *ISIJ Int.*, 34 (12), 927–942.
  86. Scholl, S. (2014) Einflussfaktoren auf das Spröbruchverhalten im Fallgewichtsversuch, PhD Thesis, RWTH Aachen, Aachen, Germany.
  87. Inagaki, H. (1988) Fractographic Study of the Formation of the Separation in a Control-Rolled, Low Carbon Nb Steel. *Z. Für Met.*, 79 (6), 364–374.
  88. Sonnleitner, M., and Kolednik, O. (2012) Effect of delaminations in Charpy specimens on impact energy in thermomechanically rolled hot strip steel. *TMP 2012 - 4th Int. Conf. Thermomechanical Process. Steels*. Sheffield, UK
  89. Morrison, W.B. (1975) Influence of testing direction on the mechanical properties of wrought steel. *Met. Technol.*, 2 (1), 33–41.
  90. Bramfitt, B.L., and Marder, A.R. (1977) A study of the delamination behavior of a very low-carbon steel. *Metall. Trans. A*, 8 (8), 1263–1273.
  91. Hawkins, D.N. (1976) Cleavage separations in warm-rolled lowcarbon steels. *Met. Technol.*, 3 (1), 417–421.
  92. Dabkowski, S.D., Konkol, P.J., and Baldy, M.F. (1976) "Splitting-Type" Fractures in High-Strength Line-Pipe Steels. *Met Eng Q*, 16 (1), 22–32.
  93. Herø, H., Evensen, J., and Embury, J.D. (1975) The occurrence of delamination in a control rolled HSLA steel. *Can. Metall. Q.*, 14 (2), 117–122.
  94. Kozasu, I., and Kubota, H. (1971) Effect of elongated sulfide inclusions of ductility and ductile fracture of structural steel. *Trans Iron Steel Inst Jpn*, 11 (5), 321–330.
  95. Bramfitt, B.L., and Marder, A.R. (1973) The influence of microstructure and crystallographic texture on the strength and notch toughness of a low-carbon steel. *Process. Prop. Low Carbon Steels'ed JM Gray*, 191–224.
  96. Coleman, T., Dulieu, D., and Gouch, A. (1973) The microstructure and design of alloys. *Proc 3rd ICSMA Met. Soc. Lond.*, 1, 70.
  97. Schofield, R., Rowntree, G., Sarma, N.V., and Weiner, R.T. (1974) 'Arrowhead'fractures in controlled-rolled pipeline steels. *Met. Technol.*, 1 (1), 325–331.
  98. Hawkins, D.N. (1978) Effect of warm working on structure and properties of low-carbon steels. *Met. Technol.*, 5 (1), 37–44.
  99. Iino, M., Mimura, H., and Nomura, N. (1977) Delamination in Linepipe Steels. *Trans Iron Steel Inst Jpn*, 17 (8), 450–458.
  100. Iino, M. (1978) The Estimation of the Delamination Effect on Impact Toughness of Steel. *Trans Iron Steel Inst Jpn*, 18 (6), 339–343.
  101. Miyoshi, E., Tanaka, T., Fukuda, M., Iwanga, H., and Okazawa, T. (1976) Propagating Shear Fracture Test of Large Diameter Gas Transmission Line Pipes for Arctic Grade. *Tetsu--Hagane*, 62 (6), 688–695.
  102. Miyoshi, E., Fukuda, M., Iwanga, H., and Okazawa, T. (1974) The Effect of Separation on the Propagating Shear Fracture. *Crack Propag. Pipelines*.

- 
103. Haskel, H.L., Pauletti, E., Martins, J de P., and Carvalho, A.L.M. de (2014) Microstructure and microtexture assessment of delamination phenomena in Charpy impact tested specimens. *Mater. Res.*, 17 (5), 1238–1250.
  104. Yang, X.-L., Xu, Y.-B., Tan, X.-D., and Wu, D. (2015) Relationships among crystallographic texture, fracture behavior and Charpy impact toughness in API X100 pipeline steel. *Mater. Sci. Eng. A*, 641, 96–106.
  105. Yang, X.-L., Xu, Y.-B., Tan, X.-D., and Wu, D. (2014) Influences of crystallography and delamination on anisotropy of Charpy impact toughness in API X100 pipeline steel. *Mater. Sci. Eng. A*, 607, 53–62.
  106. Clegg, W.J., Kendall, K., Alford, N.McN., Button, T.W., and Birchall, J.D. (1990) A simple way to make tough ceramics. *Nature*, 347 (6292), 455–457.
  107. Sakai, M., Bradt, R.C., and Fischbach, D.B. (1986) Fracture toughness anisotropy of a pyrolytic carbon. *J Mater. Sci.*, 21 (5), 1491–1501.
  108. Kimura, Y., Inoue, T., Yin, F., and Tsuzaki, K. (2008) Inverse Temperature Dependence of Toughness in an Ultrafine Grain-Structure Steel. *Science*, 320 (5879), 1057–1060.
  109. Kimura, Y., Inoue, T., Yin, F., and Tsuzaki, K. (2010) Delamination Toughening of Ultrafine Grain Structure Steels Processed through Tempforming at Elevated Temperatures. *ISIJInt.*, 50 (1), 152–161.
  110. Inoue, T., Yin, F., Kimura, Y., Tsuzaki, K., and Ochiai, S. (2009) Delamination Effect on Impact Properties of Ultrafine-Grained Low-Carbon Steel Processed by Warm Caliber Rolling. *Metall. Mater. Trans. A*, 41 (2), 341.
  111. Mintz, B., Maina, E., and Morrison, W.B. (2007) Origin of fissures on fracture surfaces of impact samples of HSLA steels with ferrite/ pearlite microstructures. *Mater. Sci. Technol.*, 23 (3), 347–354.
  112. Jafari, M., Kimura, Y., and Tsuzaki, K. (2012) Enhanced upper shelf energy by ultrafine elongated grain structures in 1100MPa high strength steel. *Mater. Sci. Eng. A*, 532, 420–429.
  113. Morito, S., Tanaka, H., Konishi, R., Furuhashi, T., and Maki, T. (2003) The morphology and crystallography of lath martensite in Fe-C alloys. *Acta Mater.*, 51 (6), 1789–1799.
  114. Morito, S., Yoshida, H., Maki, T., and Huang, X. (2006) Effect of block size on the strength of lath martensite in low carbon steels. *Mater. Sci. Eng. A*, 438–440, 237–240.
  115. Morito, S., Huang, X., Furuhashi, T., Maki, T., and Hansen, N. (2006) The morphology and crystallography of lath martensite in alloy steels. *Acta Mater.*, 54 (19), 5323–5331.
  116. Esterl, R., Sonnleitner, M., Stadler, M., Wölger, G., and Schnitzer, R. (2018) Microstructural Characterization of Ultra-High Strength Martensitic Steels. *Pract. Metallogr.*, 55 (4), 203–222.
  117. Vander Voort, G.F. (2010) Revealing Prior-Austenite Grain Boundaries in Heat Treated Steels. *Ind. Heat.*, 78, 48–52.
  118. S. Bechet and L. Beaujard (1955) New Reagent for the Micrographical Demonstration of the Austenite Grain of Hardened or Hardened-Tempered Steels. *Rev Met*, 52, 830–836.
  119. Brownrigg, A., Curcio, P., and Boelen, R. (1975) Etching of prior austenite grain boundaries in martensite. *Metallography*, 8 (6), 529–533.
  120. Brownrigg, A. (1973) The effect of austenite grain size on the strength of low carbon martensite. *Scr. Metall.*, 7 (11), 1139–1142.
  121. Barraclough, D.R. (1973) Etching of prior austenite grain boundaries in martensite. *Metallography*, 6 (6), 465–472.
  122. Cayron, C. (2007) ARPGE: a computer program to automatically reconstruct the parent grains from electron backscatter diffraction data. *J Appl. Crystallogr.*, 40 (6), 1183–1188.



123. Cayron, C., Artaud, B., and Briottet, L. (2006) Reconstruction of parent grains from EBSD data. *Mater. Charact.*, 57 (4–5), 386–401.
124. Cayron, C. (2008) GenOVA: A computer program to generate orientational variants. *J Appl. Crystallogr.*, 40, 1179–1182.
125. Cayron, C. (2014) EBSD imaging of orientation relationships and variant groupings in different martensitic alloys and Widmanstätten iron meteorites. *Mater. Charact.*, 94, 93–110.
126. Weyand, S., Britz, D., Rupp, D., and Mücklich, F. (2015) Investigation of Austenite Evolution in Low-Carbon Steel by Combining Thermo-Mechanical Simulation and EBSD Data. *Mater. Perform. Charact.*, 4 (3), MPC20150010.
127. Haslberger, P., Holly, S., Ernst, W., and Schnitzer, R. (2017) Microstructural Characterization of Martensitic All-Weld Metal Samples. *Pract. Metallogr.*, 54 (8), 513–532.
128. Haslberger, P., Holly, S., Ernst, W., and Schnitzer, R. (2018) Microstructure and mechanical properties of high-strength steel welding consumables with a minimum yield strength of 1100 MPa. *J Mater. Sci.*, 53 (9), 6968–6979.
129. Haslberger, P. (2018) Microstructure-property relationships of a novel metal-cored wire for welding of ultra-high strength steels, PhD Thesis, Montanuniversität Leoben, Austria.
130. Sosa, J.M., Huber, D.E., Welk, B., and Fraser, H.L. (2014) Development and application of MIPAR™: a novel software package for two- and three-dimensional microstructural characterization. *Integrating Mater. Manuf. Innov.*, 3 (1), 10.
131. Lin, Y.C., Chen, M.-S., and Zhong, J. (2009) Study of metadynamic recrystallization behaviors in a low alloy steel. *J Mater. Process. Technol.*, 209 (5), 2477–2482.
132. Lin, Y.C., and Chen, M.-S. (2009) Study of microstructural evolution during metadynamic recrystallization in a low-alloy steel. *Mater. Sci. Eng. A*, 501 (1–2), 229–234.
133. Morgridge, A.R. (2002) Metadynamic recrystallization in C steels. *Bull. Mater. Sci.*, 25 (4), 291–299.
134. Sun, W.P., and Hawbolt, E.B. (1997) Comparison between Static and Metadynamic Recrystallization-An Application to the Hot Rolling of Steels. *ISIJInt.*, 37 (10), 1000–1009.
135. Zahiri, S.H., and Hodgson, P.D. (2004) The static, dynamic and metadynamic recrystallisation of a medium carbon steel. *Mater. Sci. Technol.*, 20 (4), 458–464.
136. Medina, S.F., and Fabregue, P. (1991) Activation energy in the static recrystallization of austenite. *J Mater. Sci.*, 26 (20), 5427–5432.
137. Medina, S.F., and Hernandez, C.A. (1996) Modelling of the dynamic recrystallization of austenite in low alloy and microalloyed steels. *Acta Mater.*, 44 (1), 165–171.
138. Medina, S.F., and Quispe, A. (2001) Improved Model for Static Recrystallization Kinetics of Hot Deformed Austenite in Low Alloy and Nb/ V Microalloyed Steels. *ISIJInt.*, 41 (7), 774–781.
139. Andrade, H.L., Akben, M.G., and Jonas, J.J. (1983) Effect of molybdenum, niobium, and vanadium on static recovery and recrystallization and on solute strengthening in microalloyed steels. *Metall. Trans. A*, 14 (10), 1967–1977.
140. Humphreys, F.J., and Hatherly, M. (1995) *Recrystallization and related annealing phenomena*, Pergamon, Oxford, UK; Tarrytown, N.Y., U.S.A.
141. Medina, S.F., and Mancilla, J.E. (1993) Determination of Static Recrystallization Critical Temperature of Austenite in Microalloyed Steels. *ISIJInt.*, 33 (12), 1257–1264.
142. Esterl, R., Sonnleitner, M., and Schnitzer, R. (2019) Microstructural Analysis of the Recrystallization Behavior of Low Alloyed Steels. *Steel Res. Int.*, 90 (3), 382–391.
143. Vervynckt, S., Verbeken, K., Lopez, B., and Jonas, J.J. (2012) Modern HSLA steels and role of non-recrystallisation temperature. *Int. Mater. Rev.*, 57 (4), 187–207.

- 
144. Medina, S.F. (1998) Determination of no-recrystallisation temperature in Nb-V-Ti microalloyed steel and discussion of its definition. *Mater. Sci. Technol.*, 14 (3), 217–221.
  145. Lin, Y.C., Chen, M.-S., and Zhong, J (2008) Study of static recrystallization kinetics in a low alloy steel. *Comput. Mater. Sci.*, 44 (2), 316–321.
  146. Huang, K., and Logé, R.E. (2016) A review of dynamic recrystallization phenomena in metallic materials. *Mater. Des.*, 111, 548–574.
  147. Jonas, J.J., Sellars, C.M., and Tegart, W.J.M. (1969) Strength and structure under hot-working conditions. *Metall. Rev.*, 14 (1), 1–24.
  148. Sellars, C.M. (1990) Modelling microstructural development during hot rolling. *Mater. Sci. Technol.*, 6 (11), 1072–1081.
  149. Mirzadeh, H., Cabrera, J.M., Prado, J.M., and Najafizadeh, A. (2011) Hot deformation behavior of a medium carbon microalloyed steel. *Mater. Sci. Eng. A*, 528 (10–11), 3876–3882.
  150. Ryan, N.D., and McQueen, H.J (1990) Flow stress, dynamic restoration, strain hardening and ductility in hot working of 316 steel. *J Mater. Process. Technol.*, 21, 177–199.
  151. Roberts, W., and Ahlblom, B. (1978) A nucleation criterion for dynamic recrystallization during hot working. *Acta Metall.*, 26 (5), 801–813.
  152. Grange, R.A., Hribal, C.R., and Porter, L.F. (1977) Hardness of tempered martensite in carbon and low-alloy steels. *Metall. Trans. A*, 8 (11), 1775–1785.
  153. Bhadeshia, H., and Honeycombe, R. (2017) Chapter 4 - Solutes that Substitute for Iron, in *Steels: Microstructure and Properties*, Butterworth-Heinemann, Oxford, UK, pp. 101–134.
  154. Brooks, C.R. (1996) *Principles of the Heat Treatment of Plain Carbon and Low Alloy Steels*, ASM International, Materials Park, OH, USA.
  155. Bachmann, F., Hielscher, R., and Schaeben, H. (2010) Texture Analysis with MTEX, a Free and Open Source Software Toolbox. *Texture Anisotropy Polycrystals III*, 160, 63–68.
  156. Suwas, S., and Ray, R.K. (2014) *Crystallographic Texture of Materials*, Springer, London, UK.
  157. Esterl, R., Sonnleitner, M., Weißensteiner, I., Hartl, K., and Schnitzer, R. (2019) Influence of quenching conditions on texture and mechanical properties of ultra-high strength steels. *Submitt. J Mater. Sci.*
  158. Courbon, J., Lormand, G., Dudragne, G., Daguier, P., and Vincent, A. (2003) Influence of inclusion pairs, clusters and stringers on the lower bound of the endurance limit of bearing steels. *Tribol. Int.*, 36 (12), 921–928.
  159. Kaijalainen, A., Karjalainen, P., Porter, D., Suikkanen, P., Kömi, J, Kesti, V., and Saarinen, T. (2012) Effect of Inclusions on the Properties of Ultra-high-strength Low-alloy Steel with a Martensitic-bainitic Microstructure. *Proc 8th Int Conf Clean Steel*, 10.
  160. Shanmugam, P., and Pathak, S.D. (1996) Some studies on the impact behavior of banded microalloyed steel. *Eng. Fract. Mech.*, 53 (6), 991–1005.

## Part B

## Paper I

Esterl R, Sonnleitner M, Stadler M, Wölger G, Schnitzer R (2018)

*Microstructural Characterization of Ultra-High Strength Martensitic Steels*

Practical Metallography 55 (2018) 4: 203 - 222

DOI: 10.3139/ 147.110491

R. Esterl, M. Sonnleitner, M. Stadler, G. Wölger, R. Schnitzer

# Microstructural Characterization of Ultra-High Strength Martensitic Steels

## Mikrostrukturelle Charakterisierung von ultrahochfesten martensitischen Stählen

Received: November 15, 2017

Accepted: January 09, 2018

Eingegangen: 15. November 2017

Angenommen: 09. Januar 2018

Übersetzung: V. Müller

### Abstract

In the development of steels with increasing strength and toughness, ultra-high strength steel grades with a martensitic microstructure are gaining more importance. From the martensitic transformation product, however, strength-specific quantities derived from the former austenite grain cannot be accessed conveniently. A profound analysis of the prior austenite microstructure, its size distribution and aspect ratio is essential in order to allow conclusions on the mechanical properties. This paper presents an etchant to reveal the prior austenite grains of thermomechanical processed and press hardened martensitic steels. Furthermore, alternative detecting methods such as electron backscatter diffraction (EBSD) and high-temperature laser scanning confocal microscopy were evaluated. It was found that a picric-acid etchant in combination with a prior tempering treatment of the steel

### Kurzfassung

Bei der Entwicklung von Stählen mit zunehmender Festigkeit und Zähigkeit erlangen ultrahochfeste Stahlsorten mit martensitischer Mikrostruktur immer größere Bedeutung. Festigkeitsspezifische Eigenschaften, die sich hauptsächlich auf das vormalige Austenitkorn beziehen, sind jedoch vom vorliegenden martensitischen Umwandlungsprodukt nicht unmittelbar zu entnehmen. Eine fundierte Analyse der vorherigen austenitischen Mikrostruktur, ihrer Größenverteilung und ihres Seitenverhältnisses ist grundlegend, um Schlussfolgerungen bezüglich der mechanischen Eigenschaften zu ziehen. Diese Arbeit stellt ein Ätzmittel vor, welches die ursprünglichen Austenitkörner von thermomechanisch behandelten und pressgehärteten martensitischen Stählen sichtbar macht. Weiterhin werden Nachweisverfahren, wie Elektronenrückstreuung (EBSD) und Hochtemperatur-Laser-Scanning-Mikroskopie, bewertet. Es stellte sich heraus, dass ein Pikrin-

### Authors:

**Raphael Esterl, Manfred Stadler, Günter Wölger, Ronald Schnitzer** Department of Physical Metallurgy and Materials Testing, Montanuniversität Leoben, Franz Josef-Str. 18, 8700 Leoben, Austria

**Markus Sonnleitner** voestalpine Stahl GmbH, voestalpine-Straße 1, 4020 Linz, Austria

enables the visualization of prior austenite grains and their elongation in a micrometer-scale.

säure-Ätzmittel zusammen mit einer vorherigen Anlassbehandlung des Stahls das Sichtbarmachen der ursprünglichen Austenitkörner bis zu Größenordnungen weniger Mikrometer, und deren Streckung ermöglicht.

## 1. Introduction

In the last decades, martensitic steel products became increasingly popular. Multiple factors have led to its indispensable need. On the one hand side its demand is stressed

## 1. Einleitung

In den vergangenen Jahrzehnten konnten sich martensitische Stahlprodukte einer immer größer werdenden Beliebtheit erfreuen. Viele Faktoren haben zur absoluten Notwendig-

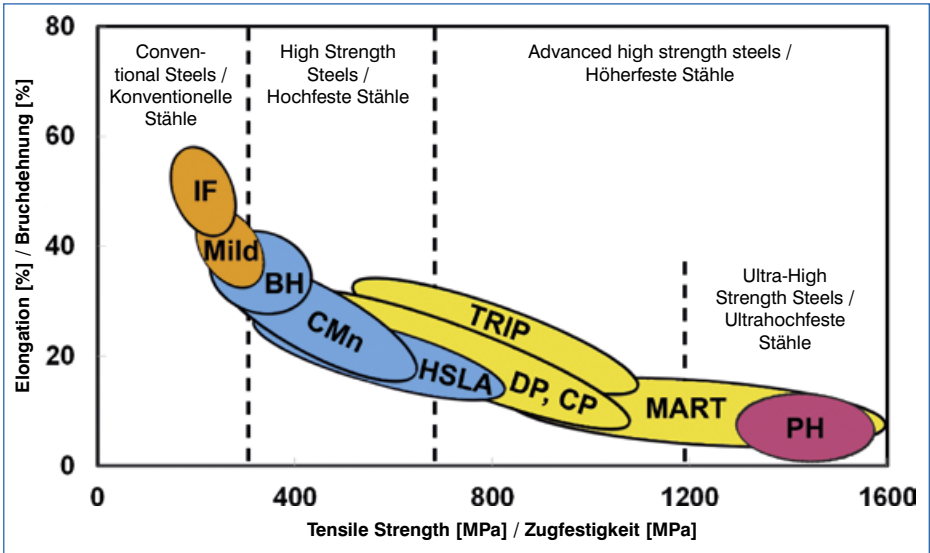


**Fig. 1:** Elongation  $A_m$  vs. tensile strength  $R_m$ , showing ductility-strength combination of several steels. With the conventional steels on the very left side, possessing high elongations and little strength: Interstitial-free (IF) and mild steels. Representatives for high-strength steels are bake-hardening steels (BH), heat-treatable quenched and tempered (Q&T) steels (CMn) and high-strength-low alloyed steels (HSLA). Transformation-induced plasticity steels (TRIP), dual-phase (DP) and complex-phase (CP) steels fill in for the advanced-high-strength steels (AHSS), closing up with martensitic and press-hardening (PH) steels as representative for the ultra-high-strength steel (UHSS) group possessing highest strength and reduced elongations.

**Bild 1:** Streckung  $A_m$  vs. Zugfestigkeit  $R_m$ , Darstellung von Zähigkeits-Festigkeits-Kombinationen verschiedener Stähle. Konventionelle Stähle ganz links, mit hoher Dehnung und geringer Festigkeit: IF-Stähle (IF) und Baustähle. Vertreter der hochfesten Stähle sind Bake-hardening-Stähle (BH), Vergütungsstähle (Q&T), CMn und hochfeste niedriglegierte Stähle (HSLA). TRIP-Stähle (TRIP), Dualphasenstähle (DP) und Komplexphasenstähle (CP) stellvertretend für AHS-Stähle, und schließlich martensitische und pressgehärtete Stähle (PH) als Vertreter der Gruppe der ultrahochfesten Stähle (UHSS) mit den höchsten Festigkeitswerten und verminderter Bruchdehnung.

through the increasing payload-to-weight ratio for both improved effectiveness and efficiency. On the other side dwindling resources and industrialization require high-strength structural steels with the simultaneous fulfillment of an economic production route [1]. The increase in strength is in immediate connection to a loss of ductility as demonstrated in Fig. 1 by the dependence of elongation on the strength of different steel categories [2]. In the course of development, a higher process purity in secondary metallurgy and advances in alloying and processing route could minimize their susceptibility of brittle fracture [3]. Moreover, an austenite grain refinement offers the simultaneous increase in strength and ductility. Ultra-high strength structural steels (UHSS), which are applied e.g. in mobile crane booms, are produced via thermomechanical processing (TMP) [4]. The combination of grain refinement and austenite pancaking with subsequent immediate quenching (direct quenching = DQ) generates a martensitic steel product with high strength and good ductility [5]. For the automotive sector this strength class can be achieved through press hardening (PH), where austenitized blanks (direct hot stamping) or pre-formed parts (indirect hot stamping) are quenched through a cooled mould. This combination of adjusting shape and microstructure in one step shows an economic benefit in process. The resulting steel product which is fully martensitic provides tensile strength up to 1500 MPa.

To provide insight into the structure-property relationship of these steels, beside the transformed martensitic structure, the prior austenitic microstructure (PAG)

keit dieser Stahlsorten geführt. Der Grund für deren Nachfrage liegt einerseits im sich stetig verbessernden Nutzlast zu Eigengewichtsverhältnis und der damit einhergehenden höheren Effizienz und Wirtschaftlichkeit. Andererseits erfordern schwindende Ressourcen und fortschreitende Industrialisierung hochfeste Baustähle unter gleichzeitiger Realisierung wirtschaftlicher Herstellungsverfahren [1]. Die Steigerung der Festigkeit steht in direktem Zusammenhang mit dem Verlust der Zähigkeit, dies wird in Bild 1 durch die Abhängigkeit der Bruchdehnung von der Festigkeit für verschiedene Stahlsorten dargestellt [2]. In der Entwicklungsgeschichte konnten durch eine höhere Prozessreinheit im Bereich der Sekundärmetallurgie und Fortschritte beim Legieren und bei Verarbeitungsprozessen deren Anfälligkeit für Sprödbrüche gemindert werden [3]. Hinzu kommt, dass eine Feinung des Austenitkorns den gleichzeitigen Anstieg von Festigkeit und Zähigkeit ermöglicht. Ultrahochfeste Baustähle (UHSS), wie sie z.B. in den Auslegern von Mobilkränen Verwendung finden, werden durch thermomechanische Behandlung (TMB) hergestellt [4]. Die Kombination aus Kornfeinung und Pancaking des Austenitkorns mit anschließendem Direkt härten (DQ, direct quenching) liefert einen martensitischen Stahl mit hoher Festigkeit und guten Zähigkeitseigenschaften [5]. Im Automobilsektor kann diese Festigkeitsklasse durch Presshärten (PH, press hardening) erreicht werden, wobei austenitisierte Rohlinge (direkte Warmumformung) oder vorgeformte Teile (indirekte Warmumformung) durch eine gekühlte Pressform abgeschreckt werden. Diese gleichzeitige Formgebung und Einstellung der Mikrostruktur stellt einen wirtschaftlichen Vorteil im Bearbeitungsprozess dar. Das so entstandene Stahlprodukt mit einem vollständig martensitischen Gefüge weist eine Zugfestigkeit von bis zu 1500 MPa auf.

Um einen Einblick in die Struktur-Eigenschaftsbeziehung dieser Stähle zu erhalten, rückt weniger die vorliegende martensitische Gefügestruktur als vielmehr das vormalige

gathers significance. For example, elongated austenite grains as which they are present in TMP steels, show pronounced dependence of mechanical properties on test direction. PH steels can show similar phenomenon through the formation of preferential directions of shear bands at their bend position [6]. In addition, mechanical properties are dependent on grain size. Similar to the acquainted Hall-Petch relation the strength of martensitic steels increases with decreasing packet sizes, which again are dependent on their former austenitic grain size. [7]

The austenite grain on which these different mechanical properties can be referred to, cannot be accessed conveniently. This is the reason why literature often depicts the process to access PAGs of martensitic steels as a demanding procedure [8]. Thus, the focus of the present paper is to show and discuss the practicability of methods to reveal PAGs of UHS steels.

The first method of choice mostly consists of an acidic etching such as Nital or picric acid with subsequent light optical analysis (LOM). As a Nital etchant originally serves to visualize the actual microstructure based on different etching reaction of its structure constituents, this instrument is only relevant in particular cases for the visualization of PAGs. Bechet and Beaujard (BB) presented in 1955 the first successful etchant on basis of picric acid to reveal the remnant austenitic microstructure [9]. Although the proposed etchant has been consistently modified, the basis of the BB etchant is considered as universal tool to reveal PAGs. Since often PAG etchants in combination with classical light-optical methods have limits, advanced high-resolution imaging via electron backscatter diffraction (EBSD) was employed. As it is now ac-

Austenitkorn (PAG, prior austenite grain) in den Vordergrund. Zum Beispiel zeigen die für thermomechanisch gewalzten Stähle typischen getreckten Austenitkörner eine ausgeprägte Richtungsabhängigkeit der mechanischen Eigenschaften auf. Pressgehärtete Stähle können ein ähnliches Phänomen durch die Bildung bevorzugter Scherband-Richtungen in ihrer Biegeposition aufweisen [6]. Daneben hängen die mechanischen Eigenschaften von der Korngröße ab. Ähnlich wie bei der bekannten Hall-Petch-Beziehung steigt die Festigkeit martensitischer Stähle mit abnehmenden Paketgrößen, die wiederum in Abhängigkeit von der Größe der ursprünglichen Austenitkörner stehen [7].

Die Austenitkörner, auf die diese verschiedenen mechanischen Eigenschaften zurückgehen, sind nicht unmittelbar zugänglich. Aus diesem Grund beschreibt selbst die Literatur, die Darstellung von Austenitkörnern von martensitischen Stählen als schweißtreibenden Prozess [8]. Als Schwerpunkt der vorliegenden Arbeit werden daher die unterschiedlichen Methoden zur Sichtbarmachung von PAGs in UHS-Stählen aufgezeigt und bewertet.

Die erste Methode der Wahl ist das Ätzen mit Nital oder Pikrinsäure mit anschließender lichtmikroskopischer Untersuchung (LOM). Da Nital eigentlich dazu dient, die tatsächliche Mikrostruktur durch unterschiedlich ausfallende Ätzangriffe des Ätzmittels auf die einzelnen Gefügebestandteile sichtbar zu machen, ist dieses Verfahren nur in speziellen Fällen zur Sichtbarmachung von PAGs von Bedeutung. Bechet und Beaujard (BB) stellten im Jahr 1955 das erste erfolgreiche Ätzmittel auf Basis von Pikrinsäure zur Sichtbarmachung des ursprünglichen Austenitgefüges vor [9]. Obwohl das seinerzeit vorgestellte Ätzmittel kontinuierlich weiterentwickelt wurde, gilt die Basis des Ätzmittels nach Bechet-Beaujard als Universalmittel zur Sichtbarmachung von PAGs. Da Ätzmittel zur Visualisierung von PAGs in Kombination mit der klassischen Lichtmikroskopie oft an gewisse Grenzen stoßen, wurde das fort-



cepted that martensitic elements including packets, laths and blocks, exhibit a transformation relation to their habitus grain, it is possible to reconstruct a PAG from its transformed product [7, 10–12]. To close the circle of common to advanced optical methods, we also present the applicability of a high-temperature laser scanning confocal microscope (HT-LSCM). Since the formation of martensite occurs out of its austenite grain, reheating to the  $\gamma$ -region will give rise to its former austenite grain, provided, that the martensitic plate is present in an undeformed condition [13, 14]. It is determined if a HT-LSCM possess this accurate resolution in order to capture and visualize the moment of formation of austenite out of martensite.

Finally, the visualization of PAGs of martensitic steels obtained via these different methods for a quantification of grains, their size and orientation in an image analysis is applied. Subsequently, a specific case of application for our established metallographic method is demonstrated to interpret the visualization of grains.

## 2. Steels Investigated and Sample Preparation

The investigations were carried out on different UHS steel samples listed in Tab. 1. "TM-UHSS 1" represents a high strength low alloyed (HSLA) structural steel with additions of recrystallization-retarding elements like V, Nb and Ti. The deformation in a non-recrystallization regime promotes a pancaking of austenite. The steel was subjected to direct quenching after hot rolling. The steel "TM - UHSS 2" has a lower alloy content,

schrittlichere und hochauflösende bildgebende Verfahren der Elektronenrückstreubeugung (EBSD) herangezogen. Da inzwischen allgemein anerkannt ist, dass Modifikationen des Martensits, darunter Pakete, Latten und Blöcke, eine Umwandlungsbeziehung zu ihrem Habituskorn zeigen, ist es möglich, die ursprüngliche austenitische Mikrostruktur ausgehend vom Umwandlungsprodukt zu rekonstruieren [7, 10–12]. Um den Kreis zwischen den üblichen und den fortschrittlicheren optischen Verfahren zu schließen, wird zusätzlich die Anwendbarkeit der Hochtemperatur-Laser-Scanning Mikroskopie (HT-LSCM, high-temperature laser scanning confocal microscopy) vorgestellt. Da sich der Martensit aus dem Austenit bildet, lässt sich durch eine Wiedererwärmung ins  $\gamma$ -Gebiet die Rückbildung der ursprünglichen Austenitkörner erreichen, vorausgesetzt, dass das martensitische Walzprodukt in einem unverformten Zustand vorliegt [13, 14]. Es wird untersucht, ob durch die HT-LSC-Mikroskopie eine geeignete Auflösung erreicht wird, um den Moment der Bildung von Austenit aus Martensit aufzunehmen und darzustellen.

Schließlich wurde, ausgehend von den unterschiedlichen Methoden zur Darstellung von PAGs in martensitischen Stählen, eine Bildanalyse durchgeführt um die Körner bezüglich Korngröße- und Orientierung zu quantifizieren. An einem konkreten Anwendungsfall wird das bewährte Verfahren zur Interpretation der Korngrößenauswertung erprobt.

## 2. Untersuchte Stähle und Proben-vorbereitung

Die Untersuchungen wurden an verschiedenen in Tab. 1 aufgeführten UHS-Stahlproben durchgeführt. "TM-UHSS 1" ist ein hochfester niedriglegierter Baustahl (HSLA-Stahl), der mit rekristallisationsverzögernden Elementen wie V, Nb und Ti legiert ist. Eine Verformung unter der Rekristallisationsstoptemperatur begünstigt ein Pancaking des Austenits. Der Stahl wurde nach dem Warmwalzen direktgehärtet. Der Stahl "TM-UHSS 2" weist einen geringeren

	C	Mn	Cr+Ni+Mo	Cu	V + Nb + Ti	Si	P	N	B	Fe
TM – UHSS 1	0.17	1.4	2.10	0.45	0.09	0.30	< 0.01	< 0.001	< 0.001	Bal.
TM – UHSS 2	0.17	2.3	0.31	0.08	0.03	0.20	< 0.01	< 0.001	0.002	Bal.
PH 1	0.20	1.2	0.25	0.02	0.04	0.19	0.01	0.003	0.003	Bal.

**Tab. 1:** Chemical composition of the steels investigated [mass-%].

**Tab. 1:** Chemische Zusammensetzung der untersuchten Stähle [Gew.-%].

especially with respect to the recrystallization retarding elements. The second fraction of investigated material for which a sufficient PAG etchant is meaningful is represented by "PH 1", a press-hardened UHS steel. A proficient visualization of the austenite grain prior to quenching might shed light on the influence of austenitization time and temperature and connect this to the mechanical properties.

The sample preparation is identical for all following analysis procedures. The specimens were hot embedded and then ground from 320 grit to 4000 grit SiC paper for at least 30 s. Subsequently, the samples were polished with 3 µm diamond paste for at least 3 min and with 1 µm for 30 s. Care needs to be taken to avoid the contamination with water, which can lead to corrosion relics influencing the following acidic etching. The samples prepared for EBSD additionally were finished with a OPU polishing for 8 min.

### 3. Visualization of PAGs in Martensitic Steels

To contrast the microstructure, different etchants were used. As Nital originally serves to visualize the actual microstructure such as ferrite – perlite to bainite – martensite, in par-

Legierungsanteil auf, speziell im Hinblick auf rekristallisationshemmende Elemente. "PH 1", ein pressgehärteter UHS-Stahl, repräsentiert die zweite Gruppe der untersuchten Werkstoffgruppe, für die ein entsprechendes Ätzmittel zur Darstellung der PAGs von Bedeutung ist. Eine Darstellung der vormaligen Austenitkörner könnte den Einfluss der Austenitisierungszeit und -temperatur darlegen und mit den daraus hervorgehenden mechanischen Eigenschaften in Zusammenhang bringen.

Die Probenvorbereitung ist für die folgenden Analyseverfahren identisch. Die Proben wurden warmeingebettet und anschließend mit SiC-Schleifpapier mit Körnungen von 320 bis 4000 über einen Zeitraum von mindestens 30 s geschliffen. Danach wurden die Proben mit einer 3 µm Diamantpaste mindestens 3 min lang poliert, schließlich mit einer 1 µm Paste für weitere 30 s. Besondere Sorgfalt ist geboten, um eine Verunreinigung mit Wasser zu vermeiden, welche zu Korrosionsrückständen führen kann, die wiederum Auswirkungen auf den anschließenden Ätzzvorgang haben. Die für die EBSD-Analyse angefertigten Proben wurden zusätzlich mit einer OP-U-Suspension über 8 min endpoliert.

### 3. Visualisierung der PAGs in martensitischen Stählen

Um die Mikrostruktur zu kontrastieren, wurden verschiedene Ätzmittel verwendet. Da Nital eigentlich dazu dient, die aktuell vorliegende Mikrostruktur, wie z. B. Ferrit – Perlit bis hin

ticular cases it is possible to reveal as well PAGs [15]. Hence, 3% of  $\text{HNO}_3$  solved in ethanol was used to etch the samples for 2–3 s.

### 3.1 The Martensitic Microstructure – Revealed through an Nital Etching Method

For pure qualitative detection of grain sizes after a solution annealing of structural steels prior to rolling, a simple Nital etching can be sufficient as displayed by Fig. 2. Here, the PAGs of a quenched 0.17% plain carbon steel (S275JR) were visualized only with a 3%  $\text{HNO}_3$  solution. The appearance of the actual microstructure which consists mainly of lath martensite infused by bainitic zones is displayed in Fig. 3. An abbreviated etching of 1 s indicates at lowered magnification a vague estimation of the existence and the dimensions of the austenite structure. After 3 s etching the martensitic blocks become visible (Fig 3b) from which the former austenitic grain can be deduced. Yet, an extended analysis of the PAGs as well as their size distribution is not possible.

zu Bainit – Martensit sichtbar zu machen, ist es in vereinzelt Fällen auch möglich, die ursprünglichen Austenitkörner darzustellen [15]. Dazu wurde eine 3%-ige alkoholische Salpetersäure ( $\text{HNO}_3$ ) zum Ätzen der Proben über 2–3 s eingesetzt.

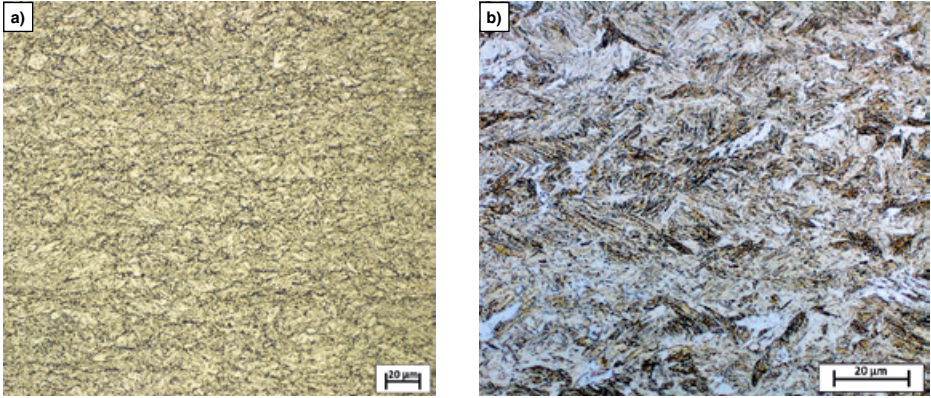
### 3.1 Die martensitische Mikrostruktur – Sichtbarmachung durch Nitalätzung

Für die rein qualitative Erfassung der Korngrößen nach dem Lösungsglühen von Baustählen und vor dem Walzen kann, wie in Bild 2 zu sehen, eine einfache Nitalätzung ausreichend sein. Hier wurden die PAGs eines gehärteten 0,17% unlegierten Stahls (S275JR) nur mit Hilfe einer 3%-igen  $\text{HNO}_3$ -Lösung sichtbar gemacht. Die tatsächliche Mikrostruktur, hauptsächlich bestehend aus lanzettenförmigem Martensit und von bainitischen Zonen, ist in Bild 3 zu sehen. Eine relativ kurze Ätzung von etwa 1 s lässt bei grober Vergrößerung eine vage Einschätzung der Lage und Größe der Austenitkörner zu. Nach 3-sekündigem Ätzen werden die Martensitblöcke sichtbar (Bild 3b), von denen auf die ursprünglichen Austenitkörner geschlossen werden kann. Eine erweiterte Analyse der PAGs und deren Größenverteilung ist jedoch nicht möglich.



**Fig. 2:** 3%  $\text{HNO}_3$  etchant revealing the PAGs after solution annealing of a quenched 0.17% plain carbon structural steel.

**Bild 2:** Mit einer 3%-igen  $\text{HNO}_3$ -Lösung wurden die PAGs eines nach Lösungsglühen abgeschreckten, unlegierten 0,17% C-Stahls sichtbar gemacht.



**Figs. 3a and b:** TM-UHSS 1 etched with a Nital etching solution: a) after 1 s soaking, slight appearance of bundle- and grain boundaries; b) after 3 s etching clear emerge of lath packages with no trace of PAGs, revealing the martensitic/bainitic microstructure, lath martensite packets and bundles.

**Bilder 3a und b:** TM-UHSS 1 geätzt mit Nitalösung: a) nach 1-sekündigem Ätzen leichtes Hervortreten von Bündel- und Korngrenzen; b) nach 3-sekündigem Ätzen deutliches Erkennen von lattenförmigen Martensitbündeln ohne Hinweise auf PAGs, zu erkennen ist die martensitische/bainitische Mikrostruktur, sowie Pakete von lanzettenförmigem Martensit.

### 3.2 Detecting PAGs With Picric-Acid Etching

In order to accentuate the prior austenite structure preserved in the material, several etchants originating from the picric acid etchant by Bechet and Beaujard were adapted to its effectiveness. Modifications such as different wetting agents or the addition of HCl can be applied [8, 9, 16–18]. Due to the fact that hydrochloric acid has been proved to be a very sensitive and

### 3.2 Nachweis von PAGs durch Pikrinsäure-Ätzung

Um das ursprüngliche Austenitgefüge, das noch im Werkstoff hinterlegt ist, hervorzuheben, wurden verschiedene Ätzmittel auf Basis des Pikrinsäure-Ätzmittels nach Bechet-Beaujard hinsichtlich ihrer Wirksamkeit angepasst. Anpassungen, z.B. durch den Einsatz verschiedener Benetzungsmittel oder die Zugabe von HCl können vorgenommen werden [8, 9, 16–18]. Aufgrund der Tatsache, dass

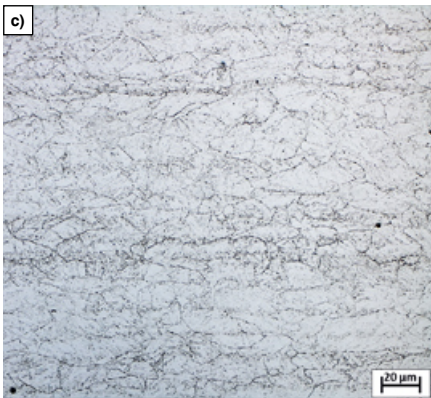
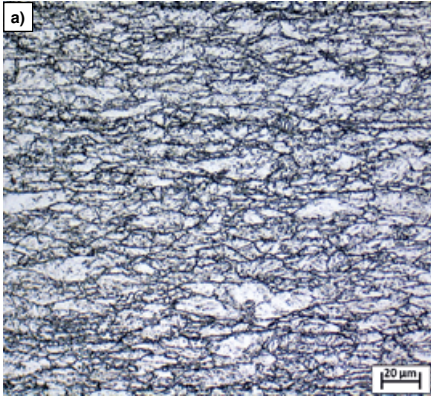
Quantity Substance / Menge Substanz	
100 ml	Picric-acid (cold saturated and filtrated) / Pikrinsäure (kaltgesättigt und filtriert)
0.7 g – 1.0 g	Sodium dodecyl sulfate / Natriumdodecylsulfat
3 drops / 3 Tropfen	HCl*

**Tab. 2:** Composition of acidic etching suspension used for PAGs of UHSS steels.

\* used conditionally.

**Tab. 2:** Zusammensetzung der Ätzlösung zur Sichtbarmachung von PAGs in UHS-Stählen.

\* bedingt eingesetzt.



**Figs. 4a to c:** a) TM-UHSS 1 etched with modified etchant using sodium dodecyl sulfate as wetting agent, composition according to Tab. 2, b) TM-UHSS 1 with refined microstructure, the etchant even reveals grain sizes  $< 1 \mu\text{m}$  c) TM-UHSS 2 etched with picric acid and wetting agent, dispensed with HCl.

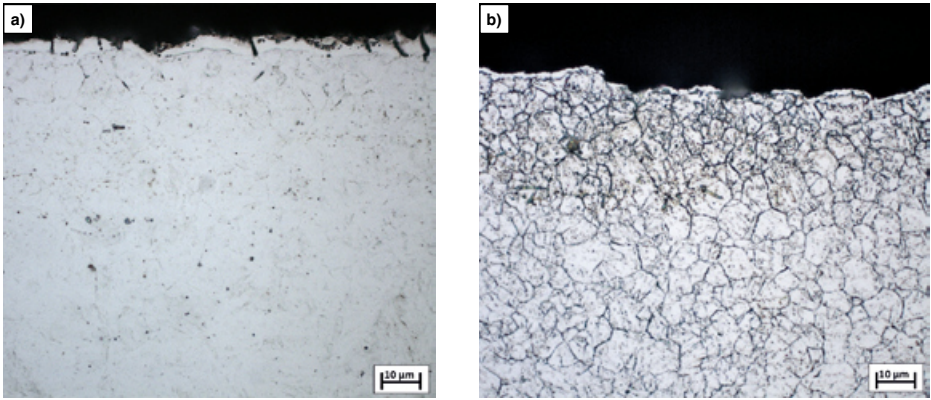
**Bilder 4a bis c:** a) TM-UHSS 1 geätzt mit modifiziertem Ätzmittel und Natriumdodecylsulfat als Benetzungsmittel, Zusammensetzung, s. Tab. 2, b) TM-UHSS 1 mit verfeinerter Mikrostruktur, das Ätzmittel zeigt sogar Korngrößen von  $< 1 \mu\text{m}$ , c) TM-UHSS 2 geätzt mit Pikrinsäure und Benetzungsmittel, Verzicht auf HCl.

critical addition, we examine its usage carefully, beside the application of a possible prior heat treatment. The composition of the established etchant is given in Tab. 2. For selected samples a heat treatment was performed. This was executed in a chamber furnace at  $600^\circ\text{C}$  for 15 min.

Fig. 4a shows the etching result of the established etchant using sodium dodecyl sulfate as wetting agent and an adjusted quantity of HCl. The established etchant expresses even small grain fractions clearly. The challenge to reveal PAGs is magnified as the grain sizes decreases. A modified milling plan yields to a refining of the mi-

Salzsäure sehr reaktiv ist und sich als heikle Zugabe erwiesen hat, wird deren Gebrauch neben der möglichen Anwendung einer vorherigen Wärmebehandlung sorgfältig untersucht. Die Zusammensetzung des Ätzmittels ist in Tab. 2 dargestellt. Bei ausgewählten Proben wurde eine Wärmebehandlung in einem Kammerofen bei  $600^\circ\text{C}$  über einen Zeitraum von 15 min durchgeführt.

Bild 4a zeigt das Ätzresultat mit Natriumdodecylsulfat als Benetzungsmittel und einer angepassten Menge HCl. Selbst kleine Kornfraktionen werden durch das Ätzmittel deutlich dargestellt. Die Herausforderung, PAGs sichtbar zu machen, steigt mit kleiner werdenden Korngrößen. Ein modifizierter Walzplan führt zu einer Verfeinerung der Mikrostruktur, das



**Figs. 5a and b:** PH 1 etched with picric acid etchant for 20 min a) as quenched state with no visible PAGs, b) after tempering at 600°C for 15 min.

**Bilder 5a und b:** PH 1 geätzt mit Pikrinsäure über 20 min, a) in vergütetem Zustand ohne sichtbare PAGs, b) nach Wärmebehandlung bei 600°C über 15 min.

crostructure, the etchant even reveals grain sizes  $< 1 \mu\text{m}$  as displayed in Fig. 4b. For TM UHSS 2 the usage of HCl was avoided due to the augmented emergence of the martensitic microstructure (Fig. 4c). Fig. 5. demonstrates the etching result on PH1 on a sample in the as-pressed condition (a) and on a tempered sample of the same steel (b). Without heat treatment, the PAGs do not appear even after 25 min of soaking in the etchant. The success of the effective emergence of PAGs in Fig. 5b emphasizes the demand for a 15 min temper treatment at 600°C in a chamber furnace.

As demonstrated, the addition of HCl can determine the success or failure of the etching. Often, a standardized quantity of 1 ml HCl per 100 ml picric acid is indicated as basic composition for numerous PAG etchants independent on the wetting agent. Though, HCl behaves as very sensitive and critical addition. Even though it supports the etching reaction by the picric acid, it as well extracts the martensitic microstructure. From experience, the use of hydrochloric acid should be avoided in the analysis of weakly alloyed UHSS. For

Ätzmittel macht sogar Korngrößen von  $< 1 \mu\text{m}$  sichtbar, vgl. Bild 4b. Für TM-UHSS 2 wurde aufgrund des stärkeren Hervortretens der martensitischen Mikrostruktur auf den Einsatz von HCl verzichtet (Bild 4c). Bild 5 zeigt das Ätzergebnis für PH 1, bei einer Probe im pressgehärteten (a) und bei einer angelassenen Probe desselben Stahls (b). Ohne Wärmebehandlung erscheinen die PAGs selbst nach 25-minütiger Ätzung nicht. Das erfolgreiche und wirksame Darstellen der PAGs in Bild 5b unterstreicht die Notwendigkeit einer 15-minütigen Anlassbehandlung bei 600°C in einem Kammerofen.

Wie bereits dargestellt, kann die Zugabe von HCl über Erfolg oder Misserfolg des Ätzens entscheiden. Oft wird eine standardisierte Menge von 1 ml HCl pro 100 ml Pikrinsäure unabhängig vom verwendeten Benetzungsmittel als Grundzusammensetzung für viele PAG-Ätzmittel angegeben. Jedoch ist HCl sehr reaktiv und somit ein heikler Zusatz. Obwohl HCl die durch Pikrinsäure hervorgerufene Ätzreaktion unterstützt, greift sie auch die martensitische Mikrostruktur an. Erfahrungsgemäß sollte bei der Untersuchung schwachlegierter UHS-Stähle auf den Gebrauch von

steels with higher alloying contents, as in the example of TM-UHSS 1, the addition of 3–5 drops of HCl increases the etching result noticeably.

The effect of a heat treatment on the success of revealing PAGs in martensitic steels is obvious. Since the suggested heat treatment of 15 min at 600 °C is equivalent to a tempering process, mechanical sampling due to the expected softening is inappropriate. Yet, since the prevailing temperatures for the annealing treatment are below the  $A_{C1}$ -temperature, no change in microstructure takes place. The PAGs remain unaffected what justifies the visualization of the austenite condition prior to the martensite transformation. The improved output through tempering can be explained by the diffusion of P at the temper-embrittlement temperature enables the accentuated emerge of the affected austenite grain boundaries [19]. Some steels, especially those which are generously alloyed with transformation-retarding elements such as Mo, Ni, Cr, Mn do by experience not require a heat treatment, as exemplified by TM-UHSS 1. Also do PAGs appear slightly in most of the untempered samples as well, which might be enough for a qualitative analysis of the grain sizes. Yet, for a quantitative evaluation, an annealing treatment significantly improves the results.

#### 4. Reconstruction of Austenite Grains through an EBSD Scan

The reconstruction of PAGs of an EBSD scan is based on the orientation relationship between martensitic blocks and their austenite habitus [11]. With respect to the fact, that the reconstruction of a deformed microstructure, as in a rolling in the non-recrystallization austenite regime or of an already-formed martensite is subject to re-

Salzsäure verzichtet werden. Bei Stählen mit höheren Legierungsgehalten, wie bspw. TM-UHSS 1, verbessert die Zugabe von 3–5 Tropfen HCl das Ätzergebnis deutlich.

Der Einfluss einer Wärmebehandlung auf das erfolgreiche Sichtbarmachen von PAGs in martensitischen Stählen ist offensichtlich. Da die vorgeschlagene Wärmebehandlung von 15 min bei 600 °C einem Tempervorgang entspricht, ist eine mechanische Beprobung hinsichtlich der erwarteten Entfestigung des Materials ungeeignet. Da jedoch die für diese Glühbehandlung übliche Temperatur unterhalb der  $A_{C1}$ -Temperatur liegt, findet keine Änderung der Mikrostruktur statt. Die PAGs bleiben unbeeinflusst, was die Situation der Austenitstruktur vor der martensitischen Umwandlung rechtfertigt. Das verbesserte Ergebnis durch den Tempervorgang lässt sich anhand der Diffusion der gelösten Atome erklären. Vor allem die Diffusion von P im Bereich der Anlassversprödung ermöglicht das deutliche Hervortreten der beeinflussten Austenitkorngrenzen [19]. Einige Stähle, besonders solche mit hohen Legierungsgehalten umwandlungsverzögernder Elemente wie Mo, Ni, Cr, Mn, erfordern erfahrungsgemäß keine Wärmebehandlung, wie am Beispiel von TM-UHSS 1 gezeigt wurde. Auch bei den meisten unvergüteten Proben sind die ursprünglichen Austenitkörner schwach zu erkennen, was für eine qualitative Analyse der Korngrößen ausreichen könnte. Für eine quantitative Bewertung werden die Ergebnisse durch eine Glühbehandlung jedoch deutlich verbessert.

#### 4. Rekonstruktion von Austenitkörnern durch EBSD -Untersuchung

Die Rekonstruktion von PAGs mit Hilfe eines EBSD-Scans basiert auf der Orientierungsbeziehung zwischen martensitischen Blöcken und deren Austenit-Habitus [11]. Da die Rekonstruktion einer verformten Mikrostruktur, wie es z. B. beim Walzen unter der Rekristallisations-Stop-Temperatur oder bei bereits gebildetem Martensit der Fall ist, Einschrän-

strictions [20], the researcher can rely on two different procedures which were presented by Haslberger [21]: a manual assembly of different colored martensitic blocks to a PAG proposed by Abbasi [22] and an automated reconstruction on basis of the theoretical transformed groupoid structure formed by the origin grain proposed by Cayron [23]. This method has been validated for both martensitic and bainitic transitions in iron [24]. It represents a reliable alternative to metallographic techniques as investigated by Weyand et al. [25], who prove its adequacy in the reconstruction of the PAG structure of TM-simulation deformed martensitic steels.

The samples were examined with an EDAX Hikari XP EBSD system, which is installed in a FIB Versa 3D DualBeam. After mounting and tilting the samples to an operation angle of 70°, a 100 × 100 μm<sup>2</sup> sized area was scanned with a working distance of 15 mm and step size of 0.10 μm. After collecting the pattern, the data was converted using the EDAX OIM Software to be then calculated through ARGPE. As the former proposed manual detection method constitutes a very demanding procedure especially for small grain sizes, it was detected to be unsuitable. Thus, only the automated reconstruction was used.

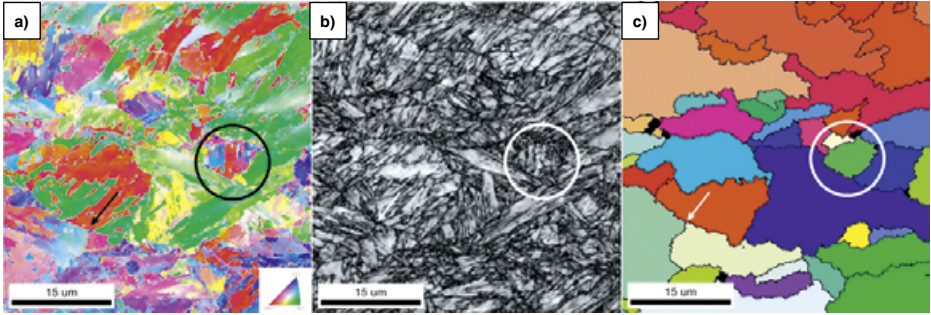
Fig. 6 reveals the result of the EBSD scan on UHSS TM 1. On behalf of the different orientations – marked by coloured contrast of the IPF map – the affiliation of the martensitic blocks emerging from a habitus austenite grain can be identified. The gray-scale map even allows a delineation of the

kungen unterworfen ist [20], stehen Wissenschaftlern zwei verschiedene Verfahren, die von Haslberger vorgestellt wurden, zur Verfügung [21]: das manuelle Zusammensetzen der unterschiedlich gefärbten Martensitblöcke zum ursprünglichen Austenitgefüge, wie von Abbasi vorgestellt [22], und eine automatische Rekonstruktion basierend auf dem theoretisch umgewandelten gruppoiden Gefüge, das durch das ursprüngliche Korn gebildet wurde, wie von Cayron vorgestellt [23]. Dieses Verfahren wurde sowohl für martensitische als auch bainitische Umwandlungen bei Eisen bestätigt [24]. Es stellt eine zuverlässige Alternative zu metallografischen Verfahren dar, wie von Weyand et al. untersucht wurde [25]. Anhand dieser Arbeit konnte die Eignung des Verfahrens zur Rekonstruktion des ursprünglichen PAG-Gefüges in martensitischen Stählen, die in einer thermomechanischen Simulation verformt wurden, nachgewiesen werden.

Die Proben wurden mit einem EDAX-Hikari-XP-EBSD-System untersucht, welches in einem FIB Versa 3D DualBeam installiert ist. Nach dem Einbringen und Neigen der Proben bis zu einem Winkel von 70° wurde eine 100 × 100 μm<sup>2</sup> große Fläche mit einem Arbeitsabstand von 15 mm und in Schrittweiten von 0,10 μm gescannt. Nach dem Aufnehmen des Patterns wurden die Daten mit Hilfe der EDAX-OIM-Software umgewandelt und anschließend durch eine automatische Rekonstruktion der Ursprungskörner ausgehend von den EBSD-Daten (ARPGE, Automatic Reconstruction of Parent Grains from EBSD data) berechnet. Da sich die zuvor genannte manuelle Rekonstruktion besonders bei geringen Korngrößen als sehr anspruchsvoll erweist, wurde sie als ungeeignet eingestuft. Folglich wurde nur das automatische Verfahren zur Rekonstruktion verwendet.

Bild 6 zeigt das Ergebnis der EBSD-Messung beim Stahl UHSS-TM 1. Durch die verschiedenen Orientierungen – angezeigt durch Farbkontraste auf der Inverse-Polfigur-Karte – kann die Zusammengehörigkeit von martensitischen Blöcken, die aus dem austenitischen Habitus Korn hervorgehen, bestimmt werden.





**Figs. 6a to c:** EBSD map with selected grain zones: a) Image quality map with inverse pole figure map, b) correlating black/white image quality map with dark shaded phase boundaries and c) unique color coded map of reconstructed PAGs with ARGPE.

**Bilder 6a bis c:** EBSD-Karte mit ausgewählten Kornbereichen: a) IQ Map mit Inverser Polfigur, b) entsprechende Schwarz/Weiß-IQ Map mit dunkel erscheinenden Phasengrenzen und c) farblich kodierte Karte der mit ARPGE rekonstruierten PAGs.

related packets. The symmetric shapes appearing in the pole figures can be used to identify and gradually compose the PAGs as it is implemented by [21, 22]. The automatic reconstruction with ARGPE delivers the unique color coded reconstructed PAG map in Fig. 6 c. Most of the grains were obviously assembled properly as highlighted by a circle in the image. Yet, some reconstructed grains are questionable, especially the former grain boundaries were structured very imprecisely. Nevertheless, the grain elongation of the TM-processed steel is evident and corresponds, including the size fractions of the grains, to the results of the light-optical analysis of the picric-etched samples.

However, a representative depiction of microstructural properties such as grain size fractions and grain elongations requires the evaluation of a large number of grains. The high interfacial density of a martensitic structure keeps the scanned area limited. Although Weyand et al. [25] report,

Die Karte in Graustufen ermöglicht sogar eine Abgrenzung der zusammengehörigen Pakete. Die symmetrischen Formen, die in der Polfigur zu sehen sind, können verwendet werden, um die PAGs zu identifizieren und stufenweise zusammensetzen, wie bei [21, 22] durchgeführt. Die automatische Rekonstruktion durch ARPGE liefert, wie in Bild 6 c dargestellt, die farblich kodierte Karte der rekonstruierten PAGs. Die Mehrzahl der Körner wurde offensichtlich richtig zusammengesetzt wie durch den mit einem Kreis markierten Bereich im Bild hervorgeht. Jedoch sind einige rekonstruierte Körner in Frage zu stellen, vor allem wurden die ursprünglichen Korngrenzen recht unpräzise strukturiert. Dennoch ist die Kornstreckung bei den thermomechanisch behandelten Stählen offensichtlich und entspricht, einschließlich der Größenfraktionen der Körner, den Ergebnissen der lichtmikroskopischen Analyse der mit Pikrinsäure geätzten Proben.

Jedoch erfordert eine repräsentative Darstellung der mikrostrukturellen Eigenschaften wie z. B. Korngrößenfraktionen und Kornstreckung die Auswertung einer großen Anzahl an Körnern. Aufgrund des hohen Anteils an Grenzflächen bei martensitischen Gefügen ist der messbare Bereich begrenzt. Obwohl

that even on large EBSD maps with sizes of  $1000\ \mu\text{m} \times 1000\ \mu\text{m}$ , PAGs can be calculated with good accuracy, the smaller microstructure magnitude of the investigated samples does not allow a proper reconstruction as the necessary resolution is dependent on the viewed area and the step size chosen for the scan. Thus, a decreasing PAG size below a few microns affects the measuring insofar as the scanned area becomes too small and a representative statistic is not feasible.

## 5. Visualization of PAGs during Reheating in a HT-LSCM

The following method indeed represents a quite uncommon procedure to reveal the PAGs of martensitic steels, yet attracts interest especially for steels which expose their austenite structure quite unwillingly. In a YONEKURA VL 2000DX high-temperature laser scanning confocal microscope, a polished sample is reheated to the  $\gamma$ -region, while the evolution of microstructure is recorded through a camera. In the immediate moment of the transformation of the martensite, the austenite structure existing prior to the transformation appears before the austenite starts to grow again. Due to the wavelength of the laser of 408 nm, the resolution is limited concerning very small PAG sizes ( $< 1\ \mu\text{m}$ ). The forming of a relief of the PAGs during reheating corresponds to a thermal etching which enables a subsequent analysis in a light microscope, which compensates for the diminished resolution of the LSCM.

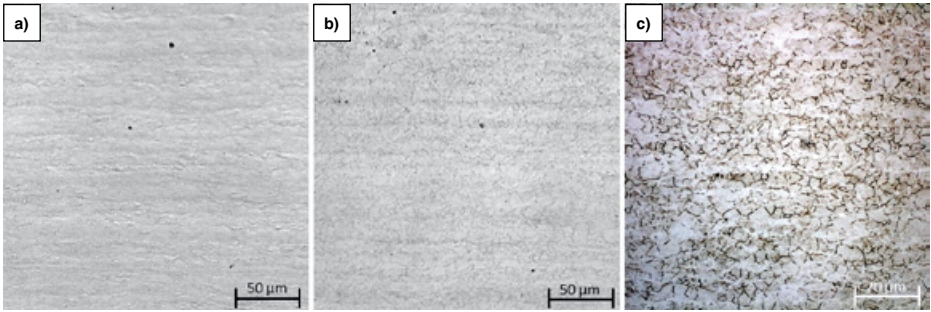
Fig. 7 represents the microstructure condition during heating at a)  $710^\circ\text{C}$  and b)  $760^\circ\text{C}$ , respectively. At  $710^\circ\text{C}$ , the sample temperature corresponds to the  $\alpha$ -region, the structure seems as expected elongat-

Weyand et al. [25] berichten, dass sogar anhand großer EBSD-Maps mit Größen von  $1000\ \mu\text{m} \times 1000\ \mu\text{m}$  PAGs mit hoher Genauigkeit errechnet werden können, ist wegen der geringeren Größenordnung der Mikrostruktur bei den untersuchten Proben eine genaue Rekonstruktion nicht möglich, da die erforderliche Auflösung vom betrachteten Bereich und von den gewählten Schrittgrößen beim Scannen abhängt. Somit beeinträchtigt die abnehmende Größe der ursprünglichen Austenitkörner auf Werte von weniger als ein paar  $\mu\text{m}$  das Messverfahren insoweit, als dass der gescannte Bereich zu klein wird und eine repräsentative Statistik nicht möglich ist.

## 5. Visualisierung von PAGs während der Erwärmung im Hochtemperatur-Laser-Scanning-Mikroskop (HT-LSCM)

Das folgende Verfahren stellt eine durchaus unübliche Vorgehensweise zur Visualisierung von PAGs bei martensitischen Stählen dar, ist jedoch vor allem bei Stahlsorten von Interesse, die ihr Austenitgefüge nur ungern preisgeben. Im Hochtemperatur-Laser-Scanning-Mikroskop VL 2000DX von YONEKURA wird eine polierte Probe bis ins  $\gamma$ -Gebiet erwärmt, während die Entwicklung der Mikrostruktur durch eine Kamera aufgezeichnet wird. Genau in dem Moment, in dem sich Martensit umwandelt, wird das Austenitgefüge wie es vor der Umwandlung vorlag, sichtbar, bevor der Austenit wieder zu wachsen beginnt. Aufgrund der Wellenlänge des Lasers von 408 nm ist die Auflösung hinsichtlich sehr geringer PAG-Größen ( $< 1\ \mu\text{m}$ ) begrenzt. Die Ausbildung eines Reliefs bei den PAGs während der Wiedererwärmung entspricht einem thermischen Ätzverfahren, wodurch eine anschließende Analyse im Lichtmikroskop ermöglicht wird, die die verminderte Auflösung des LSCM kompensiert.

Bild 7 zeigt den Zustand der Mikrostruktur während des Erwärmens bei a)  $710^\circ\text{C}$  bzw. b)  $760^\circ\text{C}$ . Bei  $710^\circ\text{C}$  entspricht die Probertemperatur dem  $\alpha$ -Gebiet und das Gefüge scheint, wie erwartet, gestreckt in Walzrichtung. Jedoch sind die Korn-



**Figs. 7a to c:** a) HT-LSCM image during heating at 710°C showing relief of elongated austenite microstructure; b) holding at 760°C, appearing of globular austenitic grains; c) light-microscope image at RT revealing thermal etched PAGs.

**Bild 7a bis c:** a) HT-LSCM-Aufnahme während der Erwärmung bei 710°C mit sichtbarem Relief der gestreckten austenitischen Mikrostruktur; b) Halten auf 760°C und Hervortreten globularer Austenitkörner; c) lichtmikroskopische Aufnahme bei RT und deutliches Erkennen thermisch geätzter PAGs.

ed in rolling direction. However, the grain boundaries are not clearly visible in order to serve for a grain size analysis; contrary to the temperature of 760°C, shown in image 7b, where the grain boundaries appear precisely. Similar to the light microscope image in 7c, the austenite grains are globular, due to a temperature-dependent globularization which obviously took place in the two phase  $\alpha$ - $\gamma$  region. It is assumed that the high degree of deformation, especially below the non-recrystallization temperature promotes the immediate forming of the austenite grain due to surface energy-minimization. This phenomenon prohibits the usage of a HT-LSCM concerning a grain size analysis of PAGs of a TMP steel. In the immediate moment in which the elongated austenite grains appear, they cannot be captured due to a diminished image contrast and an instant globularization.

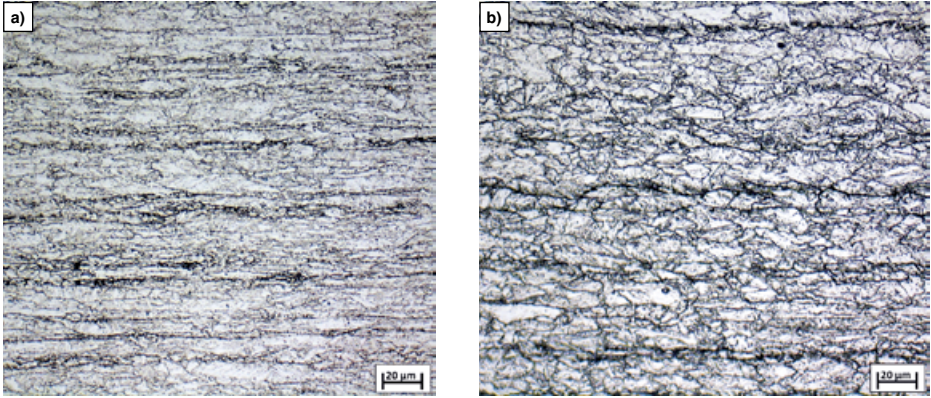
## 6. Grain Size Analysis

The effectiveness of an etchant latest is shown as the images enable a quantification of the highlighted microstructure. An automated evaluation with an image analysis software would be desirable. Yet,

grenzen für eine Korngrößenanalyse nicht deutlich genug sichtbar, im Gegensatz zum Gefüge bei 760°C, zu sehen in Bild 7b, wo die Korngrenzen klar zu erkennen sind. Ähnlich wie bei der lichtmikroskopischen Aufnahme in 7c sind die Austenitkörner globular. Der Grund hierfür ist eine temperaturabhängige Einformung, d. h. die Ausbildung von globularem Austenit, die offenbar im Zweiphasen- $\alpha$ - $\gamma$ -Gebiet erfolgte. Es ist anzunehmen, dass die starke Umformung, besonders unterhalb der Rekristallisations-Stop-Temperatur die sofortige Einformung der Austenitkörner zur Verringerung ihrer Oberflächenenergie hervorruft. Dieses Phänomen verhindert eine Korngrößenanalyse der PAGs mit Hilfe des HT-Laser-Scanning-Mikroskops bei einem thermomechanisch behandelten Stahl. In dem Moment, in dem die gestreckten Austenitkörner erscheinen, können diese aufgrund des geringeren Bildkontrasts und der sofort einsetzenden Globularisierung nicht aufgenommen werden.

## 6. Korngrößenanalyse

Der Erfolg einer Ätzung wird spätestens dann deutlich, wenn die Aufnahmen auch eine Quantifizierung der Mikrostruktur ermöglichen. Eine automatische Berechnung mit Hilfe einer Bildanalyse-Software wäre erstrebenswert.



**Figs. 8a and b:** TM - UHSS 1 etched with picric acid etchant for 20 min a) FRT of 850°C, clear elongated austenite grains due to TMP, b) FRT of 900°C, elongated PAGs, yet more globular grains compared to a).

**Bilder 8a und b:** TM-UHSS 1 geätzt mit Pikrinsäure über 20 min, a) Endwalztemperatur (FRT) von 850°C, klar erkennbare gestreckte Austenitkörner aufgrund von thermomechanischer Behandlung, b) FRT von 900°C, gestreckte PAGs, jedoch im Vergleich zu a) mehr globulare Körner.

a manual post-processing of the assessed results is inevitable, wherein the additional effort is dependent on the quality of the etching. In the present chapter listed is the application of the etchant in combination with an image analysis software "Olympus Stream".

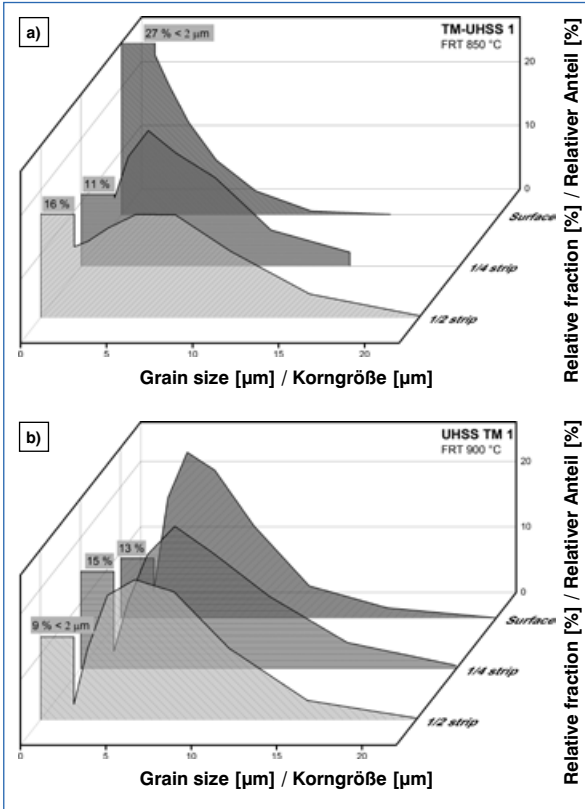
### 6.1 Grain Size Analysis and Evaluation of the Elongated PAGs due to TMP

To evaluate the etching process with respect to its applicability, steel samples of TM-UHSS 1 were analyzed. The samples were produced with different finishing rolling temperatures (FRT). Due to the different FRT, different austenite grain morphologies are expected. For investigations on the elongation of the PAGs, the transversal direction (TD) suggests itself as the width expansion alongside the rolling direction (RD) is several orders of magnitude lower than the length extension of the transversal direction. Moreover, the aspect ratio of not recrystallized elongated PAGs alongside the TD, on which almost the entire material flow occurs, allows conclusions to the

Jedoch ist eine manuelle Nachbearbeitung der Ergebnisse unerlässlich. Hierbei hängt der zusätzlich erforderliche Aufwand von der Qualität der Ätzung ab. Im vorliegenden Kapitel wird die Anwendung eines Ätzmittels in Kombination mit der Bildanalyse-Software "Olympus Stream" vorgestellt.

### 6.1 Korngrößenanalyse und Auswertung der durch TMB gestreckten PAGs

Um das Ätzverfahren hinsichtlich seiner Anwendbarkeit zu bewerten, wurden Proben des Stahls TM-UHSS 1 untersucht. Die Proben wurden mit verschiedenen Endwalztemperaturen (FRT, finishing rolling temperatures) hergestellt. Aufgrund der verschiedenen Temperaturen sind unterschiedliche Morphologien der Austenitkörner zu erwarten. Die Untersuchung der Streckung der PAGs in Querrichtung (TD, transversal direction) liegt nahe, da die Breitenausdehnung entlang der Walzrichtung (RD, rolling direction) um einige Größenordnungen geringer ausfällt als die Längenausdehnung in Querrichtung. Außerdem ermöglicht das Seitenverhältnis der nicht-rekristallisierten gestreckten PAGs entlang der Querrichtung, in der fast der



**Figs. 9a and b:** Grain size analysis of TM-UHSS 1 according to ASTM E 112–12 at a FRT of 850 °C (a) and a FRT of 900 °C (b) at three different positions. Surface, 1/4 of strip thickness and center thickness.

**Bilder 9a und b:** Korngrenzenanalyse des Stahls TM-UHSS 1 gemäß ASTM E 112–12 bei 850 °C (a) bzw. 900 °C (b) Endwalztemperatur an drei verschiedenen Messpositionen: Oberfläche, 1/4 der Blechdicke und Blechmitte.

reduction of the plate. The light-optical measurements perpendicular to the transversal direction of the DQ plate were made at three positions directing along strip thickness: near the surface of the strip, 1.5 mm and 3 mm below the strip which corresponds to 1/4 and 1/2 of the depth of the provided 6 mm strip thickness. The employed etchant revealed the PAGs of both steel samples in an excellent quality. The increased grain elongation due to a lowered FRT is obvious and can be confirmed through the image analysis (Tab. 3). Even smaller globular austenite grains smaller than 5 µm, whose presence is indicative for a recent recrystallization, are detected by the etchant. Despite the fact that the

gesamte Materialfluss stattfindet, Rückschlüsse auf den Verformungsgrad des Walzstücks. Die lichtmikroskopischen Messungen senkrecht zur Querrichtung des direkt abgeschreckten Blechs wurden an drei Messpositionen entlang der Blechdicke durchgeführt: in der Nähe der Oberfläche sowie 1,5 mm und 3 mm unterhalb der Oberfläche, was einem 1/4 bzw. 1/2 der vorliegenden Dicke von 6 mm entspricht. Das verwendete Ätzmittel lässt die PAGs beider Stahlproben in außerordentlicher Qualität sichtbar werden. Die erhöhte Kornstreckung aufgrund niedrigerer Endwalztemperaturen ist offensichtlich und kann anhand der Bildanalyse (Tab. 3) bestätigt werden. Sogar globulare Austenitkörner mit einer Größe von weniger als 5 µm, deren Vorhandensein auf eine kürzlich stattgefunden

	FRT 850 °C	FRT 900 °C
Surface / Oberfläche	3.3 µm	5.2 µm
<b>Grain size</b> ¼ plate thickness / <b>Korngröße</b> ¼ Blechdicke	5.5 µm	6.7 µm
½ plate thickness / ½ Blechdicke	6.3 µm	6.6 µm
Surface / Oberfläche	1.8	1.7
<b>Elongation</b> ¼ plate thickness / <b>Streckung</b> ¼ Blechdicke	2.2	1.6
½ plate thickness / ½ Blechdicke	2.2	1.6

**Tab. 3:** Results of the microstructure analysis, grain size and elongation at three positions for TM-UHSS 1 for a FRT of 850 °C and 900 °C.

**Tab. 3:** Ergebnis der Mikrostruktur-analyse, Korngröße und Streckung an drei Messpositionen bei TM-UHSS 1 bei Endwalztemperaturen (FRT) von 850 °C und 900 °C.

size distribution is not quite obvious in the image, grains smaller than 2 µm represent a substantial proportion (Fig. 9).

## 7. Summary

The findings can be summarized as follows:

- The microstructure of TM-processed UHS steels and of a PH steels was investigated with light optical microscopy, laser scanning confocal microscopy and electron backscatter diffraction.
- An adapted picric-acid etchant was used to reveal the PAGs, their aspect-ratio and grain-size distribution. With adjusted proportions of sodium dodecyl sulfate as wetting agent and HCl the PAGs of all investigated UHSS samples were successfully visualized. In some cases, a tempering- treatment improves the etching result significantly.
- A Nital solution can serve as PAG etchant in specific cases. However, it is difficult to visualize the PAGs as distinctive in order to perform a quantitative analysis.
- The automated reconstruction of PAGs with a EBDS scan facilitated through

Rekristallisation hinweist, wurden durch das Ätzmittel sichtbar gemacht. Obwohl die Größenverteilung aus dem Bild nicht deutlich hervorgeht, stellen Körner mit weniger als 2 µm Größe einen erheblichen Anteil dar (Bild 9).

## 7. Zusammenfassung

Die Ergebnisse lassen sich wie folgt zusammenfassen:

- Die Mikrostruktur von thermomechanisch behandelten UHS-Stählen und von pressgehärteten Stählen wurde mit Hilfe von Lichtmikroskopie, Laser-Scanning-Mikroskopie und EBSD-Messung untersucht.
- Ein speziell angepasstes Ätzmittel auf Basis von Pikrinsäure wurde zur Sichtbarmachung der PAGs, deren Seitenverhältnis und Korngrößenverteilung verwendet. Mit angepassten Anteilen von Natriumdodecylsulfat als Benetzungsmittel und HCl wurden die PAGs aller untersuchten UHS-Stahlproben erfolgreich visualisiert. In einigen Fällen wird das Ätzergebnis durch eine Anlassbehandlung deutlich verbessert.
- Eine Nitallösung kann in einigen Fällen als PAG-Ätzmittel verwendet werden. Jedoch erweist sich eine ausgeprägte Darstellung der PAGs, die die Grundlage einer quantitativen Analyse darstellt, als schwierig.
- Die automatische Rekonstruktion von PAGs mit Hilfe einer EBDS-Messung und ARPGE

ARGPE is validated. Limits are displayed regarding workload and prospected area of the investigated very fine microstructures.

- A reliable characterization of PAGs through HT-LSCM is not possible, due to the fact that reheating still below the  $\gamma$ -region results in an immediate globularization of PAGs because of the elevated surface energy of the deformed microstructure.
- The established etchant enables conclusions concerning the recrystallization behavior in the austenite region dependent on temperature and the degree of deformation. This may serve as basis for studies on the recrystallization behavior of TM-processed steel in order to highlight the influences on the microstructure with varying deformation parameters

## Acknowledgement

Funding of the Austrian BMVIT in the framework of the program "Production of the future" and the "BMVIT Professorship for Industry" is gratefully acknowledged. Special thanks to the voestalpine Stahl GmbH in Linz, providing the investigated steels.

## References / Literatur

- [1] Klein, M.; Spindler, H.; Luger, A.; Rauch, R.; Stiaszny, P.; Eigelsberger, M.: Mater. Sci. Forum 500–501 (2005), 543–550
- [2] Karbasian, H; Tekkaya, A.E.: J. Mater. Process. Technol. 210 (2010), 2103–2118  
DOI: 10.1016/j.jmatprotec.2010.07.019
- [3] Totten, G. E.: Steel Heat Treatment: Metallurgy and Technologies, 2nd edition, crc Press, 2006, pp. 21 ff

wurde bestätigt. Es gibt jedoch Einschränkungen hinsichtlich des erforderlichen Aufwandes und des untersuchten Bereichs der vorliegenden sehr feinen Mikrostrukturen.

- Eine zuverlässige Charakterisierung der PAGs mit Hilfe eines Hochtemperatur-Laser-Scanning-Mikroskop ist nicht möglich, da eine Erwärmung noch unterhalb des  $\gamma$ -Gebiets eine sofortige Globularisierung der PAGs aufgrund der erhöhten Oberflächenenergie der verformten Mikrostruktur hervorruft.
- Das gängige Ätzmittel ermöglicht Schlussfolgerungen bezüglich des Rekristallisationsverhaltens im Austenitgebiet in Abhängigkeit von Temperatur und Verformungsgrad. Dies könnte als Grundlage für Untersuchungen des Rekristallisationsverhaltens bei thermomechanisch behandelten Stählen dienen, um die Einflüsse unterschiedlicher Verformungsparameter auf die Mikrostruktur herauszustellen.

## Danksagung

Für die finanzielle Unterstützung gilt unser besonderer Dank dem österreichischen Bundesministerium für Verkehr, Innovation und Technologie (BMVIT) im Rahmen des Programms "Produktion der Zukunft" und der "BMVIT Stiftungsprofessur für Industrie". Ebenso danken wir der voestalpine Stahl GmbH in Linz für die zur Verfügung gestellten Stähle, die Gegenstand unserer Untersuchungen waren.

- [4] Tamura, I.: Thermomechanical Processing of High-Strength Low-Alloy Steels, 1st edition, Butterworths, London, Boston 1988, pp. 22 ff
- [5] Klein, M; Rauch, R.; Spindler, H.; Stiaszny, P.: BHM Berg- Hüttenmänn. Monatshefte, 2012, vol. 157, pp. 108–112.  
DOI: 10.1007/s00501-012-0062-3
- [6] Mattei, L.; Daniel, D.; Guiglionda, G.; Klöcker, H.; Driver, J.: Mater. Sci. Eng. A, 2013, vol. 559, 812–21.  
DOI: 10.1016/j.msea.2012.09.028

- [7] Morito, S.; Yoshida, H.; Maki, T.; Huang, X.: *Mater. Sci. Eng. A*, 2006, vol. 438–440, pp. 237–40.
- [8] Vander Voort, G.F.: *Ind. Heat.*, 2010, Vol. 78, pp. 48–52.
- [9] Bechet, S.; Beaujard, L.: *Rev Met Vol 52*, 1955, pp. 830–836.  
DOI: 10.1051/metal/195552100830
- [10] Miyamoto, G.; Takayama, N.; Furuhashi, T.: *Scr. Mater.*, 2009, vol. 60, pp. 1113–16.  
DOI: 10.1016/j.scriptamat.2009.02.053
- [11] Morito, S.; Tanaka, H.; Konishi, R.; Furuhashi, T.; Maki, T.: *Acta Mater.*, 2003, vol. 51, pp. 1789–99.  
DOI: 10.1016/S1359-6454(02)00577-3
- [12] Morito, S.; Huang, X.; Furuhashi, T.; Maki, T.; Hansen, N.: *Acta Mater.*, 2006, vol. 54, pp. 5323–31.  
DOI: 10.1016/j.actamat.2006.07.009
- [13] Tokizane, M.; Matsumura, N.; Tsuzaki, K.; Maki, T.; Tamura, I.: *Metall. Mater. Trans. A*, 1982, vol. 13, pp. 1379–1388.  
DOI: 10.1007/BF02642875
- [14] Law, N. C.; Edmonds, D. V.: *Metall. Mater. Trans. A*, 1980, vol. 11, pp. 33–46.  
DOI: 10.1007/BF02700436
- [15] Vander Voort, G. F.: *Metals and Practice*, p 1, 1984.
- [16] Brownrigg, A.: *Scr. Metall.*, 1973, vol. 7, pp. 1139–42.  
DOI: 10.1016/0036-9748(73)90235-4
- [17] Brownrigg, A.; Curcio, P.; Boelen, R.: *Metallography*, 1975, vol. 8, pp. 529–33.  
DOI: 10.1016/0026-0800(75)90028-2
- [18] Barraclough, D. R.: *Metallography*, 1973, vol. 6, pp. 465–472.  
DOI: 10.1016/0026-0800(73)90044-X
- [19] Ucisik, A. H.; McMahon, C. J.; Feng, H. C.: *Metall. Trans. A*, 1978, vol. 9, pp. 321–29.  
DOI: 10.1007/BF02646381
- [20] Kubota, M.; Ushioda, K.; Miyamoto, G.; Furuhashi, T.: *Scr. Mater.*, 2016, vol. 112, pp. 92–95.  
DOI: 10.1016/j.scriptamat.2015.09.020
- [21] Haslberger, P.; Holly, S.; Ernst, W.; Schnitzer, R.: *Pract. Metallogr.*, 2017, vol. 54, pp. 513–532.  
DOI: 10.3139/147.110464
- [22] Abbasi, M.; Nelson, T.W.; Sorensen, C.D.: *J. Appl. Crystallogr.*, 2013, vol. 46, pp. 716–25.  
DOI: 10.1107/S0021889813008522
- [23] Cayron, C.; Artaud, B.; Briottet, L.: *Mater. Charact.*, 2006, vol. 57, pp. 386–401.  
DOI: 10.1016/j.matchar.2006.03.008
- [24] Cayron, C.: *J. Appl. Crystallogr.*, 2007, vol. 40, pp. 1183–88.  
DOI: 10.1107/S0021889807048777
- [25] Weyand, S.; Britz, D.; Rupp, D.; Mücklich, F.: *Mater. Perform. Charact.*, 2015, vol. 4, pp. 322–340

## Bibliography

DOI 10.3139/147.110491

*Pract. Metallogr.* 55 (2018) 4; page 203–222

© Carl Hanser Verlag GmbH & Co. KG

ISSN 0032–678X

### Raphael Esterl



was born 1988 in Neumarkt-St. Veit and studied materials science at the Montanuniversität Leoben (Austria) from 2009 to 2015. He is now working on his PhD thesis dealing with the recrystallization behavior of ultra-high strength steels.

### Ronald Schnitzer



born 1981 in Eisenstadt (Austria), has studied material science. From 2010 to 2016 he was employed at the company voestalpine Böhler Welding, where he was responsible for the Research and Development Department. In 2016 he occupied

the “BMVIT Professorship for Industry” at the Montanuniversitaet Leoben (Austria).



## Paper II:

Esterl R, Sonnleitner M, Schnitzer R (2019)

*Microstructural Analysis of the Recrystallization Behavior of Low Alloyed Steels*

Steel research international 90 (2019) 3: 382 - 391

DOI: 10.1002/ srin.201800500

# Microstructural Analysis of the Recrystallization Behavior of Low Alloyed Steels

Raphael Esterl, Markus Sonnleitner, and Ronald Schnitzer

The recrystallization behavior of five low alloyed steels is investigated using double hit deformation tests. It is shown, that Niobium has the biggest influence in retarding the recrystallization kinetics. Further, the microstructural evolution dependent on strain and temperature during deformation is studied with a picric acid etchant and light-optical analysis. It is shown how the microstructure of two differently alloyed ultra-high strength steels changes along with the peculiarities of the corresponding stress–strain curves including the evolution of grain size and aspect ratio of the prior austenite grain. The findings on the different recrystallization kinetics with the role of recrystallization retarding elements are further reinforced by investigations on the Zener-Hollomon parameter and the activation energy needed for dynamic recrystallization. A rolling scenario on a deformation dilatometer is simulated on a hardenable and a micro-alloyed steel to illustrate the microstructural evolution between the rolling steps. It is shown, how the two ultra-high strength steels perform different in their microstructural evolution, as the waiving of micro-alloying elements (MAE) provides finer austenite grains.

recrystallization through their high solute drag and stable precipitates (Nb and Ti)<sup>[3–7]</sup> or stimulate the recrystallization in the austenite region (V) promoting fine grains and low rolling forces.<sup>[8,9]</sup> Their usage allows to noticeably improve the properties of structural steels and enables the production of ultra-high strength steel (UHSS) grades. For the latter, transformation retarding elements such as Mn or B are also used to reduce the critical cooling rate.<sup>[3,10–12]</sup> Besides, its effect as solid solution strengthener, in the case of Mn,<sup>[13]</sup> they both provide no prominent contribution to recrystallization, but retard the austenite to ferrite and pearlite transformation and therefore enable a bainitic or martensitic microstructure.

The application of the mentioned alloying elements mainly covers the spectrum from mild to ultra-high-strength steels with their ability to modify the microstructure in controlling the grain size and the  $\gamma$ - $\alpha$  transformation. Their influence on the static

(SRX), metadynamic (MDRX), and dynamic (DRX) recrystallization processes determined by means of double-hit deformation tests is broadly investigated.<sup>[4,14–17]</sup> There have also been reports of corresponding influences on the DRX and MRX in numerous publications.<sup>[16,18–23]</sup> Furthermore, several models exist to quantify these mechanisms mathematically, which make these microstructural phenomena, that is, the onset of the DRX and even further recrystallization-influencing factors, such as the formation of strain induced precipitations predictable.<sup>[18,23–26]</sup> Nevertheless, on the one hand, there is no clear delimitation in the recrystallization behavior of mild and hardenable steels with respect to the alloying elements influencing the  $\gamma$  to  $\alpha$  transformation. And, therefore, a sequenced analysis of microstructure evolution in a series of deformations is worth investigating. For example, in the case of a rolling process, the involved mechanisms coincide and often cannot be distinguished clearly from each other, which limits the precision of these models.

Thus, the goal of this study is the comparison of the recrystallization behavior of mild steels and hardenable steels during hot deformation. Furthermore, the present work shall solve the challenge to display the underlying microstructural processes both, in laboratory scale deformations and metallographic analysis. The motivation is to support the development of UHS steel grades with revealing the microstructural evolution.


This is done by a clear representation of the microstructural evolution of two selected steel grades through a combination of several small scale deformations with a subsequent metallographic examination. The results on the microstructural development,

## 1. Introduction

For decades micro-alloying is an attractive procedure in industrial steel production to provide high strength steel grades through an economic production route.<sup>[1]</sup> In a systematic combination of alloying and rolling, the recrystallization processes can be tuned to generate a fine grained microstructure with high strength and good ductility.<sup>[2]</sup> Nb, V, and Ti serve herein as MAE with the strongest impact on the microstructure. Both in solute as in undissolved condition they are proficient to retard the

R. Esterl, Prof. R. Schnitzer  
Chair of Design of Steels  
Department of Materials Science  
Montanuniversität Leoben  
Franz-Josef-Str. 18, 8700 Leoben, Austria

Dr. M. Sonnleitner  
voestalpine Stahl GmbH  
voestalpine-Straße 1, 4020 Linz, Austria

 The ORCID identification number(s) for the author(s) of this article can be found under <https://doi.org/10.1002/srin.201800500>.

© 2019 The Authors. Published by WILEY-VCH Verlag GmbH & Co. KGaA, Weinheim. This is an open access article under the terms of the Creative Commons Attribution-NonCommercial License, which permits use, distribution and reproduction in any medium, provided the original work is properly cited and is not used for commercial purposes.

DOI: 10.1002/srin.201800500

dependent on the imposed deformation, will be complemented by an empirical investigation of the initiation of DRX.

It is experienced, that microstructural processes in a hot rolling mill are not only based on straightforward predictable static and dynamic recrystallization sequences. Moreover, they are subject of complex combinations of both, recovery and suspended recrystallization such as MDRX. The metadynamic recrystallization, also known as postdynamic recrystallization, belongs to the static restoration processes following a preceded deformation. Metadynamic recrystallization is initiated from a partially or steadily recrystallized microstructure by DRX after straining over the critical strain.<sup>[21,22,27]</sup> In order to study the microstructural development during hot rolling of a TM-steel, we reproduce a laboratory scale deformation corresponding to the real rolling process.

## 2. Experimental Section

### 2.1. Steels Investigated

To investigate the influence of different alloying elements in combination with different process parameters on the microstructural evolution, five different low carbon steels were analyzed. For the sake of simplicity, the steels were numbered consecutively and their chemical compositions are listed in **Table 1**. Steels 1–3 are mild steels with carbon contents of 0.15%. Steel 2 is alloyed with 1.20% Cr. Steel 3 contains 0.012% Nb. Steels 4 and 5 represent hardenable steels with an elevated amount of Mn. Steel 4 was dispensed with alloying elements which influence hardenability and tempering resistance (Cr, Ni, Mo, Cu) or recrystallization behavior (V, Ti, Nb).<sup>[3,27,28]</sup> Steel 5 completes the list with the highest addition of MAE, modified for a TM treatment and meeting the requirements for high strength structural applications. With the ulterior motive of maintaining strength and increasing ductility, steel 5 is therefore alloyed with elements improving the post tempering condition such as Cr, Ni, Mo, and additionally Cu. A good weldability is given<sup>[29–31]</sup> and the relatively high amount of C of 0.17% combined with 2.3% of manganese enables a product with full martensitic strength.

For the deformation experiments, dilatometer samples were manufactured from industrially available material via wire-eroding with dimensions of 10 mm length and a diameter of 5 mm. In the following, tungsten platelets were utilized in order to reduce the thermal flow between the sample and the deformation stamp and a “type S” thermocouple was mounted on the sample to determine the sample temperature during deformation.

**Table 1.** Chemical composition of the steels investigated [m%].

Steel	Description	C	Mn	Cr	Ni	Mo	Cu	V	Ti	Nb	B
1	Mild steel	0.15	1.1	0.02	<0.01	0.01	0.01	<0.01	<0.01	<0.01	<0.001
2	Mild steel + Cr	0.15	1.2	1.20	<0.01	0.01	0.01	<0.01	<0.01	<0.01	<0.001
3	Mild steel + Nb	0.15	1.1	0.02	<0.01	0.01	0.03	<0.01	<0.01	0.01	<0.001
4	Hardenable steel	0.17	2.3	0.30	<0.01	0.01	0.08	<0.01	0.02	<0.01	0.002
5	Hardenable steel + MAE	0.17	1.4	0.70	1.0	0.50	0.45	0.05	0.02	0.04	<0.001

### 2.2. Sample Preparation and Determination of the PAG

The preparation of the samples is identical for all following analysis procedures. The specimens were hot embedded and then ground from 320 grit to 4000 grit SiC paper for at least 30 s. Subsequently, the samples were polished with 3 μm diamond paste for at least 3 min and with 1 μm for 30 s. For the metallographic investigation, a picric acid etchant was used to reveal the PAGs after direct quenching. A specially developed etching process was applied, which is described in detail elsewhere,<sup>[32]</sup> based on the picric acid presented by Bechet-Beaujard in 1955.<sup>[33]</sup> The etchant was modified by sodium dodecyl sulfate as wetting agent and performed at room temperature. Yet, selected samples were treated in a heated etching solution at 70 °C to enhance the emerge of the PAGs. For the evaluation of the grain sizes, the image analysis software “Olympus Stream” was used to determine the equivalent grain diameter. The width to height ratio of the grain was used to calculate the aspect ratio. The detailed description of the method can be found in ref.<sup>[32]</sup>

### 2.3. Dilatometer Experiments and Characterization of the Recrystallization Behavior

In order to investigate the SRX including the determination of the  $T_{NR}$ , which is of major interest regarding the design of TM steels, double hit experiments are the method of choice. This relatively straightforward technique allows a detailed sequencing of different alloyed steels regarding their recrystallization behavior. The test procedure consists of a sequence of six segments<sup>[14]</sup>: After solution annealing (1) the samples are cooled to the deformation temperature (2), and compressed with a selected strain rate and strain (3). Followed by a variable interpass time  $t_i$  (4), the specimen is deformed with a set of given parameters (5). Finally, the percentage of recrystallized fraction, respectively, fractional softening (FS) is determined (6). To analyze double-hit deformation test data, literature describes four main methods: the 0.2% and 2% offset method, the 5% strain method, the back-extrapolation method and mean flow stress method.<sup>[4,14,34–36]</sup> Due to the fact, that the 5% strain method enables an uncomplex and unambiguous evaluation of the obtained data, this method was chosen for this study. It avoids the extrapolation of the recorded curve which can lead to a misinterpretation as the first incline of the slope can be influenced by the immediate contact of the deformation stamps. Furthermore, the 5% true strain is large enough to exclude the effects of recovery, as the determined softening is controlled by

recrystallization. The extraction of the values is illustrated in **Figure 1**. The fractional softening is calculated according to Equation (1), wherein  $\sigma_{m,5\%TS}$  is the flow stress at 5% true strain of a hypothetical second curve corresponding to zero softening.  $\sigma_{0,5\%TS}$  is the stress at 5% true strain of the first deformation,  $\sigma_{r,5\%TS}$  at the second deformation.

$$FS = \frac{\sigma_{m,5\%TS} - \sigma_{r,5\%TS}}{\sigma_{m,5\%TS} - \sigma_{0,5\%TS}} \quad (1)$$

If the calculated softening is plotted against  $t_i$  for a selected temperature, the Johnson-Mehl-Avrami fit can be applied to model the recrystallization kinetics. Palmiere et al. stated, that 20% of the  $FS$  can be attributed to recovery.<sup>[25,37,38]</sup> Consequently, softening above 20% is related to SRX. Nevertheless, the present work will continue the convention using the term *fractional softening* in analogy with restriction to the recrystallized fraction,<sup>[17,18]</sup> as this fact plays a decisive role sequencing different steels concerning their recrystallization behavior. An absolute confidence about the recrystallized fraction only is gained with a corresponding metallographic analysis. Nevertheless, the effort to analyze each individual sample would exceed the benefits by far and bring the methodology to analyze the SRX behavior via flow stress curves in question.

In a set of experiments, the combination of both, deformation and subsequent metallographic analysis was realized. The scientific issue is, how accurately characteristic elements such as a decline of a stress-strain curve, which is associated with a DRX as can be seen in **Figure 2**, can be visualized in the microstructure. The sequence of deformation chosen for this study can be reconstructed by the flow stress curve displayed in **Figure 2** with an overall deformation of  $\phi = 1.0$ . These flow stress curves of steel 4 and 5 were split in deformations of  $\phi = 0.2, 0.4, 0.6,$  and  $0.8$  in order to study the microstructural evolution at these stages of deformation. After the samples were subjected to solution annealing of 5 min at 1250 °C they were cooled to deformation

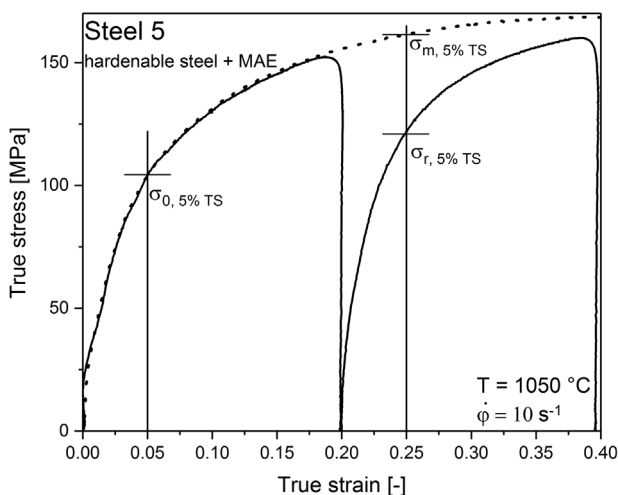


**Figure 1.** Exemplary calculation of the fractional softening with the 5% True Strain Method on steel 5 at 1050 °C.

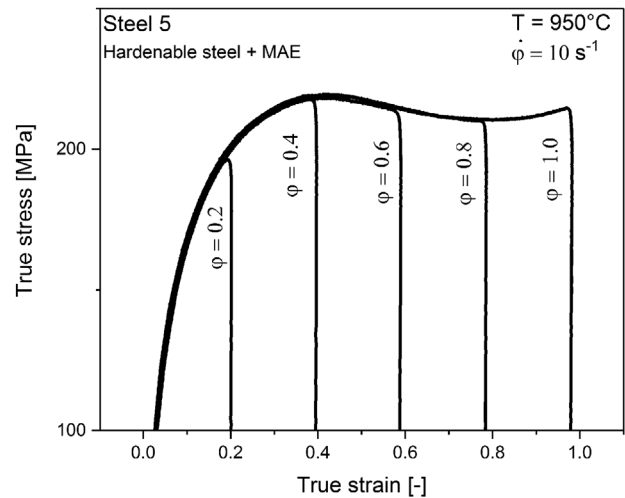


**Figure 2.** True stress–strain curves of steel 5 deformed at 950 °C with  $\phi = 0.2, 0.4, 0.6, 0.8,$  and  $1.0$  to study the microstructural condition at different degrees of deformation.

temperatures of 950 and 1000 °C, respectively. After deformation, the samples were immediately quenched in order to preserve the austenite grain condition.

To describe the yield stress in terms of temperature and strain rate, the Zener-Hollomon parameter (Equation (2)) is plotted to show the relation between strain rate and temperature on the flow stress curve.<sup>[39,40]</sup>

$$Z = f(k_f) = A^* \sin h(a^* k_f)^n \quad (2)$$

The deformation procedure of the two selected steels (steel 4 and steel 5) involved solution annealing at 1250 °C and subsequent forming at 850, 900, 950, and 1000 °C, respectively, at four different strain rates  $\phi = 0.01, 0.1, 1.0,$  and  $10$ .

This hyperbolic equation contains  $A, a$  and  $n$  as material-specific constants dependent on a corresponding strain value,  $k_f$  is the maximum of the flow stress curve. After substitution of  $f(k_f)$  and using the natural logarithm, Equation (3) arises with the relationship for  $k_f$

$$\ln(\phi) + \frac{Q}{RT} = \ln(A) + n^* \ln(\sin h(a^* k_f)) \quad (3)$$

A linear regression of the double log depiction of  $\ln(\phi)$  on the maximum of the true stress–strain curve  $\ln(k_f)$  and the single logarithmic representation of  $\ln(\phi)$  and  $k_f$  based on the least squares method, provides the material-specific constants. A partial integration of Equation (3) at constant strain rate delivers the activation energy  $Q$  (4):

$$Q = R^* n \left[ \frac{d \ln(\sin h(a^* k_f))}{d \frac{1}{T}} \right] \quad (4)$$

The calculated activation energy is used to demonstrate the influence of alloying elements on the underlying microstructural processes such as grain refinement.

In order to study the microstructural development during hot rolling of a TM-steel, a hypothetical milling process was chosen according to **Table 2** to investigate the austenite grain condition between the different rolling steps. The deformation degree decreases during rolling as the deformation resistance increases with declining temperature. The time between the rolling passes decreases as the hot strip extends in length which consequently leads to an enhancing deformation rate. Due to limitations of the deformation dilatometer, the deformation rate was kept constant at  $\dot{\varphi} = 10$ . Although, recrystallization processes are dependent on the deformation rate, the corresponding influence was classified as marginal and thus neglected in this study. After the corresponding deformation, the samples were immediately quenched in order to preserve the austenitic grain structure and adjust the martensitic grain structure intended for these steels. Due to the fact that in a milling process with subsequent quenching, the impact of water occurs delayed, after the last deformation step a holding time of 3 s was realized.

### 3. Results

#### 3.1. Static Recrystallization Behavior and Softening

The fractional softening of steel 1–5 was analyzed using the 5% true strain method described in the previous chapter. The FS of steel 1–4 was studied at 850–1000 °C, whereas steel 5 was evaluated at 900–1050 °C due to the fact that its micro-alloying and its resulting retarded recrystallization made an investigation below 900 °C not conductive. The double-hit experiments for the five different steels investigated showed the softening behavior displayed in **Figure 3a–e**. Steel 1 (**Figure 3a**) shows a clearly defined softening/static recrystallization behavior. Even at relatively low temperatures of 850 °C softening starts within seconds. Steel 2 (**Figure 3b**) behaves similar, however the recrystallization at 850 °C seems slower. **Figure 3c** illustrates the significant influence of Nb on the softening behavior of steel 3. Already the 50%-softening at 950 and 1000 °C is shifted by a factor of 10. At 900 °C the recrystallization is already slowed down so much, that especially in a hot strip mill with interpass times of a few seconds full static recrystallization does not occur. At 850 °C, recrystallization processes are suppressed so far, that a probable softening rather can be attributed to recovery. **Figure 3d** displays the softening of steel 4, with an interesting fit of the recrystallization behavior. The elevated Mn content possesses no influence on the softening, when compared to the mild steels. Although these differences are not significant, it

**Table 2.** Deformation sequence performed at a deformation Dilatometer Bähr 805 A/D to investigate the microstructural evolution of steel 4 and 5.

Deformation step/parameter	1	2	3	4	5
$\varphi$ [–]	0.25	0.25	0.15	0.15	0.1
$\dot{\varphi}$ [s <sup>−2</sup> ]	10	10	10	10	10
T [°C]	1000	950	925	900	875
T [s]	2.5	2	1.5	1.5	(3)

seems that above 900 °C the softening proceeds even faster than in mild steels, whereas at 850 °C it is clearly reduced. For steel 5 (**Figure 3e**) an examination at 850 °C was omitted since the recrystallization at 900 °C was already reduced immensely, that below this temperature softening processes are not expected. The softening distribution of steels 5 exhibits plateaus between temperatures of 1000 and 1050 °C.

#### 3.2. Dynamic Recrystallization and Corresponding Grain Size Analysis

The true stress–strain curves reveal material specific peculiarities, which can be indicative for a softening due to recovery or recrystallization. Steels 4 and 5 are classified as ultra-high strength steels, but are – due to varying applications – differently alloyed. In order to study their different recrystallization, in particular DRX, the microstructure of steel 4 and 5 was investigated following the deformation procedure described in section 2.3. **Figure 4** displays the flow stress curve of steel 4 (black curves) and steel 5 (red curves) at a temperature of 950 °C (dashed line) and 1000 °C (dotted line), respectively. The peaks, which are supposed to be an indication for the beginning of DRX are slightly shifted; the peak of Steel 4 is located at a strain of  $\varphi < 0.4$  at 1000 °C, whereas the onset of the DRX at 950 °C of steel 4 is shifted toward a higher strain  $\varphi > 0.4$ . Moreover, steel 4 responds both at 950 and 1000 °C with a more pronounced decline of the stress curve on the applied deformation than steel 5, which can be explained by a more significant softening due to DRX processes.

The light-optical images (**Figure 5a–c**) demonstrate the microstructural evolution of steel 5 with respect to the imposed deformation according to **Figure 2**. The mean grain size after solution annealing of 5 min at 1250 °C was 38 μm. With increasing deformation, the austenite grain elongates perpendicular to the axis of compression. At the peak of the flow stress curve ( $\varphi = 0.4$ ), the corresponding microstructure reveals zones of recrystallized grains. The grain size analysis (**Figure 6**) confirms this fact as the grain size distribution is shifted to smaller grain sizes. According to both light – optical analysis and the subsequent grain size investigation, full recrystallization of the austenite grain is reached at  $\varphi = 0.8$ , where the flow stress curve reaches a saturation level.

The different recrystallization behavior of steel 4 and 5 moreover is reflected by the evolution of the PAG aspect ratio displayed in **Figure 7** for two different temperatures, 950 and 1000 °C. With increasing deformation, the aspect ratio rises for both, steel 4 and 5. However, steel 4 possesses a very globular grain throughout the whole deformation. The aspect ratio does not exceed values above 1.5, at  $\varphi = 0.4$  it shows a maximum, and decreases to values of  $\approx 1$ . This trend coincides with the progression of the flow stress curve (**Figure 4**). At 950 °C an aspect ratio of 1.17 remains, whereas at 1000 °C the aspect ratio is reduced to 1.06. Steel 5, however behaves different. At 950 °C, the aspect ratio develops to a maximum at  $\varphi = 0.8$  and falls subsequently to a value of 1.98 at  $\varphi = 1.0$ . In contrast to the evolution at 950 °C, the development of the aspect ratio at 1000 °C shows only an increase till  $\varphi = 0.6$ . The recrystallization is obviously accelerated to lower deformations. The light-optical

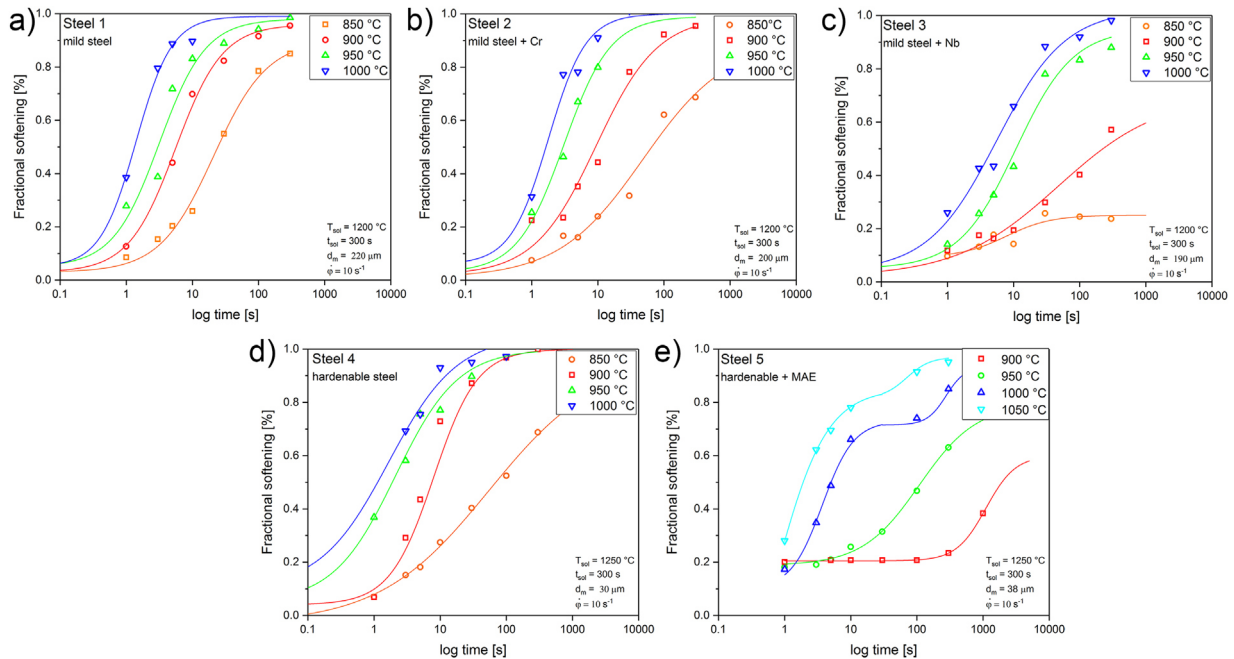


**Figure 3.** Fractional softening of Steel 1–5; Steel 1–4 were analyzed at 850–1000 °C, steel 5 at 900–1050 °C as an investigation below this temperature is due to its micro-alloying and the resulting retarded recrystallization not conducive.

images (Figure 8a–d) reflect, that compared to steel 5, steel 4 reveals no increased pancaking toward higher deformations, even at high deformations the PAGs exhibit a globular shape. The corresponding grain sizes at a deformation of  $\phi = 0.2$  are measured with 24  $\mu\text{m}$  at 950 °C (Figure 8a) and 10  $\mu\text{m}$  at 1000 °C (Figure 8c). The mean grain sizes decrease at both temperatures with increasing deformation of  $\phi = 0.8$  down to 7  $\mu\text{m}$  (950 °C – Figure 8b) and 10  $\mu\text{m}$  (1000 °C – Figure 8d), respectively.

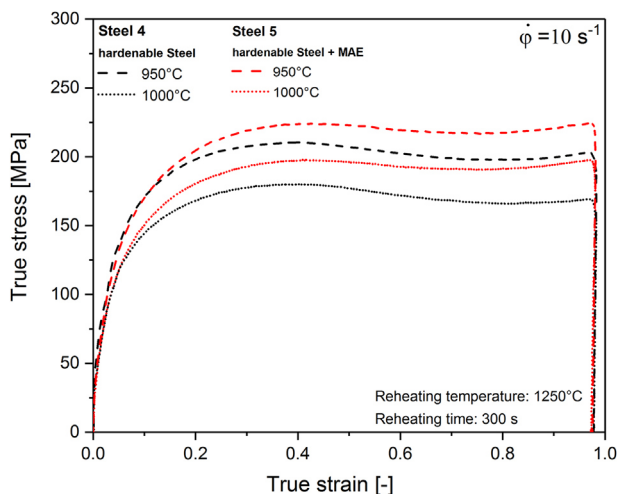


**Figure 4.** True stress–strain curve of steel 4 and steel 5 at  $T = 950$  and  $1000$  °C, showing their different DRX behavior. Steel 4 exhibits a more pronounced DRX indicated by the noticeable decline of the (black) curve after the peak stress.

### 3.3. Calculation of the Activation Energy for the Initiation of DRX

Figure 9 demonstrates the evaluation of the Zener-Hollomon parameter and the activation energy of steel 4 and 6. The determination is based on the evaluation of flow stress maxima  $k_f \text{ max}$  at four different temperatures between 850 and 1000 °C and strain rates of  $\phi = 0.01, 0.1, 1.0,$  and  $10$ . Figure 9a provides the relationship between  $k_f \text{ max}$  and  $\phi$  for steel 4 at the different temperatures. The material specific constants were determined with  $n = 6.7782$  and  $a = 0.00675 \text{ MPa}^{-1}$ . For steel 5, (Figure 9b) the constants are calculated as follows:  $n = 8.5257$  and  $a = 0.00595 \text{ MPa}^{-1}$ . Figure 9c demonstrates the relationship between the flow stress  $k_f$  as a function of the Zener-Hollomon parameter  $Z$  for both steels investigated. Following this approach, the values for  $Q$  were deduced which amounts  $Q = 199 \text{ kJ K}^{-1} \text{ mol}^{-1}$  for steel 4 and  $256 \text{ kJ K}^{-1} \text{ mol}^{-1}$  for steel 5.

### 3.4. Grain Size Evolution during Rolling-Like t-T- $\phi$ Cycles

After deforming steel 4 and steel 5 following a hot rolling scheme (Table 2), the grain size distributions as depicted in Figure 10 were detected. The grain size range of steel 4 is spread over a limited area, whereas steel 5 possesses a wider size distribution. With increasing deformation, steel 4 in general develops smaller size partitions. The mean grain sizes of steel 5 trend to smaller fractions with increasing deformation as well, that means, large grains recrystallize

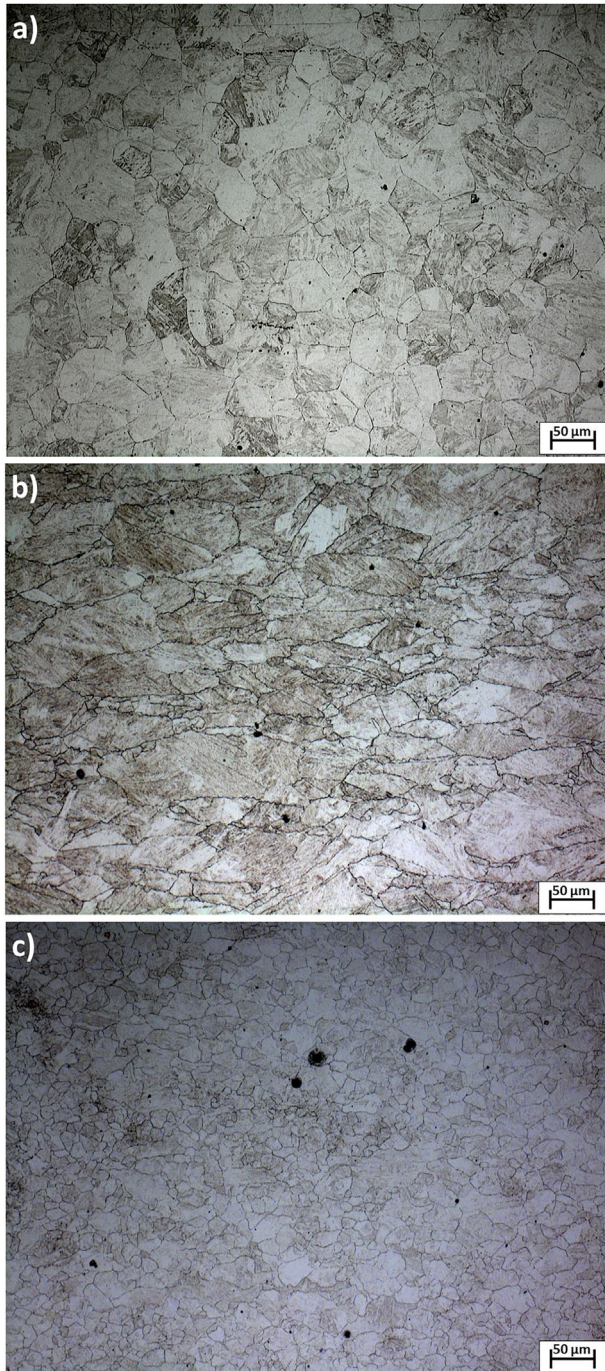


**Figure 5.** PAG microstructure of steel 5, austenite grains visualized with a picric-acid etchant. a) After solution annealing at 1250 °C for 5 min, (b) after a deformation of  $\phi = 0.4$  at 1000 °C, (c) fully recrystallized after a deformation of  $\phi = 0.8$  at 1000 °C.

in favor of smaller ones. Nevertheless, the mean grain sizes do not reach the magnitude of steel 4. Figure 10c provides an overview of the development of the microstructural characteristics. For both steels, the aspect ratio increases in general with growing deformation, whereas the mean grain sizes decrease.

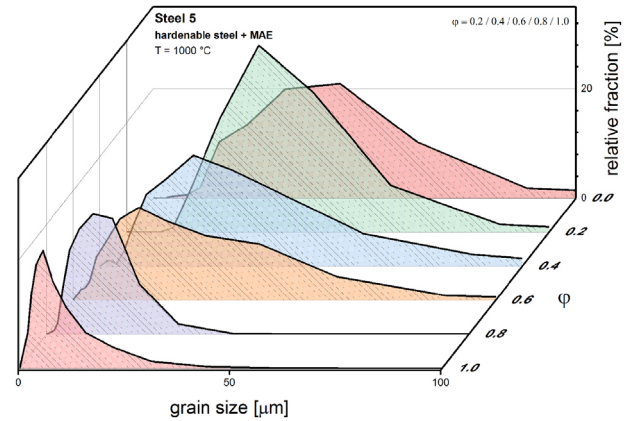


**Figure 6.** Grain size evolution after deformations of  $\phi = 0.2, 0.4, 0.6, 0.8,$  and 1.0 at 1000 °C. With increasing deformation, the grain size distribution shifts to smaller grain sizes. At  $\phi = 0.8$  the microstructure is fully recrystallized.

## 4. Discussion

### 4.1. Static Recrystallization Behavior and Fractional Softening

Double-hit experiments provided an extended survey of the softening and thus the static recrystallization behavior of the investigated low-C steels. This analysis enables a sequencing of the steels investigated regarding their different alloying elements. **Figure 11a–d** demonstrate the softening of the different steels arranged parallel at the individual temperatures of 850–1000 °C. Mild steel 1 and 2 possess a continuous fast SRX behavior. Despite the content of transformation retarding elements present in steel 4, its SRX behavior matches the behavior of mild steels. The increased levels of both Si and Mn

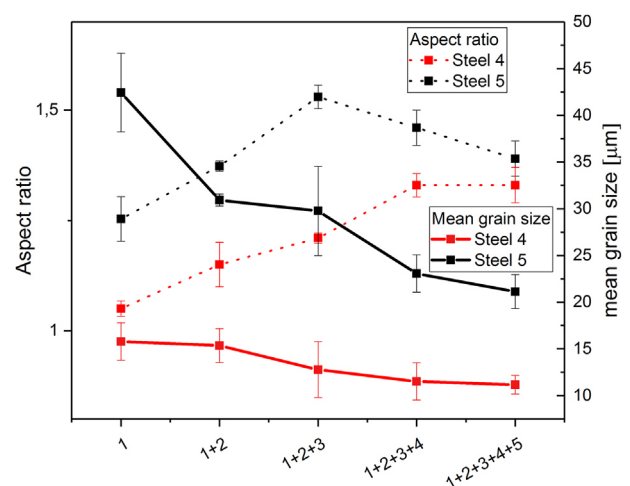


**Figure 7.** Elongation of the PAGs dependent on the deformation for steel 4 and 5. At 1000 °C and a deformation of  $\phi = 0.8$  the value for elongation of steel 5 descends to almost 1, confirming the recrystallized microstructure. At 950 °C the elongation increases with no significant full recrystallization due to the recrystallization retarding elements.

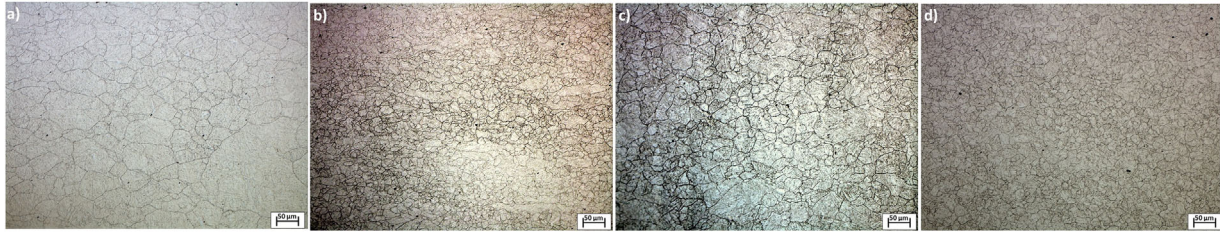


**Figure 8.** Light-optical images of steel 4–PAGs etched with a picric acid etchant, showing the microstructural evolution at deformation of a)  $\phi = 0.2$ , (b)  $\phi = 0.8$  at  $950\text{ }^{\circ}\text{C}$  and deformations of (c)  $\phi = 0.2$ , and (d)  $\phi = 0.8$  at  $1000\text{ }^{\circ}\text{C}$ .

apparently do not affect the SRX, although Medina et al. have reported a minimal influence.<sup>[41]</sup> Also, Ti seems not to affect SRX although Ti is known to possess high potential to elevate the  $T_{NR}$  in retarding the recrystallization.<sup>[7,16]</sup> A major function of Ti however, is revealed in regarding the grain sizes after solution annealing. Whereas the variants which are dispensed with Ti show a high potential to grain growth at  $1200\text{ }^{\circ}\text{C}$ , in opposite, the Ti variants, steel 4 and 5 still reveal relatively small grain sizes despite a higher solution annealing temperature of  $1250\text{ }^{\circ}\text{C}$ .

The effect of Nb on the SRX is more pronounced and thus clearly visible in the diagrams. A surcharge of  $0.01\%$  Nb in steel 3 results in a similar recrystallization behavior as this of the microalloyed hardenable variant, steel 5. Steel 5, furthermore forms plateaus at  $1000\text{ }^{\circ}\text{C}$  (Figure 11d) and  $1050\text{ }^{\circ}\text{C}$  (Figure 3f). This is an indication to the formation of strain induced precipitations, (VC and TiC), which delay the recrystallization. The amount of V however is very little ( $0.05\%$ ) and this phenomenon is not very pronounced at the other temperatures. Thus, it can be presumed that strain induced precipitations need to be attributed to NbC or TiC. For proofing this hypothesis, TEM investigation would be required.

#### 4.2. Grain Size Analysis after Deformation and DRX Behavior

Steel 4 and 5 were imposed to different deformations in order to investigate the microstructural development during deformation. The first set of deformations was performed at a constant temperature, yet different degrees of deformation. The second set contained a laboratory scale rolling-like t-T-  $\phi$  cycle. These investigations provided an interesting insight into the development of the microstructure. From the true stress curves (Figure 4) a maximum of the DRX at the peak point of  $\phi \approx 0.4$  and a saturation region of the DRX at  $\phi \approx 0.8$  can be expected. For both steels, the corresponding microstructure however showed differences in their progression at  $950$  and  $1000\text{ }^{\circ}\text{C}$ . It is evident, that the flow stress curve of both steels behave approximately congruent. The niveau of their corresponding flow stress curve is shifted upwards with descending temperature as the deformation resistance increases with decreasing temperature. Nevertheless, comparing the yield stress curves of the two steels, it is obvious, that they behave differently in their further progression as they possess a different recrystallization behavior due to their different alloy contents. At the individual temperatures, the gradient of the curves coincides

for both temperatures which indicates, that both steels exhibit similar strength. However, the stress-inclination of steel 4 declines earlier as softening processes are in progress, whereas the stress level of steel 5 rises higher as the incorporated MAE prevent a preliminary softening. Besides this accelerated creeping of steel 4, the overall appearance of the similar flow stress curves could be taken to imply that the recrystallization processes between the steels behave similar. Although it is common to declare the onset of the DRX with the relatively easy-to-interpret peak value, literature agrees, that the start of the DRX at this point is already in progress.<sup>[42,43]</sup> More precisely is the inflection point of the flow stress curve to be classified as the onset of DRX.<sup>[44,45]</sup> Both steels first show a significant peak and then reach a saturation level, at  $950^{\circ}$  as well as at  $1000^{\circ}\text{C}$ . However, the corresponding metallographic analysis demonstrates, that steel 4 which exhibits an initial grain size after annealing of  $30\text{ }\mu\text{m}$  already recrystallizes to a grain size of  $10\text{ }\mu\text{m}$  after deforming with  $\phi = 0.2$  at  $1000\text{ }^{\circ}\text{C}$ . Steel 5 though, which exhibits an initial grain size of  $37\text{ }\mu\text{m}$  starts not before  $\phi = 0.4$  with small recrystallized spots. The elongated austenite grain and zones of smaller globular grains, whose presence are indicative for an active recrystallization, can be seen in Figure 8b. The shift of the peaks presents a clear change in the microstructure through ongoing microstructural processes. The PAGs of the sample deformed with  $\phi = 0.8$  at  $1000\text{ }^{\circ}\text{C}$  (Figure 8c) illustrate, that the microstructure is fully recrystallized at this state of deformation. The grain size distribution represents a limited area of existence far below the initial grain size. With increasing deformation ( $\phi = 1.0$ ) the grain partitions are yet recrystallized and thus smaller in size, but rise in their aspect ratio. The deformation at  $950\text{ }^{\circ}\text{C}$  delivered quite different findings concerning the microstructural processes. At  $\phi = 0.4$ , some small grain fractions are recognizable, whose proportion increases constantly up to  $\phi = 0.8$ . However, full DRX was not accomplished. The empirical determination of  $T_{NR}$  with the Boratto equation<sup>[11]</sup> delivers a value of  $993\text{ }^{\circ}\text{C}$ . This value would coincide with the softening curves (Figure 11c, d), as between  $950$  and  $1000\text{ }^{\circ}\text{C}$  a significant gap in the static recrystallization kinetics is visible. However, the determination of  $T_{NR}$  with the Boratto equation needs to be accepted with reservation, as it does not include the effect of Mo. Mo is known to influence the  $T_{NR}$  and retard the recrystallization significantly.<sup>[46]</sup>

In order to extend the observed feature to the DRX, the investigations demonstrate, that below  $1000\text{ }^{\circ}\text{C}$  a fully dynamic recrystallization only can be accomplished with very high deformations ( $>\phi = 1.0$ ). This fact again stands in conflict with



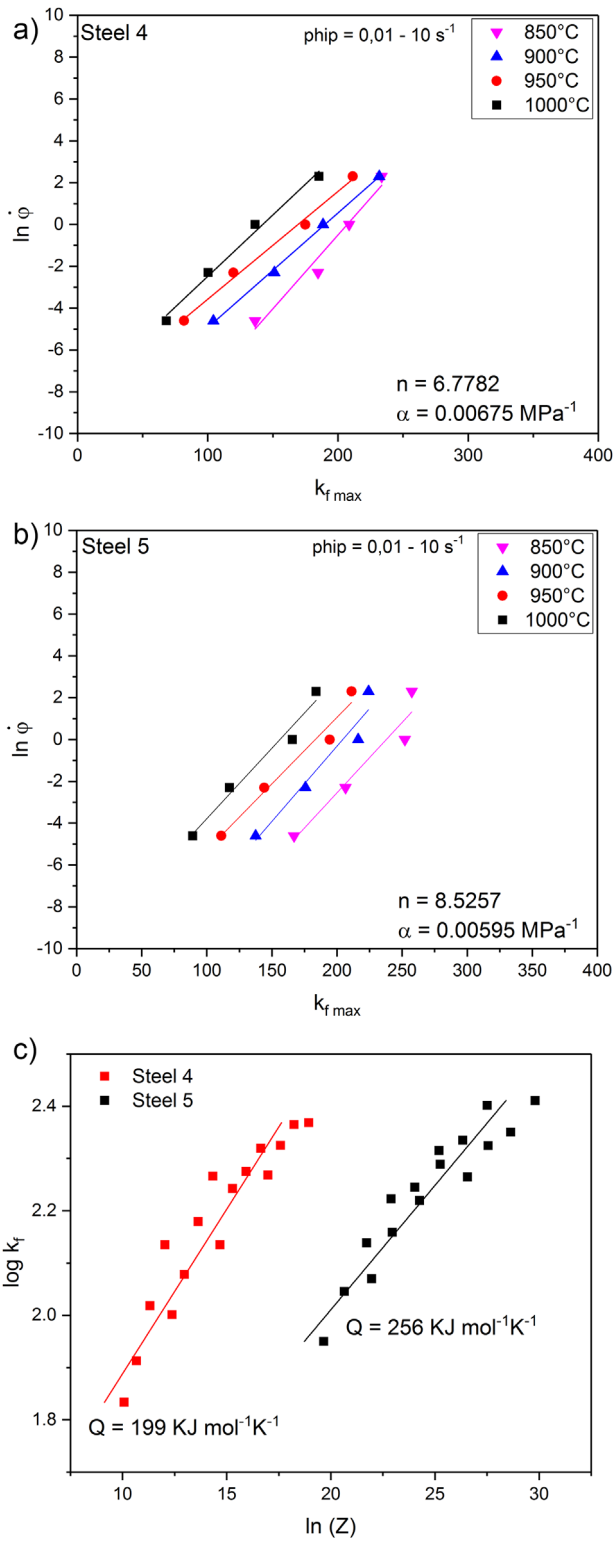


**Figure 9.** Correlation between  $k_f$  and strain rate at different temperatures of (a) steel 4 and (b) steel 5. c) The flow stress  $k_f$  is plotted as function of the Zener-Hollomon parameter  $Z$  for steel 4 and steel 5.

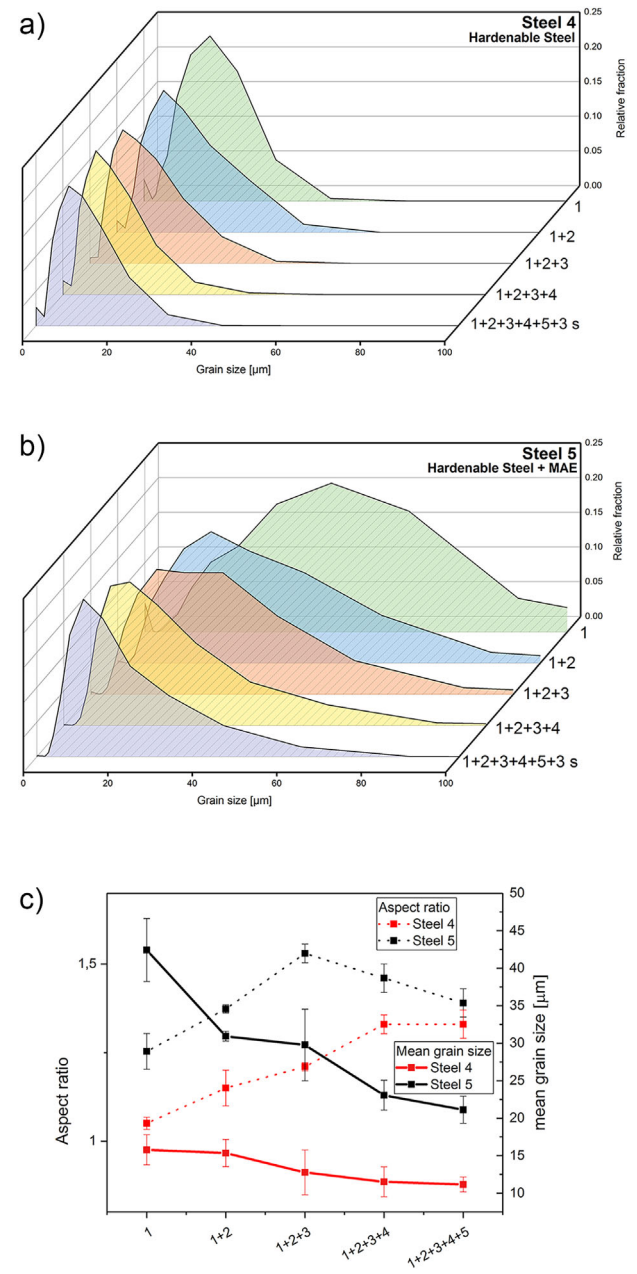


**Figure 10.** Grain size evolution after deformation according to the simulated milling process of a) steel 4 and (b) steel 5. c) Evolution of the mean grain size and aspect ratio for both steels.

the peculiarities of the flow stress curve, in which the saturation regime might lead to the assumption that a DRX is present. As discussed, steel 4 responds with a significantly accelerated recrystallization due to the reduced micro-alloying elements. Already at  $\phi = 0.2$  a clear grain refining occurs, compared to the initial state. Since steel 4 demonstrated to be very receptive for recrystallization especially in the static softening (Figure 3d and 11a–d), the small deformation of  $\phi = 0.2$  in the immediate moment before quenching could have led to recrystallization. Nevertheless, differences in the microstructure are also evident,

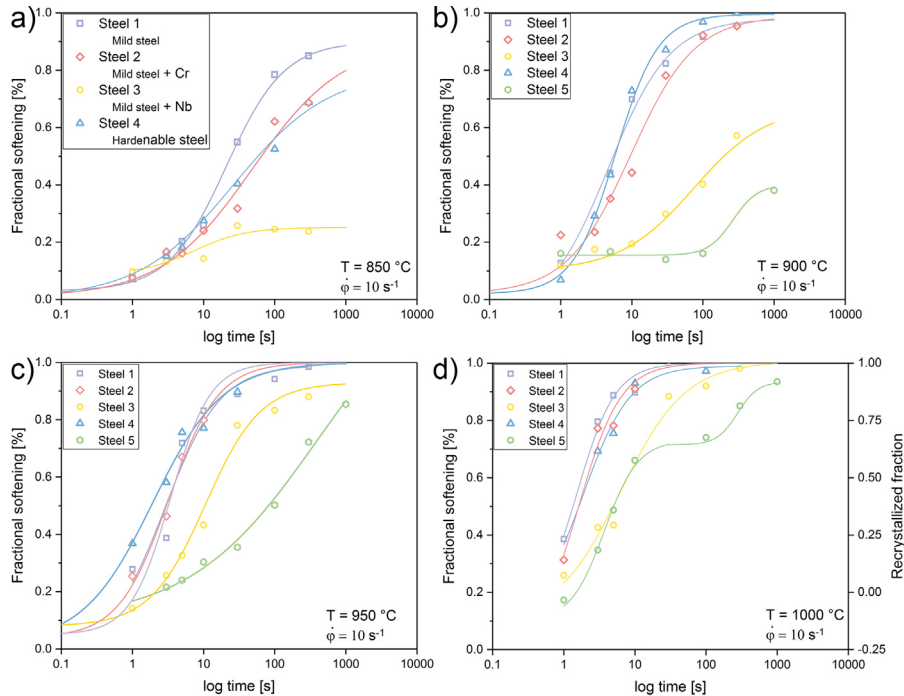


**Figure 11.** Fractional softening of Steel 1–5 sorted in the investigated temperatures of (a) 850 °C, (b) 900 °C, (c) 950 °C, and (d) 1000 °C.

as the grains are much finer at 1000 °C than at 950 °C. With increasing deformations, the grain evolution behaves almost identical for both temperatures. At 950 °C the grain size ( $\approx 7 \mu\text{m}$ ) decreases in favor of a consistent aspect ratio (1.25), while at 1000 °C a globular grain remains, marginally enlarged in size ( $\approx 10 \mu\text{m}$ ). These findings confirm the prevailing DRX processes that result in complete recrystallization at both temperatures. At 1000 °C the temperature is high enough to activate the complete globularization of the grain with a tendency to grain enlargement, whereas at 950 °C the temperature is enough to initiate grain refinement, yet leaves a remaining aspect ratio.

These findings are supported by the investigations on the Zener-Holomon parameter and the activation energy. The accelerated recrystallization of steel 4 due to the reduced content of microalloying elements is expressed by the value of the activation energy  $Q$ , which is  $199 \text{ kJ K}^{-1} \text{ mol}^{-1}$ . In contrast, steel 5 possesses a higher activation energy for DRX of  $256 \text{ kJ K}^{-1} \text{ mol}^{-1}$ . This confirms the retarded recrystallization of steel 5 as visualized in the previous microstructural analysis. According to the correlation between  $Q$  and the chemical composition of Nb alloyed steels:

$$Q_{\text{def}} = 297 + 6412[\% \text{Nb}] + 123[\% \text{Mo}] + 1[\% \text{Ni}] - 111[\% \text{Cr}] \quad (5)$$

proposed by Jonas et al.,<sup>[47]</sup> the calculated activation energy for steel 5 amounts  $288 \text{ kJ K}^{-1} \text{ mol}^{-1}$ . This value is slightly higher than the experimentally determined. This difference, however, can be related to the influence of V and Ti, which is not included in this equation.

The comparison of the microstructural evolution after both steels were subjected to a hypothetical rolling process, provided an insight into the different grain refinement behavior. Both steels

show a clear grain-refinement tendency as a result of the successive deformation steps (Figure 10a–c). However, in the case of steel 5, recrystallization is not complete. During the first two deforming steps, the grain aspect ratio increases, whereas subsequent deformations steps result in a decrease of the grain aspect ratio and grain size. Only after this degree of deformation, it appears, that enough energy has been induced to initiate at least a partial recrystallization. Steel 4 obviously recrystallizes after each deformation step. After the third step the remaining aspect ratio is elevated and differs just weakly in value from steel 5. An inauguration of the microstructure after etching the PAGs with a picric-acid etchant indicate, that the aspect ratio of steel 4 is distributed over the whole aggregation of grains. The aspect ratio calculated for steel 5 is concentrated on several big grains, whereas the microstructure possesses areas of a high amount of globular recrystallized grains which possess an aspect ratio of 1. These grains compensate the high aspect ratio of the bigger grains.

## 5. Summary

The main findings are summarized in the following:

- 1) Double-hit deformation tests performed on a dilatometer showed the softening behavior of 3 mild and 2 hardenable steels with different alloying contents. A significant gap in the SRX behavior between the Nb or V alloyed and the plain carbon steels gap could be shown. Mn and Cr, which retard the  $\gamma$  to  $\alpha$  transformation do not have any influence on the SRX behavior.
- 2) Sequenced deformations were performed to reproduce the different microstructural stages of a flow stress curve

metallographically. Is it shown, that characteristic peculiarities of a stress strain curve such as an evident peak or a saturation regime, which can be associated with microstructural features need to be interpreted with reservation. In specific, DRX can be initiated already before the inflection point of the inclining curve and a saturation regime does not necessarily mean a full recrystallization due to DRX.

- 3) Deformations with different deformation parameters ( $T$  and  $\epsilon$ ) on two UHSS steels showed the influence of MAE on the activation energy of DRX. These findings coincide with the metallographic analysis of the investigated steels, micro-alloying leads to a reduced recrystallization visible in the microstructure. The corresponding activation energy for DRX is increased.
- 4) A rolling scenario was performed on a dilatometer on two ultra-high strength steels and the microstructure development at the different deformation steps was investigated. Although both steels show the same carbon content, the particular steel dispensed with MAE recrystallizes continuously to a homogenous globular austenite grain. The second steel, alloyed with recrystallization retarding elements, such as V and Nb generated a pancaked austenite grain with wide grain size distributions.

## Acknowledgement

Funding of the Austrian BMVIT (846933) in the framework of the program "Production of the future" and the "BMVIT Professorship for Industry" was gratefully acknowledged.

## Conflict of Interest

The authors declare no conflict of interest.

## Keywords

double-hit deformation, micro-alloying, pilot rolling scenario, recrystallization, ultra-high strength steels

Received: September 24, 2018

Revised: November 27, 2018

Published online: January 2, 2019

- 
- [1] A. A. Barani, F. Li, P. Romano, D. Ponge, D. Raabe, *Mater. Sci. Eng. A* **2007**, 463, 138.
  - [2] M. Klein, R. Rauch, H. Spindler, P. Stiaszny, *BHM Berg- Hüttenmänn. Monatshefte* **2012**, 157, 108.
  - [3] T. Gladman, *The Physical Metallurgy of Microalloyed Steels*, Institute of Materials, London **1997**.
  - [4] S. Vervynck, K. Verbeken, B. Lopez, J. J. Jonas, *Int. Mater. Rev.* **2012**, 57, 187.
  - [5] L. J. Cuddy, in *Proc. 1981 Thermomechanical Processing of Microalloyed Austenite*, TMS-AIME, Warrendale, PA, **1981**, pp. 129–140.
  - [6] S. S. Hansen, J. B. V. Sande, M. Cohen, *Metall. Trans. A* **1980**, 11, 387.
  - [7] H. Adrian, F. B. Pickering, *Mater. Sci. Technol.* **1991**, 7, 176.
  - [8] R. Lagneborg, T. Siwecki, S. Zajac, B. Hutchinson, *Scand. J. Met.* **1999**, 28, 186.
  - [9] R. J. Glodowski, in *Rev. International Seminar 2005 on Application Technologies of Vanadium in Flat—Rolled Steels*, Vanitec: Suzhou, China, **2005**, 43–51.
  - [10] H. J. Jun, J. S. Kang, D. H. Seo, K. B. Kang, C. G. Park, *Mater. Sci. Eng. A* **2006**, 422, 157.
  - [11] R. Barbosa, F. Boratto, S. Yue, J. J. Jonas, in *Proc. of the International Conference on Processing Microstructure and Properties of HSLA Steels*, The Mineral, Metals and Materials Society, Pittsburgh (PA), **1987**, pp. 51–56.
  - [12] S.-H. Cho, K.-B. Kang, J. J. Jonas, *Mater. Sci. Technol.* **2002**, 18, 389.
  - [13] D. T. Llewellyn, R. C. Hudd, *Steels: Metallurgy and Applications*, 3rd ed., Butterworth-Heinemann, Oxford [England]; Woburn, MA **1998**.
  - [14] C. N. Homsher, PhD Thesis, Colorado School of Mines, **2013**.
  - [15] Y. C. Lin, M.-S. Chen, J. Zhong, *Comput. Mater. Sci.* **2008**, 44, 316.
  - [16] S. F. Medina, J. E. Mancilla, *Acta Metall. Mater.* **1994**, 42, 3945.
  - [17] H. L. Andrade, M. G. Akben, J. J. Jonas, *Metall. Trans. A* **1983**, 14, **1967**.
  - [18] S. F. Medina, C. A. Hernandez, *Acta Mater.* **1996**, 44, 165.
  - [19] Y. C. Lin, M.-S. Chen, J. Zhong, *J. Mater. Process. Technol.* **2009**, 209, 2477.
  - [20] Y. C. Lin, M.-S. Chen, *Mater. Sci. Eng. A* **2009**, 501, 229.
  - [21] W. P. Sun, E. B. Hawbolt, *ISIJ Int.* **1997**, 37, 1000.
  - [22] A. R. Morgridge, *Bull. Mater. Sci.* **2002**, 25, 291.
  - [23] S. H. Zahiri, P. D. Hodgson, *Mater. Sci. Technol.* **2004**, 20, 458.
  - [24] K. Huang, R. E. Logé, *Mater. Des.* **2016**, 111, 548.
  - [25] W. Roberts, B. Ahlblom, *Acta Metall.* **1978**, 26, 801.
  - [26] Z. Liu, S. Jiao, X. Yuan, W. U. Di, *J. Iron Steel Res. Int.* **2008**, 15, 31.
  - [27] I. Tamura, *Thermomechanical Processing of High-Strength Low-Alloy Steels*, Butterworths, London, Boston **1988**.
  - [28] G. Gottstein, *Physikalische Grundlagen der Materialkunde*, 3. Aufl., Springer, Berlin **2007**.
  - [29] R. Schnitzer, D. Zügner, P. Haslberger, W. Ernst, E. Kozeschnik, *Sci. Technol. Weld. Joining* **2017**, 22, 536.
  - [30] O. Grong, D. K. Matlock, *Int. Met. Rev.* **1986**, 31, 27.
  - [31] D. J. Abson, R. J. Pargeter, *Int. Met. Rev.* **1986**, 31, 141.
  - [32] R. Esterl, M. Sonnleitner, M. Stadler, G. Wölger, R. Schnitzer, *Pract. Metallogr.* **2018**, 55, 203.
  - [33] S. Bechet, L. Beaujard, *Rev. Met.* **1955**, 52, 830.
  - [34] B. Dutta, C. M. Sellars, *Mater. Sci. Technol.* **1987**, 3, 197.
  - [35] S. F. Medina, *Mater. Sci. Technol.* **1998**, 14, 217.
  - [36] S. F. Medina, A. Quispe, P. Valles, J. L. Bantildeos, *ISIJ Int.* **1999**, 39, 913.
  - [37] O. Kwon, A. J. De Ardo, *Acta Metall. Mater.* **1991**, 39, 529.
  - [38] E. J. Palmiere, C. I. Garcia, A. J. De Ardo, *Metall. Mater. Trans. A* **1996**, 27, 951.
  - [39] J. J. Jonas, C. M. Sellars, W. J. M. Tegart, *Metall. Rev.* **1969**, 14, 1.
  - [40] H. Mirzadeh, J. M. Cabrera, J. M. Prado, A. Najafzadeh, *Mater. Sci. Eng. A* **2011**, 528, 3876.
  - [41] S. F. Medina, A. Quispe, *ISIJ Int.* **2001**, 41, 774.
  - [42] N. D. Ryan, H. J. McQueen, *J. Mater. Process. Technol.* **1990**, 21, 177.
  - [43] S. Solhjo, *Mater. Des.* **2010**, 31, 1360.
  - [44] H. Mecking, U. F. Kocks, *Acta Metall.* **1981**, 29, 1865.
  - [45] E. I. Poliak, J. J. Jonas, *ISIJ Int.* **2003**, 43, 684.
  - [46] B. Pereda, B. Lopez, J. M. Rodriguez-Ibabe, in *Proc. International Conference on Microalloyed Steels: Processing, Microstructure, Properties and Performance*, AIST, Pittsburgh, **2007**, 151-9.
  - [47] S.-H. Cho, K.-B. Kang, J. J. Jonas, *ISIJ Int.* **2001**, 41, 766.

## Paper III:

Esterl R, Sonnleitner M, Schnitzer R (2019)

*Influences of Thermomechanical Treatment and Nb Micro-Alloying on the Hardenability of Ultra-High Strength Steels*

Metallurgical and Materials Transactions A

DOI :10.1007/ s11661-019-05235-8.

# Influences of Thermomechanical Treatment and Nb Micro-alloying on the Hardenability of Ultra-High Strength Steels



RAPHAEL ESTERL, MARKUS SONNLEITNER, and RONALD SCHNITZER

For the construction of mobile crane booms, ultra-high strength steels produced *via* thermomechanical processing (TMP) have widely substituted steels fabricated through the conventional quenching and tempering (Q+T) route. A strong deformation of the austenite grain during hot rolling followed by direct quenching (DQ) offers benefits in terms of strength and toughness. To guarantee an optimal through-hardening, alloying elements retarding the  $\gamma$  to  $\alpha$  transformation are used. To explore the influence of the processing route on the critical cooling rate and the hardenability, hot deformation tests were performed on a deformation dilatometer. Different cooling rates were applied after deformation corresponding to two different rolling cycles with varying finish rolling temperatures (FRTs). The obtained hardness values were compared to those received through conventional quenching after austenitization. These investigations conducted on three steels with varying micro-alloying contents showed that Nb in combination with TMP raises strength significantly, and promotes a bainitic and ferritic transformation in solid solution. When applying low FRTs and in combination with other micro-alloying elements, NbC coarsens and reduces the effect of precipitation hardening.

<https://doi.org/10.1007/s11661-019-05235-8>  
© The Author(s) 2019

## I. INTRODUCTION

IN the recent decades, thermomechanical processing with subsequent direct quenching (TM-DQ) has generated an attractive way to produce ultra-high-strength steels.<sup>[1–6]</sup> Their high demand arises from an improved payload-to-weight ratio for mobile crane applications. The requirements of the user and manufacturer were met through both economic and efficient production routes. The highest strength and proficient toughness as well as good weldability are realized with these steel grades.<sup>[7]</sup> This is accomplished by the systematic combination of an alloying and a rolling schedule in which the recrystallization processes are tuned to achieve a fine-grained austenitic microstructure prior to martensitic transformation. The influence of the condition of the prior austenite grain (PAG) on the properties of the emerging steel product has been investigated in depth.<sup>[8,9]</sup> The dimension of the emerging substructure

such as packets and blocks<sup>[10]</sup> is proportional to the size of the PAGs.<sup>[11]</sup> A decrease in the PAG size results in smaller martensitic constituents.<sup>[12]</sup> Consequently, the Hall–Petch correlation can also be extended on martensitic microstructures. A decrease of the size of the prior  $\gamma$ -grain promotes a strength improvement through the smaller dimensions of martensite. The number of barriers for the movement of dislocations increases, which is followed by a rise in strength. Furthermore, rolling in the nonrecrystallization  $\gamma$ -regime ( $T_{NR}$ ) promotes an elevated number of nucleation sites for the following  $\gamma$  to  $\alpha$  transformation enhancing the grain refining.<sup>[4,8,13]</sup> It has been well established that decreasing the finish rolling temperature improves both strength and toughness.<sup>[6,14–16]</sup> For a further improvement in the strength of these steels, a martensitic transformation is performed by instant quenching.<sup>[4,8,17]</sup> Therefore, alloying elements such as Mn, Cr, Mo, Si, and B come to application, which, in dissolved condition, decelerate the diffusion-controlled  $\gamma$  to  $\alpha$  transformation and enable full martensitic strength.<sup>[18]</sup> During cooling, Mo retards the pro-eutectoid ferrite and perlite transformation<sup>[19]</sup> and prevents the Nb-precipitation to Nb(CN).<sup>[20]</sup> Si, Mn, and Cr decelerate the perlite and bainite transformations through different mechanisms. The role of Si is based on its inhibition to form carbides due to its low solubility in cementite.<sup>[18]</sup> The influence of Cr on the hardenability is less pronounced than the effect of Mn, as Cr requires higher additions to decrease the critical

---

RAPHAEL ESTERL and RONALD SCHNITZER are with the Department of Materials Science, Montanuniversität Leoben, Franz Josef-Str. 18, 8700 Leoben, Austria. Contact e-mail: raphael.esterl@unileoben.ac.at MARKUS SONNLEITNER is with the voestalpine Stahl GmbH, voestalpine-Straße 1, 4020 Linz, Austria.

Manuscript submitted December 14, 2018.

cooling rate,<sup>[21]</sup> yet, like Mo, it counteracts the softening during tempering.<sup>[18,22]</sup> The strongest impact on the hardenability possesses B, which already influences the  $\gamma$  to  $\alpha$  transformation with very low alloying contents.<sup>[23–25]</sup>

It is generally recognized that the critical cooling rate and  $M_S$  are a function of alloying contents and elements.<sup>[20,26]</sup> The influences of several alloying elements retarding the  $\gamma$  to  $\alpha$  transformation have been broadly investigated. Moreover, the influences of the rolling conditions and FRTs on the mechanical properties of the martensitic steel product are largely scientifically explored.<sup>[8,16,17]</sup> Nevertheless, there is a lack of research, if the rolling conditions and especially the FRTs influence both  $M_S$  and hardening characteristics. To investigate the effect of the FRT on the hardenability, a rolling scenario with two different FRTs was performed on a Deformation Dilatometer Bähr 805 A/D. In order to examine, if micro-alloying possesses an effect on the hardenability in combination with different rolling parameters, three different steels were analyzed. In detail, two hardenable steels with different Niobium contents were compared to a hardenable and temper-resistant steel in order to investigate the hardenability depending on different production routes. Steels processed *via* TMP still are in competition to steels produced *via* the classical quenching and tempering (Q+T) route, as manufacturers promote the improved impact strength and better isotropy concerning their mechanical properties of Q+T steels.<sup>[14,27–30]</sup> Therefore, we further intend to compare the hardenability of TM steels to that of the steels produced *via* a traditional Q+T route. In addition, CCT diagrams of the investigated steels will demonstrate the influences of the processing route and the Nb content on the  $\gamma$  to  $\alpha$  phase transformation and the resulting hardness values.

## II. MATERIALS AND EXPERIMENTAL PROCEDURE

### A. Materials Investigated

The investigations on the influence of the TM processing on the hardenability have been conducted on three different steels. The corresponding melts were produced in an induction furnace according to the composition listed in Table I. The steels represent hardenable steels with a carbon content of 0.17 pct. Steels 1 and 2 are alloyed with Mn, Si, and B retarding the  $\gamma$  to  $\alpha$  transformation to ensure a martensitic microstructure under corresponding cooling conditions. These steels only differ in their Nb content in order to examine the influence of Nb on the hardenability after TMP. In Steel 3, the Mn content is reduced and is

yet alloyed with the micro-alloying element (MAE) V, optimized for a TM-processing route. In addition, steel 3 is dispensed with B, however, modified with elevated contents of Cr, Ni, Mo, and Cu compensating for the softening during tempering.<sup>[31]</sup>

### B. Experimental Procedure and Sample Preparation

To prepare the material for the investigations, the raw material was prerolled, and dilatometer samples were extracted *via* wire-eroding with dimensions of 10 mm length and a diameter of 5 mm. In the following, tungsten platelets were utilized in order to reduce the thermal conduction between the sample and the deformation stamp, and a “type S” thermocouple was mounted on the sample to determine the sample temperature during deformation. To reproduce a TM-rolling scheme, the deformation sequence according to Table II was performed using a deformation Dilatometer Bähr 805 A/D. Two different FRT were studied, the deformation program contained a nominal overall compression of  $\varphi = 1.0$ . After a solution annealing of 5 minutes at 1250 °C, the subsequent deformations were split into 5 passes, starting at a temperature of 1000 °C and finishing at 875 °C (rolling scenario FRT 1), and starting at 1075 °C, respectively, aiming for an FRT of 950 °C (rolling scenario FRT 2). The samples were quenched after deformation and an additional holding time of 3 seconds in order to portray a realistic representation of an industrial TM-rolling process, as quenching after the finish rolling steps occurs after several seconds. Five different cooling rates were performed:  $\lambda = 1, 3, 10, 30,$  and  $100$  K/s.

To compare the hardenability of the steel samples to those quenched after re-austenitization (Q+T route), prerolled samples were subjected to an austenitization of 930 °C for 5 minutes. Subsequently, the samples were quenched with the same cooling rates implemented on the deformed samples. From the dilatation data, the transformation temperatures were analyzed through the length expansion  $\Delta L/L$  occurring at the phase transformations.<sup>[32,33]</sup> The *three-tangent method* was used to determine the 5 pct—start and 95 pct—end of the phase transformation. Only the beginning and the end of the first observed transformation during cooling were taken into account.

Prior to the hardness testing, the specimens were hot embedded and then ground with 320 to 4000 grit SiC paper for at least 30 seconds. Subsequently, the samples were polished with 3- $\mu$ m diamond paste for at least 3 minutes and with 1- $\mu$ m paste for 30 seconds. Five HV10 hardness measurements were performed on each sample. Care was taken to ensure that the hardness was extracted from the center of the sample. To reveal the

Table I. Chemical Compositions of the Steels Investigated [m Percent]

Steel/Composition	C	Si	Mn	Al	Cr	Ni	Mo	Cu	V	Nb	Ti	B
Steel 1	0.17	0.2	2.3	0.05	0.25			0.08			0.02	0.002
Steel 2 (+ Nb)	0.17	0.2	2.3	0.05	0.25			0.08		0.04	0.02	0.002
Steel 3 (+ MAE)	0.17	0.2	1.4	0.05	0.70	1.0	0.4	0.5	0.03	0.04	0.02	< 0.001

**Table II. Deformation Sequence Performed at a Deformation Dilatometer Bähr 805 A/D to Investigate the Influences of Two Different FRTs on Hardenability**

Deformation Step/Parameter	1	2	3	4	5
$\varphi$ (-)	0.25	0.25	0.15	0.15	0.1
$\dot{\varphi}$ (s <sup>-1</sup> )	10	10	10	10	10
FRT 1: $T$ (°C)	1000	950	925	900	875
FRT 2: $T$ (°C)	1075	1025	1000	975	950
$t$ (s)	2.5	2	1.5	1.5	(3)

PAGs, the samples were etched with a picric acid etchant. Their compositions and procedures are described in Reference 34. For the metallographic analysis of the PAGs, the equivalent grain diameters and the aspect ratio of the PAGs were determined using the image analysis software MIPAR™.[35] For the microstructural analysis of the transformed microstructure, the samples were polished with a silicate polishing (*Struers OPS*) for 10 minutes prior to a finishing electrolytic ablation of 5 seconds with 35 V. Subsequently, the samples were dipped into a Nital etchant. The images of the microstructures were recorded using an optical microscope and a *FIB Versa FEI 3D DualBeam* scanning electron microscope (SEM). The characteristics of the emerging precipitates of NbC were evaluated by means of EDS analysis using an EDAX Octane Plus detector and the software package TEAM 4.3.

### III. RESULTS

The effect of the process route on the hardenability is shown in Figure 1. Steel 1 exhibits no significant influence of the FRT on the hardening behavior, the hardness progressions dependent on the cooling rates are congruent. Nevertheless, the hardness is noticeably increased with lower FRT (448 HV10) compared to the FRT of 950 °C (433 HV10) and the sample quenched without deformation (435 HV10) at the highest cooling rate of 100 K/s. Steel 3 possesses the same phenomenon. The hardness at high cooling rates > 3 K/s is clearly elevated for the lower FRT of 875 °C and amounts 472 HV10 at a cooling rate of 100 K/s compared to 460 HV10 for the sample deformed with an FRT of 950 °C and 451 HV10 for the undeformed, plain quenched sample. However, at a cooling rate of 1 K/s, both the undeformed quenched sample and the compressed sample with an elevated FRT possess higher hardness values: 413 HV10 and 417 HV10, respectively, compared to 372 HV10 measured for the sample deformed with an FRT of 875 °C.

Figure 1 also contrasts the hardening behaviors of steel 1 and steel 2, and therefore the influence of Nb on the hardening behavior depending on the process route. The upper diagram compares the hardness values of steels 1 to 3 in a plain hardened condition dependent on the cooling rate. At low cooling rates < 10 K/s, the Nb-alloyed steel (2) only reaches low hardness levels below 350 HV10. A full martensitic hardness only is

reached at high cooling rates of 30 and 100 K/s. Regarding the latter, the hardness of the Nb steel (2) even exceeds that of the Nb-free variant (435 HV10) with a value of 448 HV10. The additional strength contribution through Nb is even more apparent in the deformed samples at both finish deformation temperatures of 875 °C and 950 °C. At high cooling rates of 100 K/s, the hardness gain through an addition of 0.04 pct Nb amounts + 41 HV10 (from 446 HV10 to 487 HV10) at an FRT of 875 °C (middle graph). This effect is repeated at the higher FRT of 950 °C (bottom diagram). An addition of 0.04 pct Nb results in a hardness plus of 43 HV10. At low cooling rates of 3 K/s, the higher Nb content seems to retard the  $\gamma$  to  $\alpha$  transformation both at the FRTs of 875 °C and 950 °C. At the lowest FRT, martensitic hardness is even reached with a Nb content of 0.04 pct at a cooling rate of 1 K/s. The lower-temperature-deformed samples again attain higher hardness levels. At a cooling rate of 100 K/s, the samples deformed with an FRT of 950 °C reach hardness values of 433 HV10 (Nb-free) and 477 HV10 (Nb+), respectively, whereas the corresponding hardnesses at an FRT of 875 °C reach values of 446 HV10 (Nb-free) and 487 HV10 (Nb+).

Figure 2 shows the transformation start and finish temperatures of steels 1 and 2 and the resulting microstructures related to the adopted processing route and the implemented cooling rate. Steel 1 exhibits a balanced behavior concerning its phase-transformation temperatures with a slight upward trend toward the decreasing cooling rates. A martensitic microstructure is attained at cooling rates between 10 and 100 K/s, which is confirmed both through hardness measurements and metallographic analysis. At low cooling rates between 1 and 10 K/s, the microstructure contains both bainitic and martensitic segments in variable proportions. The Nb variant, steel 2, behaves differently. The martensite transformation temperatures are slightly reduced for steel 2 for all three process routes. At high cooling rates, a full martensitic microstructure is attained. However, the CCT diagrams (Figure 2) illustrate that, at low cooling rates, the  $\gamma$  to  $\alpha$  transformation occurs at elevated temperatures. These values are significantly above the theoretical  $M_s$  (calculated from Reference 26) and suggests, considering the reduced hardness values as illustrated in Figure 1 that the ferritic and bainitic phases are forming. Figure 3 presents the metallographic analyses of steels 1 and 2 quenched at 10 K/s. Despite undergoing the same cooling conditions, steel 2 forms ferritic components after re-austenitization

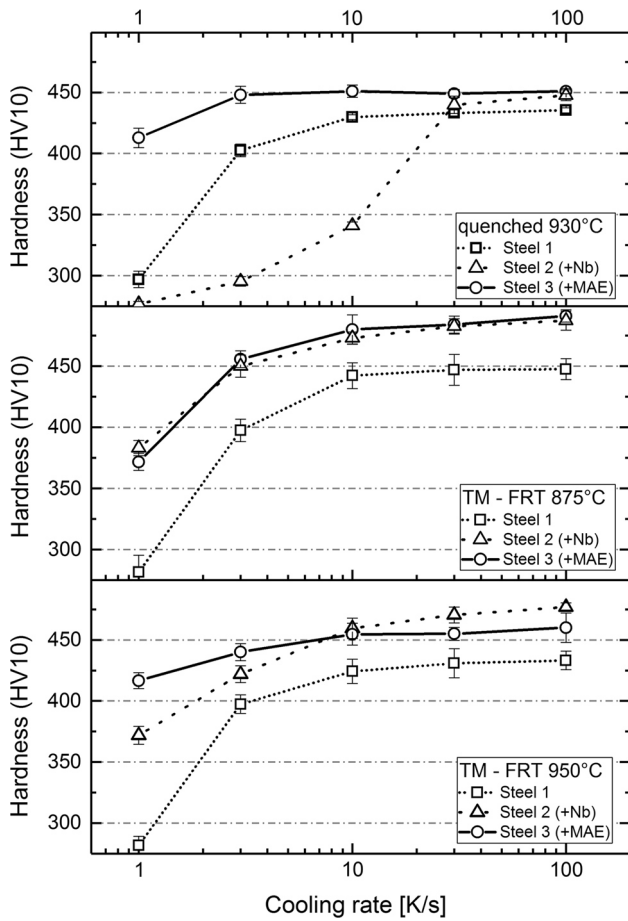


Fig. 1—Effect of FRTs on the hardenability of steels 1 to 3 compared to quenching after previous austenitization for 5 min at 930 °C. A decreased FRT delivers higher hardness values for all steels. However, steel 3 exhibits a significant hardness decrease at low cooling rates compared to the higher FRT and the Q-route. Top graph: Nb retards the hardenability on the undeformed and simple quenched samples. Middle graph: with the increasing Nb content, higher hardness values are achieved at an FRT of 875 °C. Bottom graph: Nb influencing the final hardness and retarding the  $\gamma$  to  $\alpha$  transformation at low cooling rates at an FRT of 950 °C.

(Figure 3(c)). After TMP with an FRT 875 °C, it becomes fully martensitic (Figure 3(b)).

Figure 4 displays the corresponding phase transformations and the resulting hardness values and microstructures of steel 3, dependent on the processing route. At medium cooling rates, the phase transformations occur at analogical temperatures for all three different processing routes. Starting with a  $M_S$  of  $\sim 400$  °C at a cooling rate of 3 K/s with a descending trend to values of  $M_S \sim 370$  °C at 30 K/s. However, this trend is disrupted at low cooling rates. The phase transformations are shifted toward the elevated temperatures to values of  $M_S \sim 484$  °C (FRT 875 °C) and  $\sim 486$  °C (FRT 950 °C) for a cooling rate of 1 K/s and to  $M_S \sim 417$  °C (FRT 875 °C) and  $\sim 403$  °C (FRT 950 °C) for a cooling rate of 100 K/s, respectively. Nevertheless, compared to steel 2, a fully martensitic microstructure is reached down to cooling rates of 10 K/s. It is shown that an increase in cooling rate above 10 K/s not necessarily increases the hardness of the respective production route.

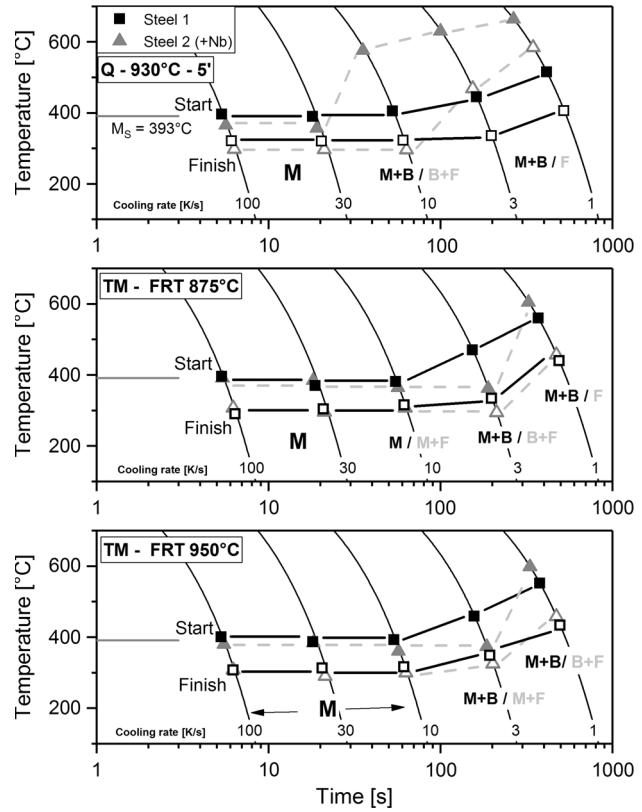


Fig. 2—Phase-transformation temperatures of steels 1 and 2 depending on cooling rates and processing route. Whereas  $M_S$  and  $M_F$  are dependent on the chemical composition, the cooling rates necessary for a complete martensite formation differ between the processing routes. The  $M_S$  was calculated according to Ref. [26].

However, at cooling rates  $< 10$  K/s, also sections of bainitic or even ferritic phases (quenched sample at cooling rate of 1 K/s) appear. Figure 5 reveals selected PAGs (a to c) and the transformed microstructure (d to f) of steel 1 to 3 at a cooling rate of 100 K/s. Processed with an FRT of 875 °C, steel 1 exhibits still a coarse and globular PAG structure (Figure 5(a)). The corresponding transformed microstructure of steel 1 (Figure 5(d)) is by far coarser than the counterpart of steel 2 (Figure 5(e)). After re-austenitization, the PAGs of steel 2 and 3 very fine, as displayed in Figure 5(b) and (c). The quantification of the dimensions of the PAGs are listed in Table III. The size of the resulting  $\alpha$  substructures, such as ferritic grains, bainitic laths, and martensitic blocks, are proportional to their originating  $\gamma$ -grains.<sup>[8,9,11]</sup> According to Table III, the finest grains are achieved through TMP at a finish processing at 875 °C, whereas, as aforementioned, steel 2 and 3 show a tendency to produce the finest grains through re-austenitization at 930 °C (Figures 5(b) and (c)).

#### IV. DISCUSSION

In order to investigate the influence of the production route on the hardenability of UHSS strength, three steels with different alloying contents were subjected to varying cooling rates after applying different



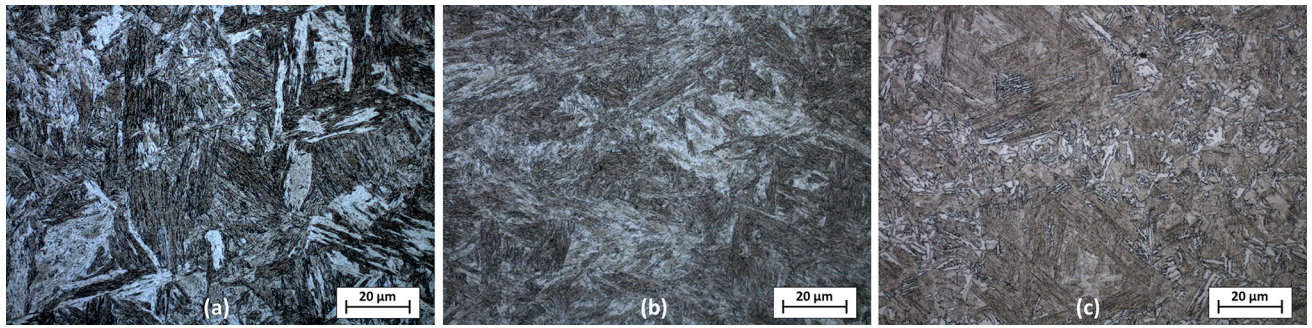


Fig. 3—Microstructures of samples cooled at 10 K/s: (a) steel 1 after re-austenitization and quenching, steel 2 after (b) TMP with an FRT of 875 °C, and (c) quenching after re-austenitization. The microstructure of steel 1 is slightly coarsened compared to the Nb variant. Direct quenching of steel 2 with 10 K/s creates a martensitic microstructure, whereas from the quenching route, ferritic segments arise.

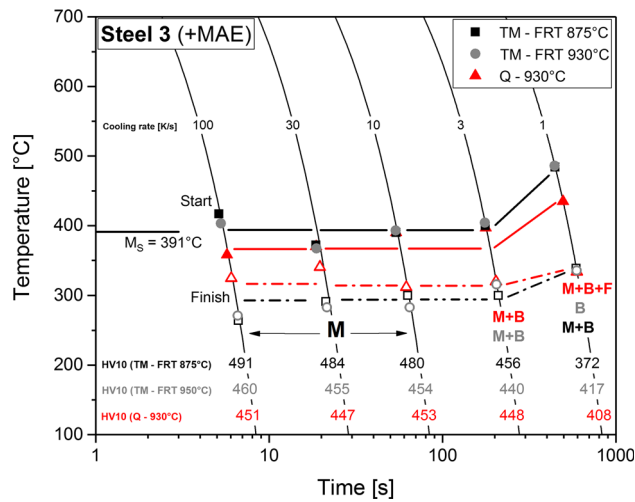


Fig. 4—Phase-transformation temperatures of steel 3. Effects of cooling rates and FRTs compared to plain quenching (Q) on the martensite start ( $M_s$ ) and finish temperatures ( $M_f$ ). The corresponding hardness values obtained after applying the different cooling rates are in correspondence with the obtained microstructures.

compressions on a deformation dilatometer. The dilatometer is a simple, yet, unique tool to bring industrial-scale processes down to laboratory dimensions. However, it cannot picture a whole rolling scenario. Further, the given nominal strains are distributed unequally over the deformed sample. Nevertheless, these points were considered through withdrawing both hardness and microstructural investigations consequently only from the middle of the deformed samples.

For all three steels investigated, the highest hardness values were attained at an FRT of 875 °C, compared to the samples compressed at an FRT of 950 °C and the plain-quenched (after an austenitization of 5 minutes at 930 °C) processing route. The influence of the processing route is less pronounced at steel 1. However, the steel grades alloyed with Nb (steel 2 and 3) show a significant increase in hardness when deformation is imposed prior to quenching. This effect can be attributed to the increased reduction in the nonrecrystallization regime,

as Nb shifts the  $T_{NR}$  to higher temperatures and promotes pancaking as demonstrated in Figure 6. This is in accordance to literature.<sup>[2,6,8,14,16]</sup>

The comparison of the hardening behavior between the three steels emphasizes the significance of micro-alloying in combination with TMP concerning the achievable strengths. While the gain in strength through an addition of 0.04 pct Nb (steel 2) is only marginal for a conventional hardening after re-austenitization (+ 3 pct), TMP with subsequent DQ with 100 K/s gives a hardness plus of 9 pct (FRT 875 °C) and 10 pct (FRT 950 °C) compared to the Nb free variant steel 1. Furthermore, at lower cooling rates of <30 K/s, the hardenability of steel 1 and 2 diverge clearly. Whereas steel 1 possesses at a cooling rate of 1 K/s still martensitic constituents, steel 2 consists mainly of ferritic and bainitic components already at a cooling rate of 30 K/s. The reported effect that Nb micro-alloying and deformation promotes bainite formation by Kajjalainen *et al.*<sup>[16]</sup> is in accordance with the present investigations. Moreover, it is shown that the accelerated  $\gamma$  to  $\alpha$  transformation is further enhanced through both, lowering the FRT in TMP and quenching after re-austenitization, from which even ferritic components emerge. This can be attributed to the much smaller austenite grains after re-austenitization through the addition of Nb in steel 2, in which the austenite grains are pinned by precipitates prohibiting grain growth. A decrease in the austenite grain size shifts the time-temperature-transformation diagram to shorter times and promotes a ferritic transformation.<sup>[36,37]</sup> Steel 3, however, is stronger alloyed with  $\gamma$ -stabilizer and does not exhibit this phenomenon. Whether Nb eliminates the effect of the  $\gamma$  to  $\alpha$  transformation retarding elements in a solved or precipitated condition, needs to be clarified by TEM investigations. Nevertheless, the hardening behavior of steel 3 already gives an indication to this hypothesis. A surcharge of further alloying elements in steel 3 with additions of V, Cu, Mo and Ni, does not significantly increase the strength, but influence the hardenability. After the TM processing at an elevated FRT of 950 °C or after quenching from austenitization at 930 °C, the hardness does not considerably decrease after a low cooling rate of 1 K/s. Metallographic investigations reveal both, martensitic and bainitic

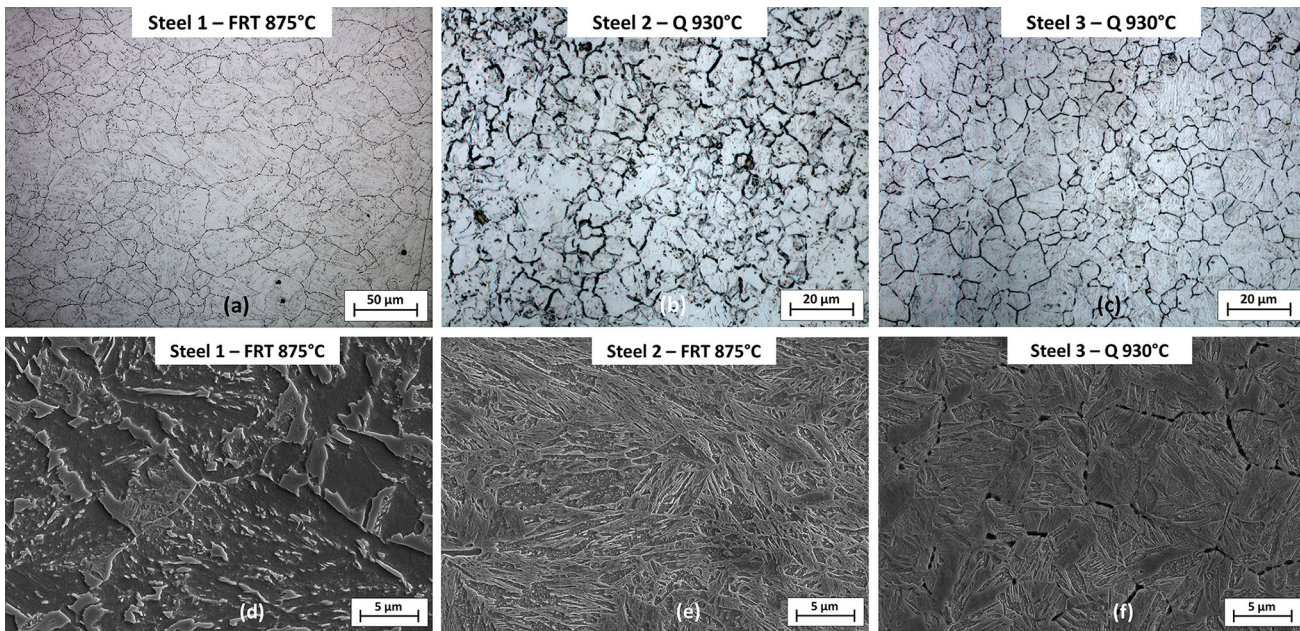


Fig. 5—Prior austenite grains (*a* through *c*) and transformed microstructures (*d* through *f*) of steels 1 to 3, at a cooling rate of 100 K/s. Despite a low FRT, the microstructure of steel 1 (*a* + *d*) is coarse and globular. Steels 2 (*b*) and 3 (*c*) clearly refine through re-austenitization. Steel 2 possesses a very fine lath structure after an FRT of 875 °C (*e*). Due to the described proportionality, the substructure originating from the PAG (*c*) of steel 3 is refined too (*f*).

**Table III. Grain Sizes of the Prior Austenite Grains Achieved Through Different Processing Routes**

Steel/ Process	Q 930 °C ( $\mu\text{m}$ )	FRT 875 °C ( $\mu\text{m}$ )	FRT 950 °C ( $\mu\text{m}$ )
1	26.7	11.2	21.8
2	8.9	9.0	13.0
3	8.1	21.3	11.7

microstructures. The decreased hardness after processing with an FRT of 875 °C would lead to the assumption that Nb is fully precipitated, whereas regarding the other processing routes, Nb might be still remaining in solution, and thus, according to the hardness values retards in a dissolved state the formation of ferrite. However, SEM investigations showed that the decreased hardness can be attributed to the size of the precipitated NbC as can be seen in Figure 7. As investigated by Maugis *et al.*,<sup>[38]</sup> NbC particles become incoherent when they exceed a size of 5 nm. Regarding the dimensions of the particles found in the SEM examinations, which are significantly larger than 5 nm, Orowan's theory of precipitation hardening<sup>[39]</sup> can be applied. However, the sizes of the NbC precipitates that emerged at an FRT of 875 °C (Figure 7(b)) are too large to contribute to reach sufficient precipitation hardening.<sup>[40]</sup> Similar phenomenon was observed by Klinkenberg *et al.*<sup>[41]</sup> In contrast, the small sizes of the NbC particles at an FRT of 950 °C and after re-austenitization at 930 °C possess the ability to achieve a high hardness at a low cooling rate of 1 K/s. It can be assumed that those alloying elements in steel 3 (Cr, Ni, and Mo and foremost the

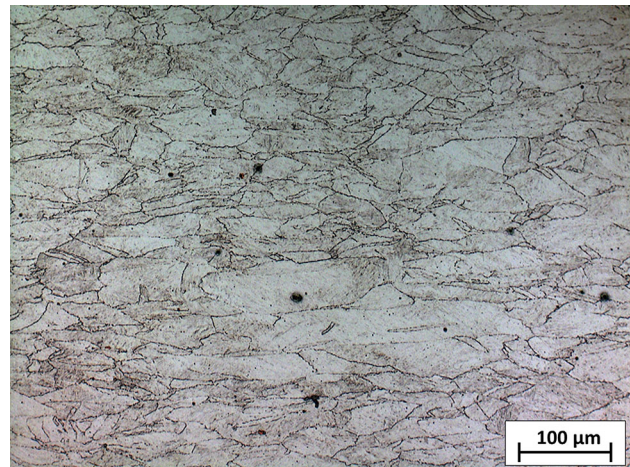


Fig. 6—PAGs of steel 3 processed at an FRT of 975 °C. The highly pancake-shaped  $\gamma$  grains explain the increased hardness over steel 1.

MAE V which is a very strong carbide former) promote precipitation of Nb and stabilizes it as NbC, under which condition it has no influence on the hardenability itself. On the contrary, Nb, which in steel 2 remains still dissolved in the matrix, stimulates bainite and ferrite.

Due to the fact that the size of the microstructural components contributes to the strength according to the Hall-Petch relation, the attainable microstructures and substructures were assessed through Nital and picric acid etchants. Regardless of the cooling rate, steel 1 exhibits a very coarse microstructure (Figures 3(a) and 5(a) and (d)) due to the dispensing of MAE which prohibits accelerated grain growth through the

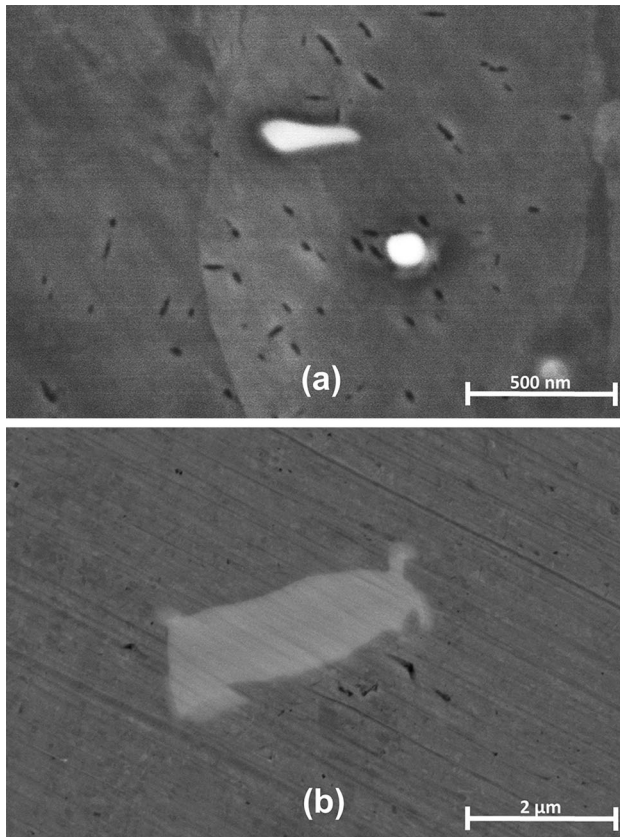


Fig. 7—SEM images of Nb carbides in steel 3 under different processing conditions with a cooling rate of 1 K/s: (a) Undeformed and quenched from 930 °C: NbC particles have a size range from 100 to 120 nm. (b) Processed with an FRT of 875 °C: NbC particles emerge with a size in the range from 2 to 3  $\mu\text{m}$ .

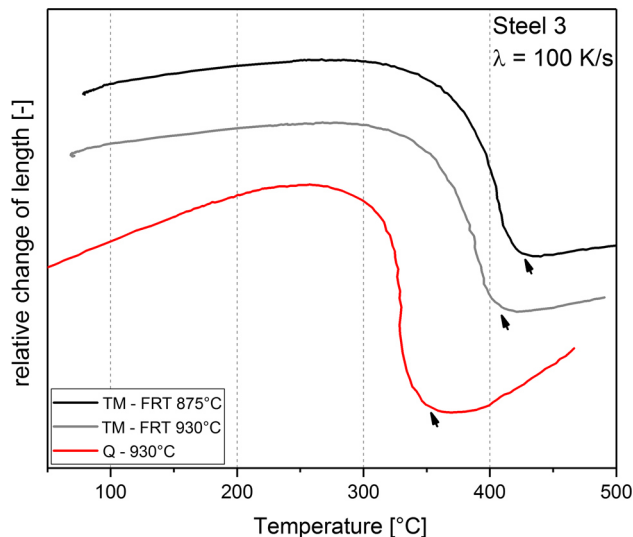


Fig. 8—Dilatation curves of steel 3 cooled at 100 K/s. The  $M_S$  temperatures of the TM-processed samples differ clearly from the re-austenitized and quenched samples.

formation of carbides and a low solute drag. In contrast, the micro-alloyed variants, steels 2 and 3, reached the smallest grain sizes, whereby their dimensions differ

depending on the process route. In accordance with literature, the lower the reduction below the FRT is, the finer the microstructure becomes. Steel 3, however, further refines after re-austenitization (Figure 5(c)). This refining can be attributed to the combination of a highly deformed austenite prior to quenching (Figure 6), which recrystallizes during reheating in the  $\gamma$ -region reducing the grain boundary energy. Furthermore, precipitated carbides inhibit an augmented grain growth.

The  $M_S$  and  $M_F$  temperatures are dependent on the chemical composition<sup>[20,36,42]</sup> and as reported by several authors on the PAG size.<sup>[36,43,44]</sup> As Figure 2 demonstrates,  $M_S$  and  $M_F$  are independent of the processing routes for steel 1 and 2. At slow cooling rates, transformation starts at higher temperatures due to the formation of ferritic or bainitic phases. Dilatation data do not allow a precise identification of the originating phase through blurring boundaries. However, microstructural analysis provided the proof with respect to the existence of martensitic, bainitic, and ferritic phases. Nevertheless, for steel 3, the  $M_S$  and  $M_F$  temperatures differ clearly from each other depending on the different process routes and the cooling rates (Figure 3). At the highest cooling rate of 100 K/s, both TM-processed steels start their martensitic transformation clearly above the calculated  $M_S$  of 391 °C,<sup>[26]</sup> whereas the quenched steel is delayed in its transformation, yet reaches  $M_F$  very close just below  $M_S$  (Figure 8). This could lead to the assumption that in a TM-deformed state, the martensite transformation is accelerated, which, however, needs further undercooling for a complete conversion, whereas in a plain austenitized state, the full martensitic transformation is accomplished with less undercooling. Due to the fact that a decrease in the PAG size leads to an elevated  $M_S$ ,<sup>[36,43-45]</sup> the  $M_S$  of the re-austenitized and quenched sample is expected to be above the TM-processed sample, as the determined microstructural dimensions for steel 3 are significantly smaller after re-austenitization. However, it is reported that a high deformation of the austenite as it is performed during TMP triggers the  $M_S$  to elevate to higher temperatures.<sup>[16]</sup> This argument is supported by the observation that increasing the reduction in the nonrecrystallization regime with lowering of the FRT from 950 °C to 875 °C further elevates the  $M_S$  to higher temperatures (Figure 8). On the contrary, re-austenitization releases these deformations by recrystallization. This leads to the assumption that the effect of elevating  $M_S$  through a highly deformed austenite dominates over the increased  $M_S$  through a finer austenite grain. However, this phenomenon only occurs at very high cooling rates and thus leaves room for a more in-depth investigation concerning this hypothesis.

## V. CONCLUSIONS

The aim of this investigation was to study the influences of Nb and different process routes on the achievable hardness and hardenability of ultra-high strength steels. The main findings and conclusions are summarized in the following:

1. TM processing with subsequent direct quenching increases the strength significantly compared to conventional quenching after re-austenitization. The finish rolling temperature plays a major role during TMP: decreasing the FRT leads to a further strength gain.
2. Further hardness increase is observed by additions of Nb. However, investigations showed that the addition of Nb leads to an expedited formation of bainite and ferrite. This is explained by a grain refinement after re-austenitization resulting in an accelerated  $\gamma$  to  $\alpha$  transformation, shifting the time transformations curves to shorter times. Finer grains additionally elevate the  $M_S$  temperature.
3. Increasing the reduction in the nonrecrystallizing austenite regime elevates the  $M_S$  temperature. This effect dominates over an accelerated formation of martensite due to smaller austenitic grain sizes.

### ACKNOWLEDGMENTS

Open access funding provided by Montanuniversität Leoben. Funding of the Austrian BMVIT within the framework of the program “Production of the future” and the “BMVIT Professorship for Industry” is gratefully acknowledged.

### CONFLICT OF INTEREST

Authors declare no conflict of interest.

### OPEN ACCESS

This article is distributed under the terms of the Creative Commons Attribution 4.0 International License (<http://creativecommons.org/licenses/by/4.0/>), which permits unrestricted use, distribution, and reproduction in any medium, provided you give appropriate credit to the original author(s) and the source, provide a link to the Creative Commons license, and indicate if changes were made.

### REFERENCES

1. *Thermomechanical Processing of High-Strength Low-Alloy Steels*, 2nd ed., I. Tamura, ed., *Thermomechanical Processing of High-Strength Low-Alloy Steels*, Butterworths, London, Boston, 1988.
2. M. Klein, H. Spindler, A. Luger, R. Rauch, P. Stiaszny, and M. Eigelsberger: *Mater. Sci. Forum*, 2005, vols. 500–501, pp. 543–50.
3. K.E. Hensger and M.L. Bernštejn: *Thermomechanische Veredlung von Stahl*, VEB Deutscher Verlag für Grundstoffindustrie, 1984.
4. C. Ouchi: *ISIJ Int.*, 2001, vol. 41, pp. 542–53.
5. D.K. Matlock and J.G. Speer: *Mater. Sci. Technol.*, 2009, vol. 25, pp. 1118–25.
6. M. Klein, R. Rauch, H. Spindler, and P. Stiaszny: *BHM Berg-Hüttenmänn. Monatshefte*, 2012, vol. 157, pp. 108–12.
7. P. Haslberger, S. Holly, W. Ernst, and R. Schnitzer: *J. Mater. Sci.*, 2018, vol. 53, pp. 6968–79.
8. L. Bracke, W. Xu, and T. Waterschoot: *Mater. Today Proc.*, 2015, vol. 2, pp. S659–62.
9. T. Swarr and G. Krauss: *Metall. Trans. A*, 1976, vol. 7, pp. 41–48.
10. G. Krauss and A.R. Marder: *Metall. Trans.*, 1971, vol. 2, pp. 2343–57.
11. R.G. Davies and C.L. Magee: *Metall. Trans.*, 1971, vol. 2, pp. 1939–47.
12. Y. Prawoto, N. Jasmawati, and K. Sumeru: *J. Mater. Sci. Technol.*, 2012, vol. 28, pp. 461–66.
13. P.D. Hodgson, H. Beladi, and M.R. Barnett: *Mater. Sci. Forum*, 2005, vols. 500–501, pp. 39–48.
14. A.J. Kajjalainen, P. Suikkanen, L.P. Karjalainen, and J.J. Jonas: *Metall. Mater. Trans. A*, 2014, vol. 45A, pp. 1273–83.
15. A.J. Kajjalainen, P.P. Suikkanen, T.J. Linnell, L.P. Karjalainen, J.I. Kömi, and D.A. Porter: *J. Alloys Compd.*, 2013, vol. 577, pp. S642–48.
16. A. Kajjalainen, N. Vähäkuopus, M. Somani, S. Mehtonen, D. Porter, and J. Kömi: *Arch. Metall. Mater.*, 2017, vol. 62, pp. 619–26.
17. O. Haiko, I. Miettunen, D. Porter, N. Ojala, V. Ratia, V. Heino, and A. Kempainen: vol. 35, p. 17.
18. H.J. Bargel: *Werkstoffkunde*, VDI-Verlag, Düsseldorf, 1987.
19. O. Girina, N. Fonstein, D. Panahi, D. Bhattacharya, and S. Jansto: in *HSLA Steels 2015, Microalloying 2015 & Offshore Engineering Steels 2015*, Tms, ed., Wiley, Hoboken, NJ, 2015, pp. 237–45.
20. A.I.H. Committee: *ASM Handbook: Heat Treating*, ASM International, New York, 1991.
21. M. Yamada, L. Yan, R. Takaku, S. Ohsaki, K. Miki, K. Kajikawa, and T. Azuma: *ISIJ Int.*, 2014, vol. 54, pp. 240–47.
22. E.C. Bain and H.W. Paxton: *Alloying Elements in Steel*, 2nd ed., American Society for Metals, Metals Park, Ohio, 1961.
23. W.C. Leslie: *The Physical Metallurgy of Steels*, Washington: Hemisphere Pub, McGraw-Hill, Corp.; New York, 1981.
24. T.G. Digges, C.R. Irish, and N.L. Carwile: *J. Res. Natl. Bur. Stand.*, 1948, vol. 41, p. 545.
25. W.J. Foy: *Bachelors Theses Rep.*, 1943, pp. 1928–70, 185.
26. V.D. Eisenhüttenleute: *Steel - A Handbook for Materials Research and Engineering: Volume 1: Fundamentals*, Springer, Berlin, 1991.
27. M.S. Joo, D.-W. Suh, J.H. Bae, N.S. Mouriño, R. Petrov, L.A.I. Kestens, and H.K.D.H. Bhadeshia: *Mater. Sci. Eng. A*, 2012, vol. 556, pp. 601–06.
28. H.L. Haskel, E. Pauletti, J.D.P. Martins, and A.L.M. de Carvalho: *Mater. Res.*, 2014, vol. 17, pp. 1238–50.
29. A. Kajjalainen, S. Pallaspuuro, and D.A. Porter: *Adv. Mater. Res.*, 2014, vol. 922, pp. 316–21.
30. S. Pallaspuuro, A. Kajjalainen, T. Linnell, and D.A. Porter: *Adv. Mater. Res.*, 2014, vol. 922, pp. 580–85.
31. T. Gladman: *The Physical Metallurgy of Microalloyed Steels*, Institute of Materials, 1997.
32. M. Takahashi and H.K.D.H. Bhadeshia: *J. Mater. Sci. Lett.*, 1989, vol. 8, pp. 477–78.
33. G.F. Vander Voort: *Atlas of Time-Temperature Diagrams for Irons and Steels*, 7th edn., ASM International, New York, 1991.
34. R. Esterl, M. Sonnleitner, M. Stadler, G. Wölger, and R. Schnitzer: *Pract. Metallogr.*, 2018, vol. 55, pp. 203–22.
35. J.M. Sosa, D.E. Huber, B. Welk, and H.L. Fraser: *Integrating Mater. Manuf. Innov.*, 2014, vol. 3, p. 10.
36. C.R. Brooks: *Principles of the Heat Treatment of Plain Carbon and Low Alloy Steels*, 1st edn., ASM International, New York, 1996.
37. A.S. for M.M.H. Committee: *Metals Handbook, Vol. 8: Metallography, Structures and Phase Diagrams*, ASM, New York, 1973.
38. P. Maugis, D. Gendt, S. Lanteri, and P. Barges: *Defect Diffus. Forum*, 2001, vols. 194–199, pp. 1767–72.
39. E. Orowan: London: The Institute of Metals, 1948, pp. 451–53.
40. T. Gladman: *Mater. Sci. Technol.*, 1999, vol. 15, pp. 30–36.
41. C. Klinkenberg, K. Hulka, and W. Bleck: *Steel Res. Int.*, 2004, vol. 75, pp. 744–52.
42. G.E. Totten: *Steel Heat Treatment: Metallurgy and Technologies*, CRC Press, 2006.
43. H. Yang and H. Bhadeshia: *Scr. Mater.*, 2009, vol. 60, pp. 493–95.
44. T.G. Digges: *J. Res. Natl. Bur. Stand.*, 1940, vol. 24, p. 723.
45. P.J. Brofman and G.S. Ansell: *Metall. Trans. A*, 1983, vol. 14, pp. 1929–31.

**Publisher's Note** Springer Nature remains neutral with regard to jurisdictional claims in published maps and institutional affiliations.

## Paper IV:

Esterl R, Sonnleitner M, Gschöpf B, Schnitzer R (2019)

*Influence of V and Nb Micro-Alloying on Direct Quenched and Tempered  
Ultra-High Strength Steels*

Steel research international (2019): 800640

DOI: 10.1002/ srin.201800640

# Influence of V and Nb Micro-Alloying on Direct Quenched and Tempered Ultra-High Strength Steels

Raphael Esterl,\* Markus Sonnleitner, Boris Gschöpf, and Ronald Schnitzer


The construction of mobile crane booms requires the usage of ultra-high strength steels. Micro-alloying elements promote grain refinement during hot rolling and result in increased toughness. The relevant strength is given through a martensitic microstructure, which is accomplished by elements retarding the  $\gamma$  to  $\alpha$  transformation. Direct quenching (DQ) from the rolling heat and quenching after a preceding re-austenitization (RQ) are two different production routes. They differ regarding their productivity, their achievable strength levels, and their resulting microstructures. In order to explore the influence of the production route in combination with prominent micro-alloying elements, which come to application during hot-rolling, six steels with varying content of V and Nb are investigated concerning their different properties after DQ and RQ as well as their behavior after tempering. It is found, that Nb strongly improves the strength after thermomechanical processing in the as-rolled condition. Furthermore, Nb compensates the loss of strength during tempering. This effect is not thoroughly discussed in literature so far. Although Nb leads to grain refining during re-austenitization, the effects on the strength of RQ steels are minimal. The effect after tempering is also weaker than after direct quenching. It is also shown, that V offers a high strength potential after tempering, however weakens the impact toughness significantly.

## 1. Introduction

Steels with a yield strength above 1100 MPa are necessary to optimize the payload-to-weight ratio for the design of advanced mobile crane booms. Ultra-high strength steels (UHSS) meet these extreme strength requirements and simultaneously offer good

R. Esterl, B. Gschöpf, Prof. R. Schnitzer  
Chair of Design of Steels  
Department of Materials Science  
Montanuniversität Leoben  
Franz-Josef-Str. 18, 8700 Leoben, Austria  
E-mail: raphael.esterl@unileoben.ac.at

Dr. M. Sonnleitner  
voestalpine Stahl GmbH  
voestalpine-Straße 1  
4020 Linz, Austria

 The ORCID identification number(s) for the author(s) of this article can be found under <https://doi.org/10.1002/srin.201800640>.

© 2019 The Authors. Published by Wiley-VCH Verlag GmbH & Co. KGaA. This is an open access article under the terms of the Creative Commons Attribution-NonCommercial License, which permits use, distribution and reproduction in any medium, provided the original work is properly cited and is not used for commercial purposes.

DOI: 10.1002/srin.201800640

ductility and thus excellent notch impact values.<sup>[1,2]</sup> For the production of UHSS, two processing routes are facing each other: the conventional route consists of quenching (Q) after re-austenitization followed by a tempering (T) process to relax the residual stresses of the martensite,<sup>[3]</sup> and the thermomechanical (TM) route, in which quenching is performed directly after hot-rolling (DQ). The globularization of the prior austenite grain (PAG) accomplished by normalization and reheating to the  $\gamma$ -region offers the advantage of an isotropic microstructure.<sup>[4–6]</sup> TM processing of UHSS represents the alternative route, offering an economic benefit by avoiding a supplementary reheating step. Furthermore, the production via TM can provide an additional strength contribution through direct quenching from the rolling heat.<sup>[1,7–9]</sup> This additional asset in strength, accomplished through a strongly deformed non-recrystallizing austenite, offers the benefit over Q + T steels, that for a given strength, alloying elements can be reduced. In turn, the waiver of mainly carbon has a favorable effect on the weldability.<sup>[10–13]</sup> Prominent micro-

alloying elements (MAE) which come to application are Ti, Nb, and V, which increase the non-recrystallization temperature ( $T_{NR}$ ) in dissolved condition and by formation of strain-induced precipitates. Consequently, they promote an elevated number of nucleation sites for the subsequent  $\gamma$  to  $\alpha$  transformation through a highly deformed austenite grain.<sup>[14–17]</sup> For Q + T steels, they also serve as grain refiners during hot rolling and promote additional refinement during re-austenitization. Furthermore, the emerging precipitations possess a significant strength contribution, which compensates the loss of strength during tempering.<sup>[18–20]</sup>

The influence of several MAE during hot-rolling has been broadly investigated.<sup>[14,16,19,21–24]</sup> Moreover, the role of processing conditions such as the finish-rolling temperature (FRT) is considered to be also well explored.<sup>[25–29]</sup> However, there is a lack of information on the combined effect of the processing route and MAE on the final mechanical properties. Particularly, the influence of MAE on a tempering treatment, in which it is distinguished between DQ and re-austenitization and quenching is an open scientific and technological field. The present work is therefore intended to cover the microstructural development, including the resulting grain sizes, depending on the process conditions, and the type and content of MAE. These investigations are supported by the mathematical description of the underlying microstructural processes through

**Table 1.** Chemical composition of the six steels investigated.

Base alloy	Variation	C	Si	Mn	Al	Cr	Cu	V	Nb	Ti	B
1		0.167	0.20	2.38	0.049	0.280	0.089	0.005	<0.002	0.021	0.0025
	Nb+	0.173	0.19	2.36	0.043	0.280	0.079	0.005	0.021	0.020	0.0024
	Nb++	0.175	0.20	2.37	0.041	0.280	0.089	0.005	0.040	0.020	0.0026
2		0.169	0.20	2.30	0.057	0.710	0.078	0.005	<0.002	0.021	0.0024
	V+	0.170	0.21	2.30	0.053	0.700	0.078	0.097	<0.002	0.021	0.0026
	V++	0.179	0.22	2.29	0.049	0.700	0.081	0.194	0.002	0.021	0.0026

the calculation of the activation energy  $E_A$  for dynamic recrystallization (DRX) via the Zener-Hollomon parameter.<sup>[30,31]</sup> Finally, the present work should stretch the bow between the microstructural and mechanical anisotropy. It will be established, whether a correlation between an elongated austenitic grain and the anisotropy in the mechanical properties between the longitudinal and transversal direction exists. For this matter, six steels with varying contents of Nb and V, processed via TM are investigated and compared to the conventional RQ-route. Mechanical properties were determined for the longitudinal and transversal direction in the as-rolled condition and after tempering. In addition, two different FRT were performed in the DQ route. Thereby it should be established, whether an increasing grain elongation, which is accompanied with a decreasing rolling temperature influences the mechanical anisotropy.

## 2. Experimental Section

### 2.1. Materials and Processing

The six steels tested were melted in an induction furnace in quantities of 300 kg each and their chemical composition is listed in Table 1. Based on the basic composition of steel 1, which represents a UHS steel, successive additions of Nb and V were applied. Besides the carbon content  $\approx 0.17\%$ , the base alloy contains  $\approx 0.2\%$  Si,  $\approx 2.3\%$  Mn, and  $\approx 0.002\%$  B to guarantee a through-hardening during quenching. Further surcharges of Cr and Cu control temper resistance.<sup>[32,33]</sup> Al and Ti are responsible for grain refinement and additional strength increase.<sup>[14,15,34,35]</sup> The variants of steel 1 possess additions of Nb of 0.02% and 0.04%, respectively. The second base alloy, contains an elevated amount of Cr (0.7%), which increases hardenability and enhances temper resistance.<sup>[33]</sup> In addition, Cr acts as grain refiner,<sup>[36]</sup> whereas its influence on recrystallization during hot rolling is negligible.<sup>[37]</sup> The modifications of base alloy 2 are alloyed with amounts of  $\approx 0.1\%$  and  $\approx 0.2\%$  V to compare the microstructural processes during hot rolling and after tempering to the Nb variants of base alloy 1.

After solution-annealing of 15 min at 1220 °C, the steels were rolled in a hot-rolling simulation unit in nine passes with a  $\varphi_{tot} = 2.3$  from 55 to 6 mm thick plates with a length of 2.000 mm. Each alloy was rolled with two different rolling schemes in order to achieve two different FRT of 1) 850 °C and 2) 930 °C. The plates were immediately water quenched after leaving the runout table and are hereinafter referred to as DQ850

and DQ930. A tempering treatment was performed on samples of each alloy for 5 min at 600 °C. Additionally, sheets of each alloy were quenched after re-austenitization at 930 °C for 5 min (in the following listed as “RQ”) and compared to others tempered after quenching (RQ + T). Thus, in sum six different conditions of each alloy were tested: two different FRTs in an as-rolled and tempered condition, as well as a RQ and a RQ + T condition. An overview of the processing cycles and conditions and the used nomenclature is given in Table 2.

Tensile tests were performed according to DIN EN ISO 6892–1 on flat tensile specimens in longitudinal and transversal direction of the rolled plates of each condition. The notch impact tests at 0, –20, and –40 °C were performed according to DIN EN ISO 148–1 on 6 mm thick specimens and the obtained notch impact work was standardly converted to 10 × 10 mm full-sized samples by linear upscaling. In order to exclude possible outliers in the tests, tensile tests were applied twice in each direction and for impact tests three samples of each condition were tested. Error bars were indicated in the diagrams only in case of larger deviations, otherwise avoided for the sake of better clarity.

### 2.2. Determination of the Activation Energy and Non-Recrystallization Temperature

To derive the activation energy for dynamic recrystallization and describe the yield stress in terms of temperature and strain rate, the Zener-Hollomon parameter was determined for the selected steels. For the experiments, which were conducted on a deformation Dilatometer Bähr 805 A/D, cylindrical samples with a diameter of 6.0 mm and a length of 10 mm were machined from the milled plates with a wire-electro discharge machine. The deformation procedure of the six investigated steels involved

**Table 2.** Overview of the processing cycles and conditions and the used nomenclature.

Processing cycles	Direct quenched		Re-austenitized and quenched
	FRT = 850 °C	FRT = 930 °C	930 °C 5 min <sup>-1</sup>
As-rolled	DQ850	DQ930	RQ
Tempered	DQ850 + T	DQ930 + T	RQ + T

FRT = finish rolling temperature.

solution annealing at 1250 °C and subsequent forming at 850, 900, 950, 1000, and 1050 °C, respectively, at four different strain rates  $\dot{\varphi} = 0.01, 0.1, 1.0, \text{ and } 10 \text{ s}^{-1}$ . The peak strain of the flow stress curves was used for the calculation of the activation energy and the Zener-Hollomon parameter according to refs. [30,31]. For the calculation of  $T_{NR}$ , which is dependent on the chemical composition, the mathematical model described by Boratto [24] was applied.

### 2.3. Sample Preparation for Metallographic Analysis

To study the microstructure dependent on the processing route and MAE, specimens of the hot rolled sheets were hot embedded and then ground from 320 grit to 4.000 grit SiC paper for at least 30 s. Subsequently, the samples were polished with 3  $\mu\text{m}$  diamond paste for at least 3 min and with 1  $\mu\text{m}$  for 30 s. To reveal the PAGs, the samples were etched with a picric-acid etchant. The composition and procedure is described in ref. [38]. To reveal the transformed martensitic microstructure, the samples were dipped in a Nital etchant. The images were recorded with an optical microscope and a *FIB Versa FEI 3D DualBeam* scanning electron microscope (SEM). For the metallographic analysis of the PAGs, the equivalent grain diameters and the aspect ratio of the PAGs were determined with the image analysis software MIPAR<sup>TM</sup>. [39] Since the temper treatment has no influence on the PAGs, only those samples were examined due to a favorable impact of the etchant on the tempered specimens. [38]

## 3. Results

### 3.1. Microstructural Analysis

Light-optical microscopy and SEM investigations of the transformed microstructure revealed a mainly martensitic microstructure with small bainitic sections as depicted in **Figure 1**. The samples, which were directly quenched from the rolling heat (DQ850) showed martensitic blocks, which are orientated in 45° toward the rolling direction (Figure 1a). These laths and blocks emerge from the highly pancaked  $\gamma$  grain, as **Figure 2a** reveals on a tempered sample of Base alloy 1 Nb + +. After re-austenitization, the PAGs develop a globular shape (Figure 1c), the blocks are not arranged in a preferential orientation and rather randomly organized. After T, carbides emerge from the supersaturated  $\alpha$ -grains.

The analysis of the PAGs, which were revealed with a picric-acid etchant, illustrates the influence of the processing route and the content of MAE. As expected, the lower FRT of 850 °C leads to an increased aspect ratio compared to the FRT of 930 °C as demonstrated by Figure 2. Already small additions of Nb strongly promote the pancaking of the PAGs, however, this effect seems to be effective only at lower final rolling temperatures. Further additions of Nb lead to grain refinement. This can be observed as well after re-austenitization. The influence of the Cr surcharge to base alloy 2 seems negligible concerning the microstructural appearance. Cr has no influence in retarding recrystallization, the aspect ratio and mean grain size of base

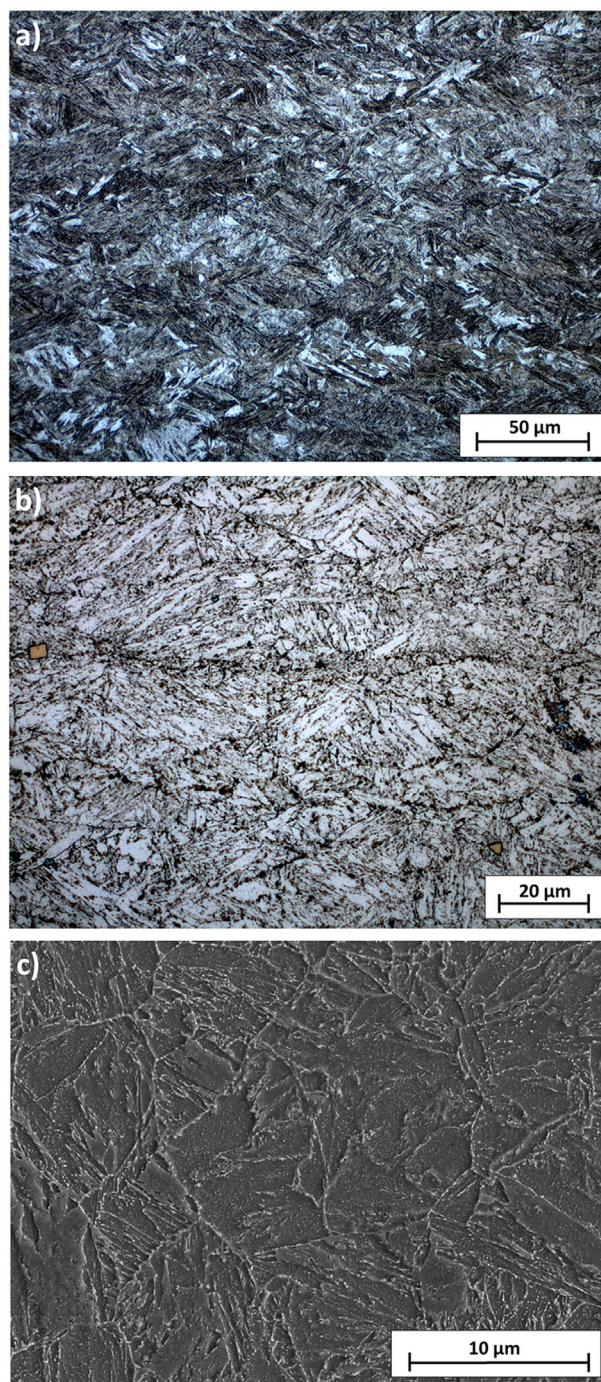


**Figure 1.** Transformed microstructure etched with a Nital etchant and revealed with light-optical microscopy (a + b) and SEM (c). a) The laths and blocks of base alloy 1 with Nb + + are orientated in 45° toward the rolling direction after DQ with a FRT 850 °C. b) After tempering, it can be observed that these blocks origin from the highly pancaked  $\gamma$  grain in 45°. c) After RQ, the microstructure is randomly arranged with no specific orientation toward the RD, furthermore carbides emerge after T.

alloy coincides with base alloy 1, however with increasing V, the aspect ratio increases slightly but not in the same extent as through Nb. The light-optical images of the steels investigated,



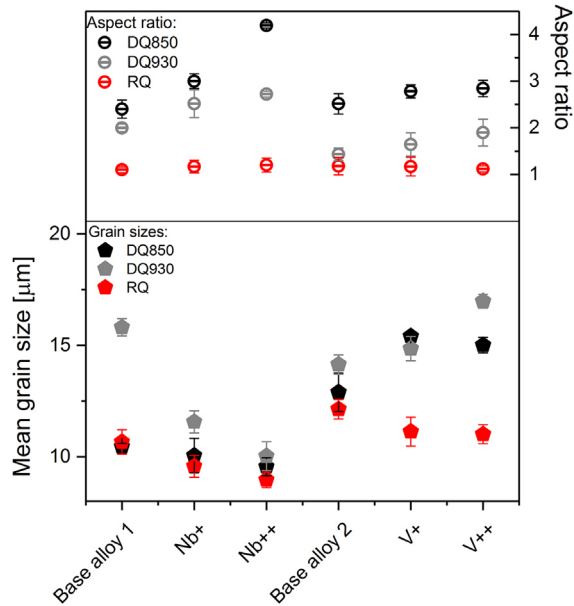


**Figure 2.** Prior austenite grain sizes and aspect ratio of the investigated steels depending on the processing route and the FRT. A lower FRT promotes pancaking of the PAGs. Even small additions of Nb noticeably increase the elongation, whereas V has little influence. Further, Nb decreases the mean grain sizes.

are displayed in **Figure 3**, and compare the TM route, processed with a FRT of 850 °C (a–c) to the condition after re-austenitization (d–f). The PAGs of base-alloy 1 are almost equiaxed in the DQ850 condition (Figure 3a). Niobium promotes immensely the pancaking of the  $\gamma$ -grains (Figure 3b), the effect

of Vanadium however is less pronounced (Figure 3c). Re-austenitization delivers equiaxed grains as the light optical images (Figure 3d–f) reveal. RQ of base alloy 1 leads to the same mean grain size (Figure 3d), yet, globularized PAGs. Nb (Figure 3e) and V (Figure 3f) both act as grain refiner after re-austenitization. Nevertheless, Nb refines the grains in every processing route significantly. The influence of V general, the influence of the FRT on the mean prior austenite grain size cannot be determined with certainty, yet, re-austenitization clearly refines the  $\gamma$ -grains (Figure 3d–f).

### 3.2. Mechanical Properties

The ultimate tensile strength (UTS) values are displayed in **Figure 4** for the different compositions investigated. Regarding the strength values of the steels in the as-rolled condition, the DQ variants with a FRT of 850 °C are clearly above those of the DQ variant with a FRT of 930 °C (60–70 MPa) and as well above the RQ samples (30–100 MPa). Base alloy 2, which is alloyed with 0.7% Cr, possesses compared to the low-Cr variant (base alloy 1) in the as-rolled condition less strength. The surcharge of Cr however leads to a slight increase in strength when tempered. The effect of the alloying elements Nb and V becomes evident in TM processing route, whereas no influence is visible in the RQ condition. Processed with a FRT of 850 °C, 0.02% Nb increase the UTS by an amount of 49 MPa and at a FRT of 930 °C by 42 MPa. The strength increase however saturates, which is visible in the weaker strength increase with double the amount of Nb. The same effect can be observed when alloying with V. However, the strength contribution of 0.1% V is less pronounced than the one of Nb, although V is alloyed with fivefold the

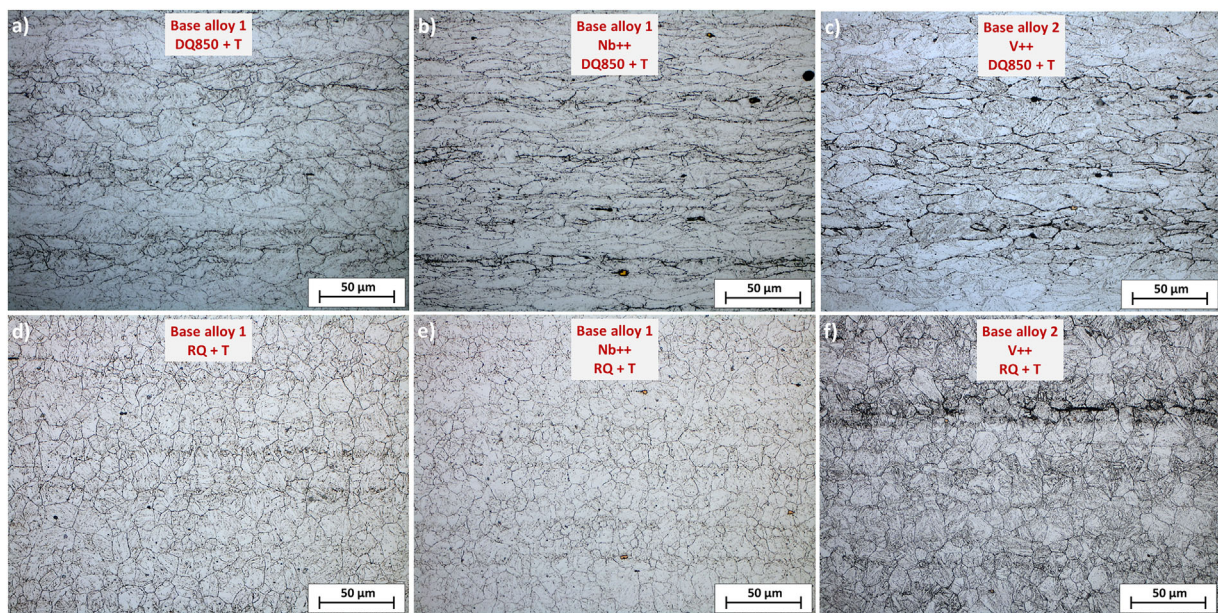


**Figure 3.** Light-optical images of the steels investigated, processed with a FRT of 850 °C (a–c) and after re-austenitization (d–f). a) Base-alloy 1 exhibits almost equiaxed PAGs, b) alloyed with Nb, the aspect ratio rises significantly. c) The influence of V in base alloy 2 on the aspect ratio is less pronounced as through Nb. d) RQ of base alloy 1 leads to the same mean grain size, yet, globularized PAGs. e) Nb and f) V both act as grain refiner after re-austenitization, the effect of Vanadium however is less pronounced.

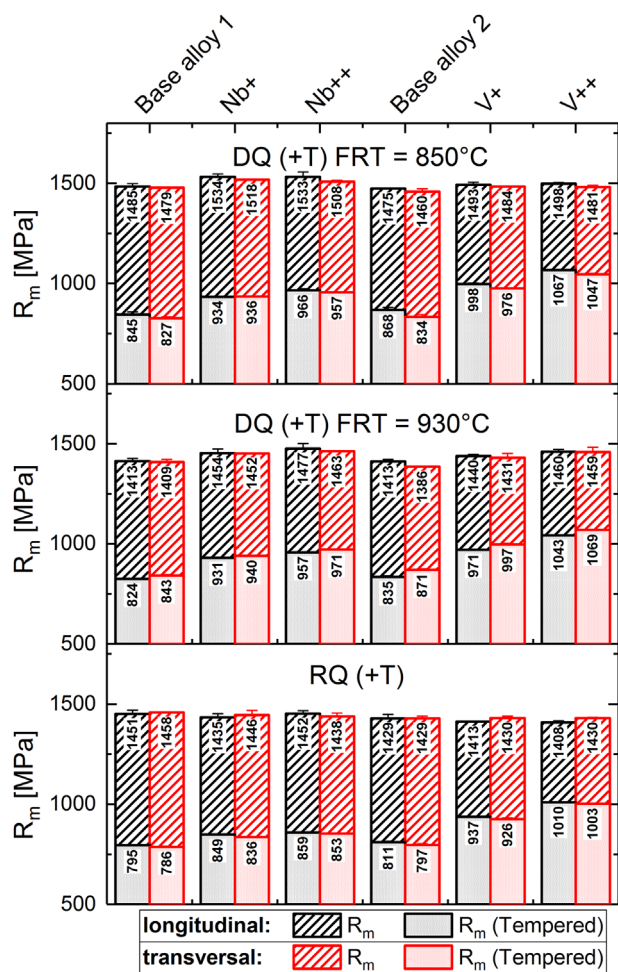


**Figure 4.** UTS values of the investigated steels, both in hardened and tempered condition for the DQ and Q variants. A lower FRT results in higher strength. In as-rolled condition, micro-alloying elements have no significant influence on the strength of the RQ variants, however, V and Nb result in strength increase after tempering. This effect is even more pronounced for the DQ cycles.

quantity. Even more pronounced is the strength contribution of Nb and V after tempering. 0.02% Nb achieve an additional strength of  $\approx 100$  MPa of the TM rolled steels, and  $\approx 50$  MPa after tempering the RQ steel. V counteracts even stronger with a strength contribution of  $\approx 130$  MPa by the addition of 0.1% V and with  $\approx 200$  MPa by the addition of 0.2% V. Nevertheless, the effect of both, Nb and V alloying, seems to saturate after tempering too.

**Figure 5** exhibits the impact toughness for the as-rolled conditions (left) and the tempered state (right) for the 6 steels investigated at 0 °C (upper graphs), -20 °C (middle), and -40 °C (bottom part). The DQ variants with a FRT of 850 °C and the RQ variants possess the best toughness values followed by the TM processed variants with a FRT of 930 °C. The micro-alloying with Nb and V has no significant influence on the impact toughness values of the as-rolled specimens at 0 and -20 °C. Yet, at -40 °C, V seems to deteriorate the notch impact values considerably. As expected, tempering generally improves

the toughness, but when comparing the variants clear differences appear. The RQ variants show slight advantages over the DQ variants. Nb and Cr exhibit no significant improvement, however, Vanadium decreases the toughness after tempering noticeably.

In order to evaluate the influence of the processing route (DQ and RQ) on the mechanical properties in longitudinal and transversal direction, the comparison of the notch impact test results is useful. Microstructural variations affect Charpy impact tests (Figure 5) more than tensile tests (Figure 4). The differences of the impact test results of the longitudinal and transversal direction at 0, -20, and -40 °C can be found in **Figure 6**. Comparing both TM routes, the higher FRT of 930 °C (gray bars) possesses an improved isotropy as the FRT of 850 °C (black bars). This can be identified at all three temperatures. However, RQ does not show an optimization of the mechanical isotropy (red bars), especially at 0 and -20 °C, despite having globular PAGs. For all process routes an improvement is accomplished through tempering (dashed bars). For the Vanadium alloyed variants, the anisotropy even seems to be eliminated completely. However, as can be seen in Figure 5, the impact toughness decreases considerably after tempering for variant 4 and 5. Also the decrease in anisotropy with decreasing test temperatures can be related to the fundamental deterioration of the notch impact values at lower temperatures. Nb exhibits no comprehensive influence in modifying the longitudinal-transversal isotropy of the TM rolled variants. Nevertheless, all surcharges to base alloy 1, Nb, V, and Cr reveals benefits concerning the isotropy of the RQ samples.

### 3.3. Flow Stress Behavior and Activation Energy for Dynamic Recrystallization

For the evaluation of the recrystallization behavior and the influence of V and Nb on the activation energy for the dynamic recrystallization (DRX), dilatometer experiments were performed with deformation temperatures between 850 and 1050 °C, at strain rates of 0.01, 0.1, 1.0, and 10 s<sup>-1</sup>. **Figure 7** shows the corresponding true stress-strain curves at a strain rate of  $\dot{\varphi} = 1.0$  for the five temperatures. For the sake of a better clarity, only the base alloys (black and gray curves) and their corresponding “high” alloy variants (Nb + +: blue dashed line and V + +: red dashed line) are plotted. The flow stress increases significantly with decreasing deformation temperatures, the  $k_{fmax}$  increases from  $\approx 130$  MPa at 1050 °C to 300 MPa at 850 °C. At both 850 and 1050 °C, only a small effect of V and Nb can be observed with a slightly elevated flow stress compared to base alloy 1 and 2, which behave almost congruent regarding their flow stress behavior. However, at the temperatures between 900 and 1000 °C, the effect of the MAE becomes evident. At 1000 °C, the Nb + + variant is clearly elevated above the others and maintains the level of flow stress, while the other curves show a decrease at high strains. The decline of the curve of the V variant is also decelerated. This effect is repeated at 950 °C, where the curve of Nb clearly stands out and shows no significant decrease. Also at 900 °C the Nb + + steel has elevated flow stress behavior,

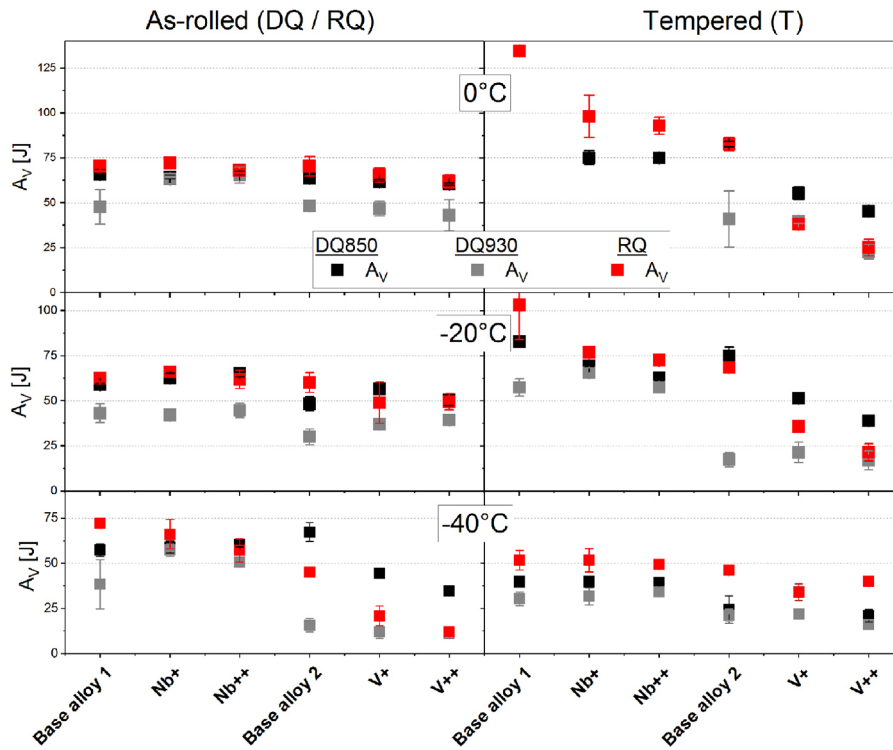


**Figure 5.** Comparison of the impact toughness at 0, -20, and -40 °C of the TM rolled and the re-austenitized steels in the as-rolled condition (left) and in a tempered condition (right). The toughness of base alloy 1 and its variants increases significantly through tempering. Base alloy 2 as well shows an addition in toughness through tempering, yet, alloyed with V, the toughness diminishes considerably through tempering.

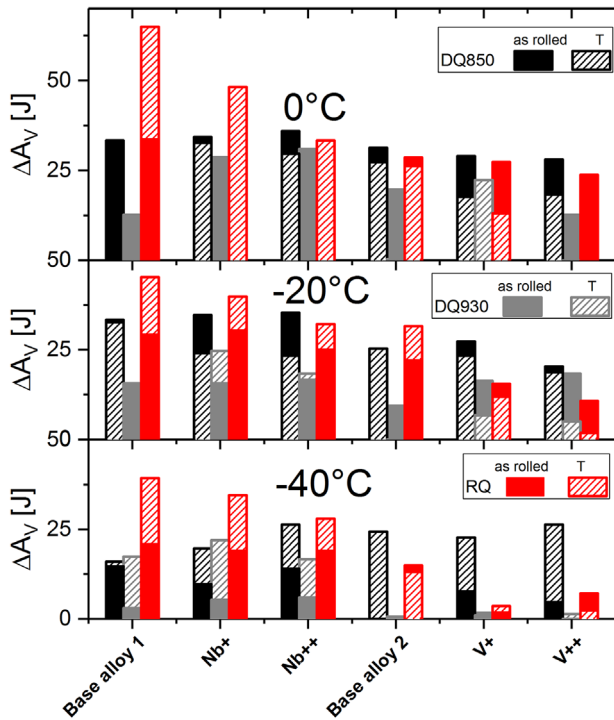


**Figure 6.** Differences of Charpy impact toughness between longitudinal and transverse direction for the 6 steels investigated, depending on their processing route. Re-austenitization has no influence on the mechanical isotropy. However, a high FRT and tempering after quenching slightly reduces the differences between the longitudinal and transversal direction.

whereas the V++ variant enqueues in the behavior of base alloy 1 and 2.

**Figure 8** shows the activation energy for DRX and the  $T_{NR}$ , which were calculated based on the Boratto model.<sup>[24]</sup> Nb possesses the biggest influence on  $E_A$ , already 0.02 wt% increase the activation energy for  $38 \text{ kJ mol}^{-1} \text{ K}^{-1}$ . Cr has no impact on the activation energy, the effect of V is less pronounced compared to Nb, a relatively high amount of 0.2 wt% V rise  $E_A$  only for  $18 \text{ kJ mol}^{-1} \text{ K}^{-1}$ .

#### 4. Discussion

In order to examine the influence of the production route in combination with MAE, six steels with varying contents of V and Nb were rolled in a hot-mill simulation unit with two different FRT of 850 and 930 °C, respectively. To evaluate differences between TM rolling with subsequent quenching and quenching after re-austenitization, the six different steels were additionally subjected to a conventional quenching after reheating to 930 °C for 5 min. The mechanical properties of the as-rolled plates were compared to tempered specimens to study the role of the production route and MAE on their behavior after tempering. TM processing with a low FRT results in improved UTS (Figure 4). The increasing deformation in the non-recrystallization regime and pancaking of the  $\gamma$ -grains (Figure 3) at lower FRT leads to refinement of lath and block size<sup>[40,41]</sup> which contributes to the strengthening. DQ with an elevated FRT and RQ possess comparable strength values, despite both processes result in different PAG sizes. The strength increase

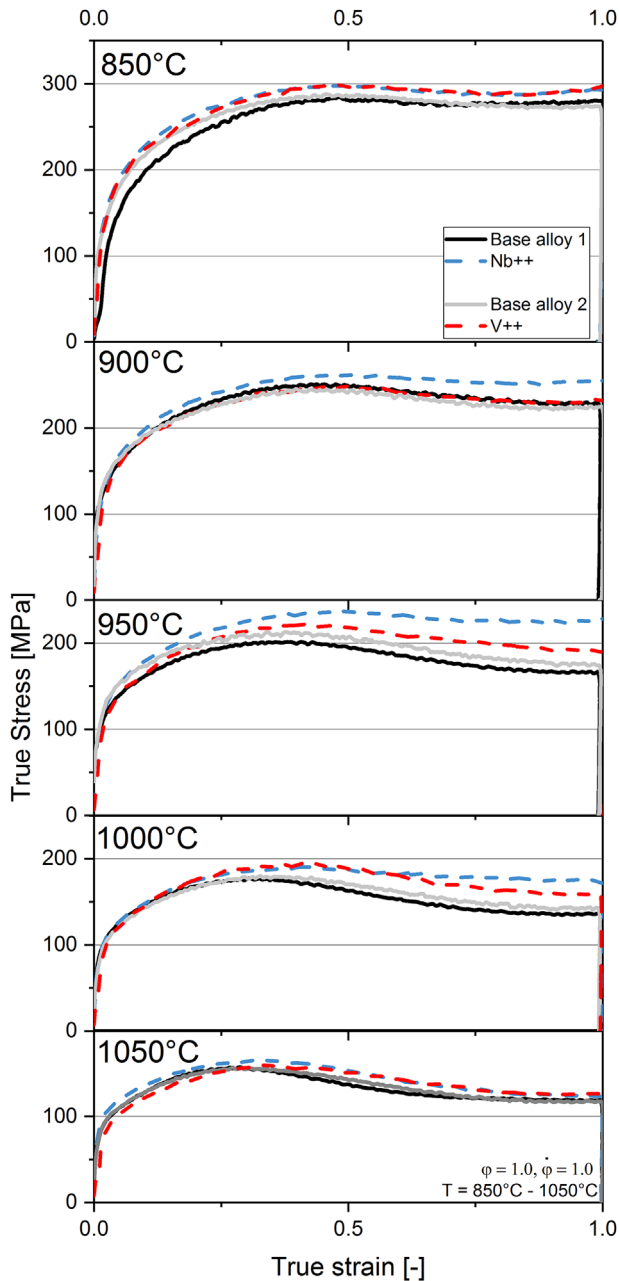


**Figure 7.** True stress–strain curves of base alloy 1 and 2 and its variants. At 1050 °C Nb and V have no effect on the flow stress, at 950 and 1000 °C Nb significantly increases flow stress and prohibits DRX, the effect of V is less pronounced. At 850 °C very little DRX appears, the yield stress curves of the individual alloys are almost congruent.

resulting from a subsequent quenching from the rolling heat compensates the strength improvement through grain refining after re-austenitization of the RQ probes so that similar strength values emerge. Comparing DQ930 and RQ, the mechanical properties of the TM rolled and direct-quenched route shows benefits, when alloyed with Nb. An elevation of  $T_{NR}$  promotes an increased deformation in the non-recrystallization regime (Figure 8), so that even the higher FRT profits from a certain TM contribution, as the last rolling steps are already below  $T_{NR}$ .

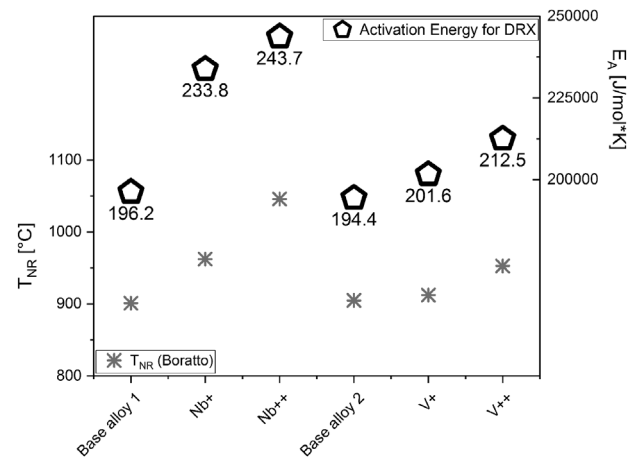


**Figure 8.** Activation energy  $E_A$  and the non-recrystallization temperature  $T_{NR}$ , calculated based on the Boratto model.<sup>[24]</sup> Nb increases  $E_A$  significantly, whereas V exhibits only little effect. Same trend can be observed regarding their role on the  $T_{NR}$ .

This profit is expressed by the aforementioned refinement. The effect of V on the  $T_{NR}$ , which includes the influence on the  $E_A$  for DRX, is very weak (Figure 8). This is reflected in the reduced pancaking (Figure 1, 2) and thus in the quasi non-existent TM-contribution to the DQ route. In **Figure 9**, the strength contribution of V and Nb is summarized as a function of the alloying content and contrasts the influence of the MAE on the strength in the as-rolled condition and after tempering. The strength potential of V is reached after tempering and is attributable to the precipitation of VC and  $V_4C_3$  and substitution of cementite carbides.<sup>[3,14,42]</sup> As in Figure 9 visible, the higher FRT even gains more strength through T, then the counterpart

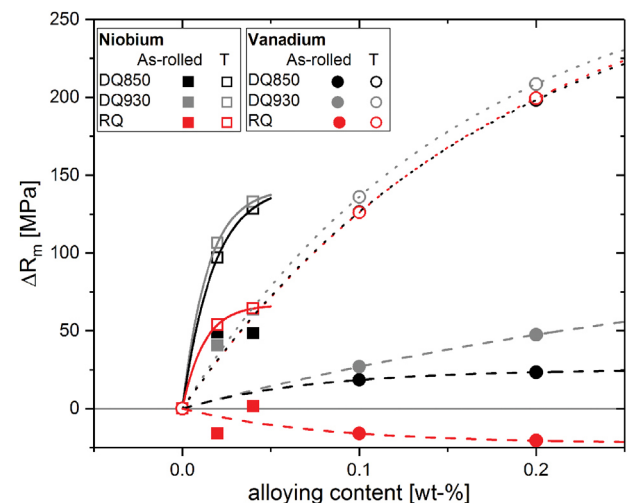


**Figure 9.** Strength contribution of Nb and V. The effect of V for strength improvement during TM rolling is very small (dashed lines), and even negative if re-austenitized. However, during tempering it significantly increases the UTS by 200 MPa (dotted lines). Nb has no effect as strengthener after re-austenitization and Q, however, delivers a plus of >50 MPa after tempering. During TM processing (DQ850, DQ930), little amounts of Nb already contribute to a strengthening. After tempering, again the effect is even more pronounced.

with the lower FRT or the RQ variant, respectively. It is assumed, that V carbides, which are responsible for the strength improvement are precipitated in a higher amount at lower rolling temperatures of 850 than at 930 °C, where a sufficient portion is still available for an improved strength gain during tempering. Despite the improvement of strength, Vanadium shows a negative effect on the impact toughness after tempering. This effect is portrayed by **Figure 10**, which contrasts the elongation at fracture and the notch impact toughness at 0 °C to the ultimate tensile strength. During tempering, the strength decreases in favor of the elongation at fracture. Although, the V variants follow this well-known trend concerning their elongation values, the impact values deteriorate significantly, whereas the other variants are improved concerning their impact toughness. This effect can be deduced to the embrittlement through vanadium carbides.<sup>[43,44]</sup>

Regarding the Charpy impact values in the as-rolled condition, neither V nor Nb result in a significant improvement or deterioration (Figure 5). However, the TM rolled plates with a FRT of 930 °C are generally lower. The DQ850 samples possess surprisingly similar values as the RQ variants, although their strength is remarkably higher. At -40 °C, the values of the DQ850 probes are even above those produced via

RQ. This can be attributed to the aforementioned refinement of lath and blocks through the increased pancaking: the resulting grain refinement offers enhanced strength and toughness and shifts the ductile-to-brittle temperature to lower temperatures.<sup>[14,33,45,46]</sup>

The comparison of the PAG aspect ratio to the Charpy impact toughness in longitudinal and transversal direction did not deliver a clear correlation. Although the reduced pancaking through an elevated FRT in DQ930 exhibits an improved isotropy of the notch impact values compared to DQ850, a globularization of the PAGs through re-austenitization (RQ) deteriorates the anisotropy again. The orientation of the martensitic blocks, which are arranged in 45° toward the RD (Figure 1a, b) and originate from the pancaked  $\gamma$  grain in an angle of 45°,<sup>[47]</sup> obviously play no significant role on the anisotropy either. The longitudinal-transversal differences of RQ, in which the martensitic components are aligned randomly are even higher compared to DQ. Increasing the pancaking through Nb has no obvious effect on the anisotropy. However, annealing after quenching seems to enhance those differences. As proposed by Kaijalainen et al.<sup>[40,48,49]</sup> rolling textures, which are dependent on the FRT are responsible for unfavorable bending properties.<sup>[50]</sup> These preferred orientations cannot be eliminated by quenching or normalizing and thus can be an explanation for the remaining anisotropy. However, further investigations are necessary to provide information on this matter.

Investigations on the flow stress behavior and the DRX have confirmed the different roles of Nb and V micro-alloying. Nb comes already to affect at relatively high temperatures (>1000 °C), and retards the recrystallization with very small additions (0.02 m%) through the formation of carbides.<sup>[14]</sup> These observations are visible in the flow stress curves (Figure 7). Although Vanadium is a strong carbide former, the high solubility product compared to Ti and Nb<sup>[51]</sup> and the low solute drag<sup>[52]</sup> attribute V only a weak effect in retarding recrystallization. As visible in Figure 8, even large amounts of vanadium, which exceed conventional micro-alloying contents, have just little effect on the DRX. These calculations are supported by the similar trend of  $T_{NR}$  dependent on DRX (Figure 8).

## 5. Summary

In order to explore the influence of the production route in combination with micro-alloying elements, six steels with varying content of V and Nb were investigated in their as-rolled and tempered condition. Their mechanical properties after direct quenching and quenching after re-austenitization were examined. The main findings are summarized in the following:

- 1) Nb is confirmed in its important role in retarding recrystallization. However, its strong impact on the improvement of mechanical properties after tempering is unattended till now. It counteracts in compensating the softening during tempering. This effect is enhanced by a previous TM rolling.
- 2) Vanadium has a negligible effect on the mechanical properties of both DQ and RQ steels in the as-rolled condition, as it is not capable in retarding recrystallization considerably. However, it manifests its effect after tempering, 0.1 m% of V lead to an additional strength of 130 MPa after tempering. Despite of the positive effect on UTS, Vanadium

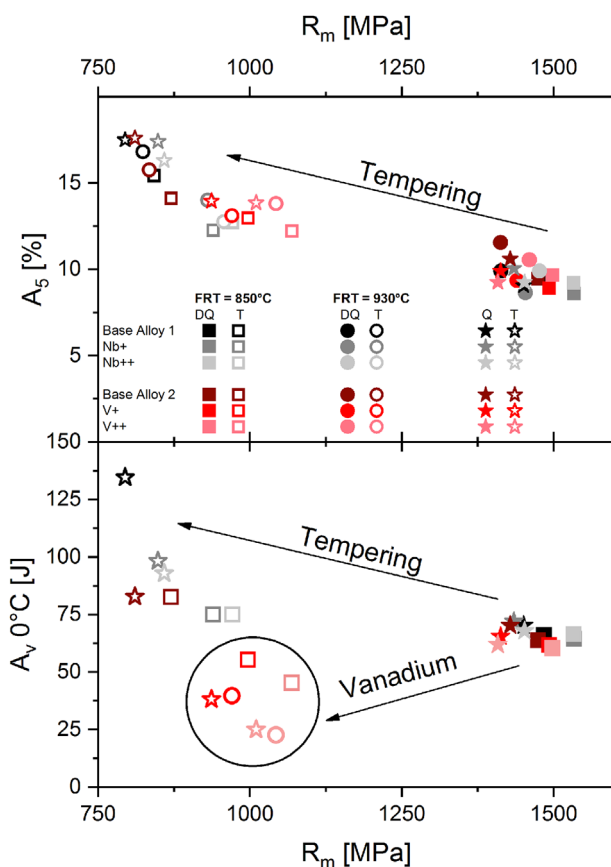


**Figure 10.** Elongation at fracture and notch impact toughness at 0 °C versus UTS. During tempering, the strength decreases in favor of the elongation at fracture. This trend is expected for the impact toughness too, however as alloyed with Vanadium, the toughness decreases significantly after tempering.

alloyed steels suffer from embrittlement after tempering, followed by a deterioration of the impact toughness. Positive effects of Cr on the temper resistance were not observed.

- 3) Re-austenitization previous to quenching does not improve the longitudinal–transversal anisotropy despite of a globular PAG. In contradiction, a reduced pancaking through a higher FRT results in an improvement of this anisotropy. Nevertheless, higher FRT have a negative effect on UTS and Charpy impact toughness.

## Acknowledgement

Funding of the Austrian BMVIT (846933) in the framework of the program “Production of the future” and the “BMVIT Professorship for Industry” was gratefully acknowledged.

## Conflict of Interest

The authors declare no conflict of interest.

## Keywords

direct quenching, finish rolling temperature, mechanical anisotropy, Nb micro-alloying, thermomechanical processing, V micro-alloying

Received: December 20, 2018

Revised: February 18, 2019

Published online:

- [1] M. Klein, R. Rauch, H. Spindler, P. Stiaszny, *BHM Berg- Hüttenmänn. Monatsh.* **2012**, 157, 108.
- [2] M. Klein, H. Spindler, A. Luger, R. Rauch, P. Stiaszny, M. Eigelsberger, *Mater. Sci. Forum* **2005**, 500–501, 543.
- [3] H. Bhadeshia, R. Honeycombe, *Steels: Microstructure and Properties*, 4th edn., Butterworth-Heinemann, Oxford, UK **2017**, pp. 237.
- [4] T. Tanaka, *Int. Met. Rev.* **1981**, 26, 185.
- [5] D. T. Llewellyn, R. C. Hudd, *Steels: Metallurgy and Applications*, 3rd edn., Butterworth-Heinemann, Oxford [England], Woburn, MA **1998**.
- [6] C. R. Brooks, *Principles of the Heat Treatment of Plain Carbon and Low Alloy Steels*, 1st edn., ASM International, Ohio, USA **1996**, pp. 3.
- [7] C. Ouchi, *ISIJ Int.* **2001**, 41, 542.
- [8] A. Kaijalainen, S. Pallaspuro, D. A. Porter, *Adv. Mater. Res.* **2014**, 922, 316.
- [9] S. Pallaspuro, A. Kaijalainen, T. Limnell, D. A. Porter, *Adv. Mater. Res.* **2014**, 922, 580.
- [10] R. Schnitzer, D. Zügner, P. Haslberger, W. Ernst, E. Kozeschnik, *Sci. Technol. Weld. Join.* **2017**, 22, 536.
- [11] P. Haslberger, S. Holly, W. Ernst, R. Schnitzer, *J. Mater. Sci.* **2018**, 53, 6968.
- [12] O. Grong, D. K. Matlock, *Int. Met. Rev.* **1986**, 31, 27.
- [13] D. J. Abson, R. J. Pargeter, *Int. Met. Rev.* **1986**, 31, 141.
- [14] T. Gladman, *The Physical Metallurgy of Microalloyed Steels*, Institute of Materials, London **1997**.
- [15] I. Tamura, *Thermomechanical Processing of High-Strength Low-Alloy Steels*, Butterworths, London, Boston **1988**.
- [16] W. B. Morrison, *Mater. Sci. Technol.* **2009**, 25, 1066.
- [17] A. A. Barani, F. Li, P. Romano, D. Ponge, D. Raabe, *Mater. Sci. Eng. A* **2007**, 463, 138.
- [18] T. Gladman, *Mater. Sci. Technol.* **1999**, 15, 30.
- [19] O. Kwon, A. J. DeArdo, *Acta Metall. Mater.* **1991**, 39, 529.
- [20] R. A. Grange, C. R. Hribal, L. F. Porter, *Metall. Trans. A* **1977**, 8, 1775.
- [21] H. L. Andrade, M. G. Akben, J. J. Jonas, *Metall. Trans. A* **1983**, 14, 1967.
- [22] S. F. Medina, *Mater. Sci. Technol.* **1998**, 14, 217.
- [23] L. J. Cuddy, in *Proc. 1981 Thermomechanical Processing of Microalloyed Austenite*, TMS-AIME, Warrendale, PA **1981**, pp. 129–140.
- [24] R. Barbosa, F. Boratto, S. Yue, J. J. Jonas, in *Proc. of the International Conference on Processing Microstructure and Properties of HSLA Steels*, The Mineral, Metals and Materials Society, Pittsburgh, PA **1987**, pp. 51–56.
- [25] C. N. Homsher, *PhD thesis*, Colorado School of Mines, **2013**.
- [26] B. Pereda, B. Lopez, J. M. Rodriguez-Ibabe, in *Proc. International Conference on Microalloyed Steels: Processing, Microstructure, Properties and Performance*, AIST, Pittsburgh **2007**, pp. 151.
- [27] S. Vervynckt, K. Verbeken, B. Lopez, J. J. Jonas, *Int. Mater. Rev.* **2012**, 57, 187.
- [28] L. Bracke, W. Xu, T. Waterschoot, *Mater. Today Proc.* **2015**, 2, 659.
- [29] A. Kaijalainen, N. Vähäkuopus, M. Somani, S. Mehtonen, D. Porter, J. Kömi, *Arch. Metall. Mater.* **2017**, 62, 619.
- [30] J. J. Jonas, C. M. Sellars, W. J. M. Tegart, *Metall. Rev.* **1969**, 14, 1.
- [31] H. Mirzadeh, J. M. Cabrera, J. M. Prado, A. Najafizadeh, *Mater. Sci. Eng. A* **2011**, 528, 3876.
- [32] G. Krauss, *Steels: Processing, Structure, and Performance*, 3rd edn., ASM International, Ohio, USA **2005**.
- [33] D. T. Llewellyn, R. C. Hudd, *Steels: Metallurgy and Applications*, 3rd ed., Butterworth-Heinemann, Oxford [England]; Woburn, MA **1998**.
- [34] D. K. Matlock, J. G. Speer, *Mater. Sci. Technol.* **2009**, 25, 1118.
- [35] P. D. Hodgson, H. Beladi, M. R. Barnett, *Mater. Sci. Forum* **2005**, 500–501, 39.
- [36] G. E. Totten, *Steel Heat Treatment: Metallurgy and Technologies*, CRC Press, Boca Raton **2006**.
- [37] R. Esterl, M. Sonnleitner, R. Schnitzer, *Steel Res. Int.* **2019**, DOI: 10.1002/srin.201800500.
- [38] R. Esterl, M. Sonnleitner, M. Stadler, G. Wölger, R. Schnitzer, *Pract. Metallogr.* **2018**, 55, 203.
- [39] J. M. Sosa, D. E. Huber, B. Welk, H. L. Fraser, *Integrating Mater. Manuf. Innov.* **2014**, 3, 10.
- [40] A. J. Kaijalainen, P. P. Suikkanen, T. J. Limnell, L. P. Karjalainen, J. I. Kömi, D. A. Porter, *J. Alloys Compd.* **2013**, 577, 642.
- [41] Y. Prawoto, N. Jasmawati, K. Sumeru, *J. Mater. Sci. Technol.* **2012**, 28, 461.
- [42] A. I. H. Committee, *ASM Handbook: Heat Treating*, ASM International, Metals Park, Ohio **1991**.
- [43] R. Lagneborg, T. Siwecki, S. Zajac, B. Hutchinson, *Scand. J. Met.* **1999**, 28, 186.
- [44] A. P. V. Wyk, G. Pienaar, *J. Afr. Inst. Min. Met.* **1987**, 87, 73.
- [45] G. Gottstein, *Physikalische Grundlagen der Materialkunde*, 3. Aufl., Springer, Berlin, **2007**.
- [46] A. Brownrigg, *Scr. Metall.* **1973**, 7, 1139.
- [47] S. Zajac, V. Schwinn, K. H. Tacke, *Mater. Sci. Forum* **2005**, 500–501, 387.
- [48] A. J. Kaijalainen, P. P. Suikkanen, L. P. Karjalainen, D. A. Porter, *Mater. Sci. Eng. A* **2016**, 654, 151.
- [49] A. J. Kaijalainen, P. Suikkanen, L. P. Karjalainen, J. J. Jonas, *Metall. Mater. Trans. A* **2014**, 45, 1273.
- [50] W. Bleck, R. Grossterlinden, U. Lotter, C.-P. Reip, *Steel Res.* **1991**, 62, 580.
- [51] H. Bhadeshia, R. Honeycombe, in *Steels: Microstructure and Properties*, 4th edn., Butterworth-Heinemann, Oxford, UK **2017**, p. 101.
- [52] R. J. Glodowski, in *Application Technologies of Vanadium in Flat-rolled Steels -Vanitec Symposium*, Suzhou, China, **2005**, p. 43.

## Paper V:

Esterl R, Sonnleitner M, Weißensteiner I, Hartl K, Schnitzer R (2019)

*Influence of quenching conditions on texture and mechanical properties of  
ultra-high strength steels*

Submitted to Journal of Materials Science

# Influence of quenching conditions on texture and mechanical properties of ultra-high strength steels

Raphael Esterl<sup>1</sup>, Markus Sonnleitner<sup>2</sup>, Irmgard Weißensteiner<sup>3</sup>, Karin Hartl<sup>1</sup>, Ronald Schnitzer<sup>1</sup>

<sup>1</sup> Department of Materials Science, Montanuniversität Leoben, Franz Josef-Str. 18, 8700 Leoben, Austria

<sup>2</sup> voestalpine Stahl GmbH, voestalpine-Straße 1, 4020 Linz, Austria

<sup>3</sup> Christian Doppler Laboratory for Advanced Aluminum Alloys, Chair of Nonferrous Metallurgy, Montanuniversität Leoben, Franz Josef-Str. 18, 8700 Leoben, Austria

**Keywords:** ultra-high strength steels, thermomechanical processing, direct quenching, texture analysis, micro-alloying

## Abstract:

Direct quenching of thermomechanical processed low-carbon steels is a preferred production route to increase strength and toughness of ultra-high strength steels and thus enhance the payload to weight ratio e.g. of mobile cranes. However, during hot rolling, certain crystallographic textures emerge, which can generate unfavorable mechanical properties or mechanical anisotropy. In order to investigate the role of the processing route and the effect of micro-alloying elements on the texture formation and its relationship to differences between different testing directions, four different ultra-high strength steels were subjected to various quenching procedures. It was found, that despite of a globularization of the prior austenite grain after re-austenitization, differences in the longitudinal and transversal direction remain. The extinction of a rolling texture after re-austenitization is dependent on the austenitization condition and the addition of micro-alloying elements. Especially Nb promotes the formation of rolling texture components and prevents the extinction thereof even through intense austenitization treatments. However, remaining preferred orientations exhibit only little influence on the anisotropy of the mechanical properties.

## 1. Introduction

For the production of mobile crane booms, ultra-high strength steels (UHSS) are in application to provide an optimized payload-to weight ratio <sup>[1-3]</sup>. The strength is accomplished by a grain refinement by means of a systematic combination of micro-alloying elements (MAE) and process parameters. This includes as well a targeted temperature control during hot rolling <sup>[4-6]</sup>. A martensitic microstructure, achieved through a subsequent quenching delivers a yield strength (YS) up to 1500 MPa <sup>[1,3,7-9]</sup>. The fine grained microstructure not only meets highest strength requirements but also guarantees proficient toughness <sup>[3,10]</sup>. UHSS produced via thermomechanical processing (TMP) have widely substituted steels, which are



fabricated through the conventional re-austenitization and quenching (RQ) route. High deformation rates in the non-recrystallizing austenite region provide enhanced refinement during the following  $\gamma$  to  $\alpha'$  transformation, thus offering further benefits in strength and toughness [1,4,6,11].

The influence of the processing route on the mechanical properties has been broadly investigated [1,5,9,10,12-16]. So exists not only a proportional correlation between the dimension of the austenite grain prior to the martensitic transformation and to the emerging substructure such as blocks and packets [17-19]. Furthermore, increased reduction in the non-recrystallization region promotes the austenite pancaking and thus a finer microstructure during  $\gamma$  to  $\alpha'$  transformation [1,20-22]. These effects are exploited in steel production to optimize the mechanical properties. Nevertheless, it is also known that after hot rolling certain features remain in the microstructure, which result in an anisotropy of the mechanical properties [23]. On the one hand, non-metallic inclusions lead to insoluble inclusion ligaments during rolling and thus affect differences in the longitudinal (L) and transversal (T) directions [23,24]. However, process optimizations in the secondary metallurgy are nowadays capable to limit these disadvantages through an adjustment of the inclusion structure [23-26]. Notwithstanding of the mentioned positive effects on the mechanical properties, on the other hand, an increased reduction below the non-recrystallization temperature ( $T_{NR}$ ), is also known to provoke the L-T anisotropy [20]. In a previous work we showed that RQ does not eliminate the L-T anisotropy despite of a globular PAG [10]. From these observations it can be concluded that, in fact the reduction in the non-recrystallization region, but not the shape of the PAG, influences the mechanical anisotropy. It has been observed, that process parameters and MAE influence the inheritance of several characteristics, so that the newly recrystallized austenite grain remains grain size, shape and orientation of the previous microstructure [27,28]. Several researchers have found, that typical texture components of a  $\alpha$ -fiber ( $\langle 110 \rangle \parallel RD$ ), such as  $\{001\}\langle 110 \rangle$ ,  $\{112\}\langle 110 \rangle$  and  $\{111\}\langle 110 \rangle$  can lead to unfavorable properties [20,29-33]. These rolling texture components have detrimental effects on the bending properties including deviations of L and T. In this case, the finish rolling temperature (FRT) possesses a major influence.

In order to gain a deeper insight into the L-T anisotropy, the present work establishes possible correlations between the differences in the mechanical properties and a preferred texture arising during rolling. For this matter, four direct quenched UHS steels with different contents of MAE were investigated. Their mechanical properties in L and T were characterized and compared to the corresponding properties after RQ. In order to answer the question, if the re-austenitization conditions have an influence on these properties, three different heat treatments with varying austenitization temperature and cooling times were performed before quenching. X-Ray diffraction (XRD) measurements were conducted to study the texture developments as a result of the performed heat treatments. The present work should shed light on the anisotropy of hot-rolled steels and help to understand the role of MAE and processing route on the formation of an unfavorable texture resulting in differences of the mechanical properties between L and T.

## 2. Materials investigated and experimental procedure

### 2.1 Materials, heat treatment and mechanical testing

The investigations on the influence of the processing route were performed on four different steels. The steels display industrial available UHS steel grades and their chemical composition is listed in Table 1. All steels experienced the same rolling conditions, the FRT was set to 850° C. The steels were labeled according to their strength classes and are numbered from 1 – 4. Steel 1 and 2 represent temper resistant UHS steels and possess a carbon content of 0.09%. Additions of Mn, Si and B retard the  $\gamma$  to  $\alpha$  transformation to ensure a martensitic microstructure [34–38]. Mo and V facilitate a TM process route through an elevation of  $T_{NR}$  [22,34,39,40]. Moreover, they compensate for the softening during tempering and enhance weldability [41]. Compared to the base alloy 1, steel 2 has higher additions of Cr, and additionally Ni is added for further temper resistance [37,42]. Alloy 3 represents a wear resistant steel with a carbon content of 0.17%. Elevated additions of Si and Mn enable a through-hardening [35]. Compared to steel 3, temper resistance is given in Steel 4 with elevated amounts of Cr, Ni, Mo and Cu. Further, steel 4 is alloyed with Nb, which serves as strongest MAE in retarding recrystallization and providing additional strength after tempering [10,43].

Table 1: Chemical composition of the steels investigated [m%]

Steel	Description	C	Si	Mn	Cr	Ni	Mo	Cu	V	Ti	Nb	B
1	0.09 C, base alloy	0.09	0.1	1.6	0.70	0.01	0.20	0.03	0.10	0.02	<0.01	0.002
2	0.09 C, increased alloy content	0.09	0.1	1.6	0.90	0.50	0.20	0.03	0.10	0.02	<0.01	0.002
3	0.17 C, lean alloy	0.17	0.2	2.3	0.30	0.01	0.02	0.03	0.001	0.02	<0.01	0.002
4	0.17 C, increased alloy content	0.17	0.3	1.4	0.70	1.0	0.40	0.50	0.05	0.02	0.04	<0.001

The steels were investigated in the as-rolled condition and compared to re-austenitization and quenching, for which three different austenitization procedures were performed. The different heat treatments are listed in table 2. The conventional re-austenitization and quenching (RQ) consists of an austenitization at a temperature of 930° C for 5 min followed by water quenching. In the second route, quenching is performed after normalization treatment and an extended austenitization time of 30 min (NRQ). In the third route quenching was executed after a higher austenitization temperature of 1050° C (HRQ).

Table 2: Heat treatment and quenching procedures,  $T_Q$  displays the quenching time and  $t_Q$  the austenitization time

Description	1. Heat treatment			2. Heat treatment		
	$T_Q$ [°C]	$t_Q$ [min]	Cooling medium	$T_Q$ [°C]	$t_Q$ [min]	Cooling medium
DQ Direct quenched			water			
RQ Re-austenitized and quenched	930	5	water			
NRQ Normalized, re-austenitized and quenched	930	30	air	930	30	water
HRQ High-temperature re-austenitized and quenched	1050	5	water			

Tensile tests were performed according to DIN EN ISO 6892-1 on flat tensile specimens in longitudinal and transversal direction of the rolled plates of each condition. The notch impact tests at 0°, -20° C and -40° C were performed according to DIN EN ISO 148-1 on 6 mm thick specimens and the obtained notch impact work was standardly converted to 10x10 mm full-sized samples by linear upscaling. In order to exclude possible outliers in the tests, tensile tests were applied twice in each direction and for impact tests three samples of each condition were tested.

## 2.2 Sample preparation and parameters for XRD and EBSD analysis

For the microstructural analysis, three different conditions (DQ, RQ and NRQ) of the four steels were investigated. Since the measuring principles of XRD and EBSD differ, the perspective on the plate is also different. The relevant position to detect rolling textures was set to  $\frac{1}{4}$  of the sheet thickness [44]. For EBSD measurements, the transversal direction (TD) of the sheet is observed, as the electron beam can be focused to the significant position on the sheet.

The samples were hot embedded and then ground from 320 grit to 4.000 grit SiC paper for at least 30 s. Subsequently, the samples were polished with 3  $\mu\text{m}$  diamond paste for at least 3 min and with 1  $\mu\text{m}$  for 30 s. A silicate polishing was used (*Struers OPS*) for 10 min prior to a finishing electrolytic ablation of 5 s with 35 V. The samples were dipped in a diluted Nital etchant and plasma cleaned for 9 h before performing EBSD measurements. The measurements were performed on a EDAX Hikari XP EBSD system, installed in a *FIB Versa FEI 3D DualBeam*. An acceleration voltage of 30 kV was applied and a step size of 100 nm was chosen. The data acquisition was performed with *EDAX Team 32*. The data was evaluated with *EDAX OIM Analysis 7.3*, in which a *grain dilatation cleanup* with one single iteration was executed.

In contrast to the electron beam, the X-ray beam cannot be focused. Therefore, the surface of the plate was milled down to  $\frac{1}{4}$  of the thickness prior to grounding and polishing in order to place the beam on

the relevant position of the plate. In the following, electrolytic polishing was performed for 1 min with 35 V. The utilized XRD, *Bruker-ASX*, was operated with a voltage of 40 kV at 40 mA and a  $K_{\alpha}$  Cu X-ray tube. In steps of  $5^{\circ}$ ,  $\{110\}$ ,  $\{200\}$  and  $\{211\}$  pole figures were measured by means of a *LYNXEYE XE* detector and evaluated with the program *DiFFRAC.SUITE.measurement<sup>TM</sup>*. The orientation distribution functions (ODF) of the individual sample conditions were calculated from the obtained pole figures in the software package *MTEX* at an applied half width of  $5^{\circ}$  [45]. Volume portions are then calculated to describe the relative volume of the relevant crystals, which obtain a certain orientation.

### 3. Results

#### 3.1 Mechanical properties

The yield strength of the four steels investigated are provided in Figure 1. Steel 3 and 4 possess significantly higher YS compared to steel 1 and 2. The strength of the DQ condition is considerably above those after re-austenitization (RQ) for each of the steels investigated. The additional normalization (NRQ) and the higher austenitization temperature (HRQ) result in a minor decrease in strength for steel 1 and 4. Yet, this phenomenon is less pronounced as compared to DQ. The L - T differences are decreasing after re-austenitization, NRQ and HRQ for steel 1 and 2. Steel 3 and steel 4 however do not reveal a clear trend. The strength in the T direction is still marginal higher compared to the absolute values (<50 MPa). Clearer differences in the L-T

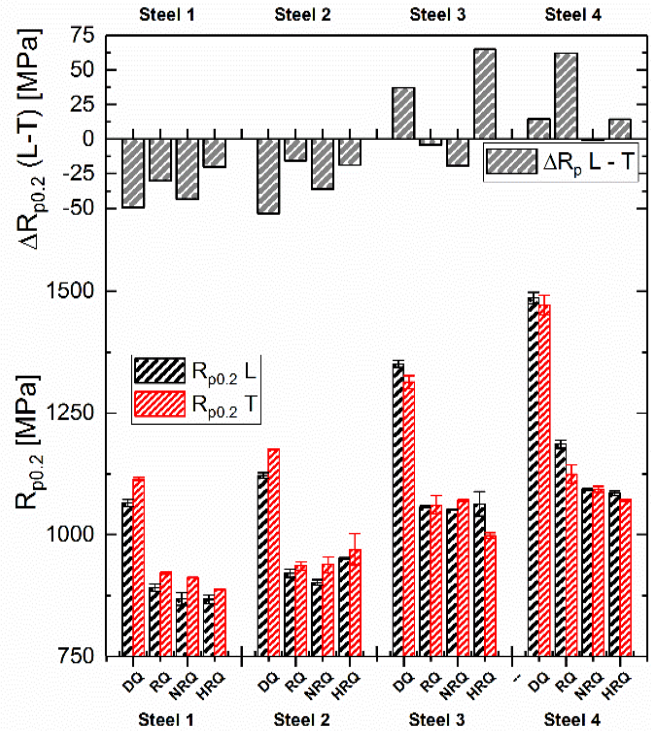


Fig. 1: YS and L - T difference values dependent on the heat treatment of the four steels investigated. The strength decreases significantly through re-austenitization and quenching. Steel 1 and 2 improve regarding their L-T anisotropy, however, the differences are very little regarding the absolute UTS values of >900 MPa. Steel 3 and 4 exhibit no clear trend.

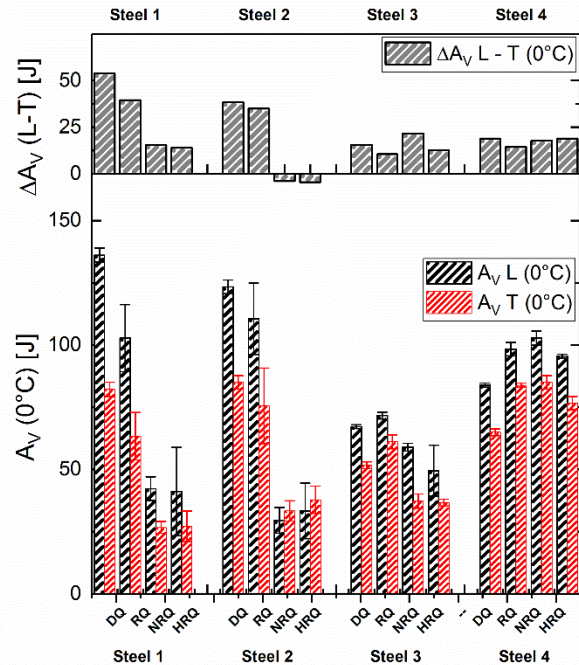


Fig. 2: Charpy impact toughness values and L - T difference values at 0°C dependent on the heat treatment of the four steels investigated. Steel 1 - 3 experience a deterioration of the impact toughness through re-austenitization and quenching, whereas steel 4 delivers an improvement in toughness. The L-T anisotropy of steel 1 and 2 seems to benefit from re-austenitization, whereas steel 4 does not show any reaction not even through high quenching temperatures.

anisotropy are evident in the Charpy impact toughness, which are displayed in Figure 2 for the investigated steels at a testing temperature of 0°C. The toughness behaves diametrical to the strength, steel 1 and 2 have the highest Charpy impact toughness values, followed by steel 4 and 3. Steel 1 – 2 experience a deterioration of the impact toughness values through re-austenitization and quenching, steel 3 first after normalization. The toughness of steel 4, however increases through re-austenitization. The L-T anisotropy of steel 1 and 2 benefits from the re-austenitization. The more intense the annealing in the  $\gamma$  region is (e.g. NRQ and HRQ), the smaller the L-T difference becomes. For steel 2 it disappears completely. The anisotropy for steel 3 and 4 are neither deteriorated nor improved through different treatments in the  $\gamma$  region. The temperature dependence of the Charpy impact

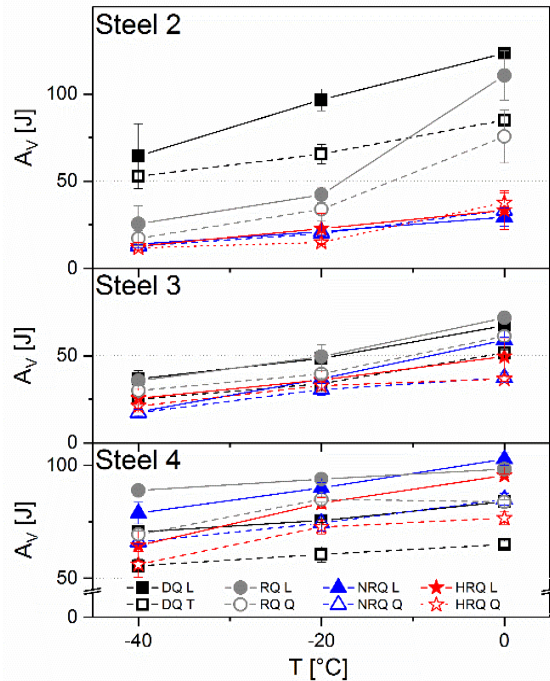


Figure 3: Charpy impact toughness between -40°C and 0°C for steel 2 – 4. Steel 2 deteriorates significantly through re-austenitization, whereas steel 3 does not show pronounced influence of the hardening treatment due to generally lower impact strength values. The impact toughness values of steel 4, which are already very high are little improved through both RQ and NRQ.

toughness is displayed in Figure 3 for temperatures between -40°C and 0°C for steel 2 – 4. The decrease of the impact toughness of steel 2 is less pronounced at 0°C, however at -20°C, it deteriorates to values below 50 J. The impact toughness of steel 4 is clearly improved through re-austenitization and amounts even at -40°C almost 100 J for the normalized and quenched variant NRQ.

### 3.2 EBSD analysis

The inverse pole figure maps for steels 2 – 4 in the TD are given in Figure 4. In the DQ condition, steel 2 (a) and 4 (c) show a strong deformation of the former  $\gamma$ -grains towards the rolling direction. Steel 4 exhibits a very fine martensitic microstructure, which, divided in blocks and laths, originates from the also very fine prior austenite grains. The martensitic microstructure of steel 3 originates from globular PAGs, which are obviously larger than in steel 4. During re-austenitization, the PAGs form to a globular shape, which can be seen in Figure 4 d – f. Whereas steel 2 (d) and 3 (e) coarsens significantly through reheating in the  $\gamma$ -region, the grain growth of steel 4 is limited. Both, the PAGs as well as the martensitic components are still extremely fine after re-austenitization.

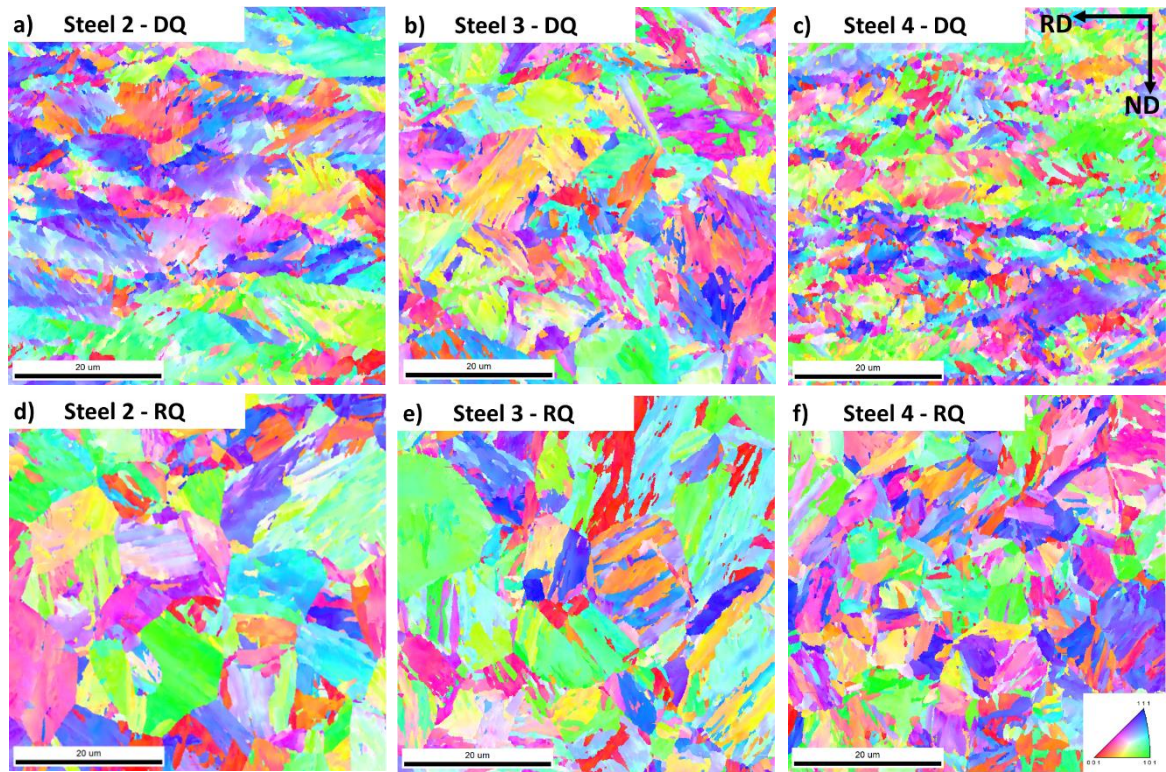


Fig. 4: EBSD inverse pole figures for the TD in the as-rolled condition for a) steel 2, b) steel 3 and c) steel 4. The MAE in steel 2 (a) and 4 (c) promote a pancaking towards the RD, the PAGs are clearly visible as elongated grains. Steel 4 (c) exhibits the finest microstructure (martensitic block and laths). Steel 2 (b) possesses globular PAGs. d-f) Although, after re-austenitization and quenching (RQ) the PAGs increase and globularize for d) steel 2 and e) steel 3, steel 4 (f) still maintains the finest microstructure.

### 3.3 XRD measurements: ODF maps and quantitative texture analysis

Figure 5 illustrates the ODF at a constant angle  $\varphi_2 = 45^\circ$  of steel 1 – 4 dependent on the processing condition. A significant increase of the rotated cube component  $\{001\} \langle 110 \rangle$ , evaluated from the ODF with an angular tolerance of  $10^\circ$  was observed for steel 1 – 3, especially in the DQ condition. The volume portions, Figure 6 amount 10% for steel 1 and 2 and 12% for steel 3. During re-austenitization and quenching, all texture components decrease in favor of a slight increase of  $\{112\} \langle 110 \rangle$ . After an additional normalization prior to quenching, Steel 2 experiences an increase of  $\{001\}$  planes parallel to the sheet plane, accompanied with the extinction of all other components. All texture components of steel 3 fall below 5% even after a single re-austenitization, concluding, that only little fragments from the rolling history remain. In opposite to the aforementioned, steel 4 exhibits increased intensities in  $\{111\} \langle 112 \rangle$ ,  $\{112\} \langle 131 \rangle$  and  $\{554\} \langle 225 \rangle$  after DQ. These components are marginally reduced on behalf of a growth of the  $\{001\} \langle 110 \rangle$  constituent during RQ and NRQ. However, all texture components of steel 4 are still present in an increased extent.

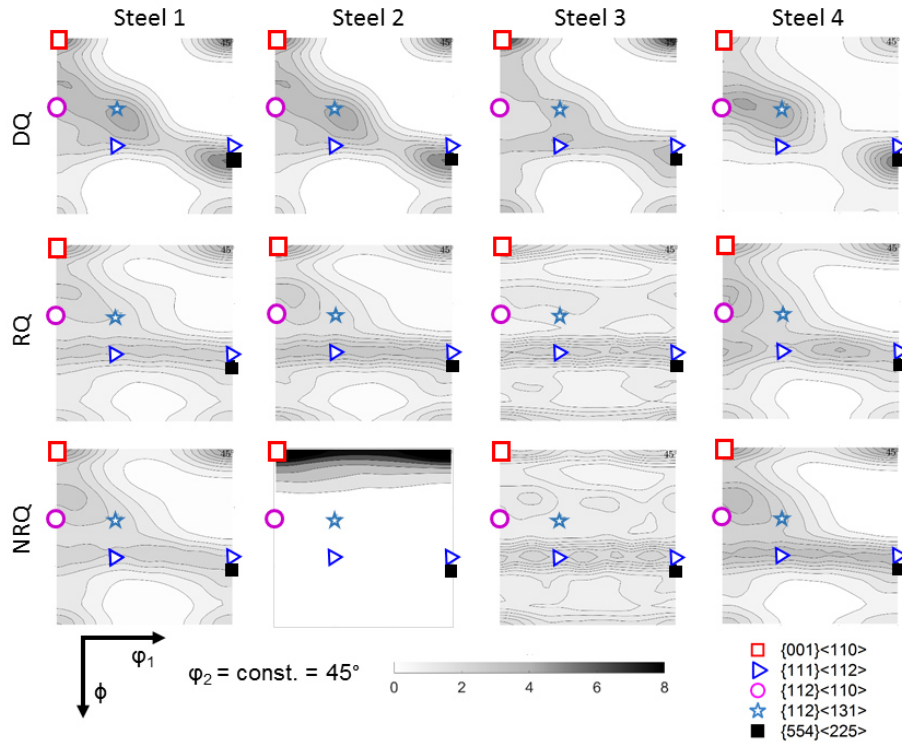


Fig. 5: ODF sections at  $\phi_2=45^\circ$  demonstrating the textures at  $\frac{1}{4}$  of the plate depth for steels 1 - 4 in DQ, RQ and NRQ condition. Steel 1 possesses a weak preferential orientation after re-austenitization, which almost disappear after normalization + quenching (NRQ). The texture components of steel 2 decrease after re-austenitization, after normalization, however the orientations fully disappear in favor of a strong cube  $\{001\}\langle 110 \rangle$  texture. Steel 4 even shows after two time austenitization augmented texture fibers.

#### 4. Discussion

In order to investigate the influence of hardening and varying austenitization conditions on the mechanical properties, four low-C UHS steels were examined regarding their mechanical anisotropy and microstructure. These findings and their relevance are discussed in detail below.

##### 4.1 Mechanical properties

An observation of the YS revealed, that an intense austenitization with a prior normalization can have a positive effect on the L-T anisotropy, especially regarding the 0.09% - C steels 1 and 2. Although, the difference is very little regarding the absolute YS values, it seems, that the globularization of the  $\gamma$ -grains supports the reduction of the different longitudinal and transversal YS. However, this improvement in isotropy reduces the YS significantly. Regarding steel 1, the YS decreases by  $\sim 17\%$ , steel 2 and 3 by 20% and steel 4 even by 24% after a single re-austenitization in the T direction. These observations can be attributed to the grain growth during re-austenitization, as depicted by the IPF map in Figure 4, but cannot alone be the reason for this significant decrease. Although, for all steels the YS is deteriorated in the same amount, the microstructure of steel 4 still maintains very fine after re-austenitization, whereas the grain size of steel 1 - 3 increase unambiguously. A detailed explanation can be given with a view on the different alloying concepts. All investigated steels were rolled with a FRT of  $850^\circ\text{C}$ . The rolling below  $T_{NR}$  leads to a high deformed  $\gamma$  grain (pancaking), which results in a very fine transformed microstructure. Nb (in steel 4) has a by far stronger effect than V (steel 1 and 2) to retard

recrystallization [10,21,22,34,43,46]. The consequence is, that the strength contribution through TMP for steel 4 is much more augmented than compared to steel 1 and 2. Although, the grain coarsening of steel 4 through RQ is less pronounced, the lack of an high deformed  $\gamma$  grain accompanied by the recrystallized austenite contributes to the YS decrease of 24%. These effects as well are observed in the temperature-dependence of the Charpy impact toughness, which is displayed in Figure 3. The detected grain coarsening of steel 2 not only reduces the impact toughness, but shifts the transition temperature to higher values. Although, steel 3 is dispensed with alloying elements which are known to optimize the impact toughness (Mo, V, Ni) [41,47] the toughness still is above 50 J at 0°C and does not deteriorate noticeably through re-austenitization. Steel 4 profits from the fine grain, which is still maintained after re-austenitization and results in higher impact toughness, which is even improved through RQ in elevating the entire level of the DBTT to higher toughness.

#### 4.2 Microstructure and Texture

The investigations on the microstructure delivered details on the different behavior of the four investigated low-C steels regarding their microstructure – property relationship. Several peculiarities of the mechanical properties have been explained through the grain size and structure by means of EBSD measurements. However, there is still a missing link of the remaining anisotropy which in case of steel 3 and 4 cannot be eliminated completely and therefore measurements of the texture were performed. EBSD reaches its limit if the detected microstructure is very small as for the present case [48]. For a proper texture analysis, at least 10.000 grains are suggested to be measured [49]. The step size needs to be reduced immensely when detecting microstructures with high grain boundary densities, as it is the case for martensitic steels. This would result in an extremely high effort for textures analysis with EBSD. The XRD measurements however provided the orientation distributions over the whole sample

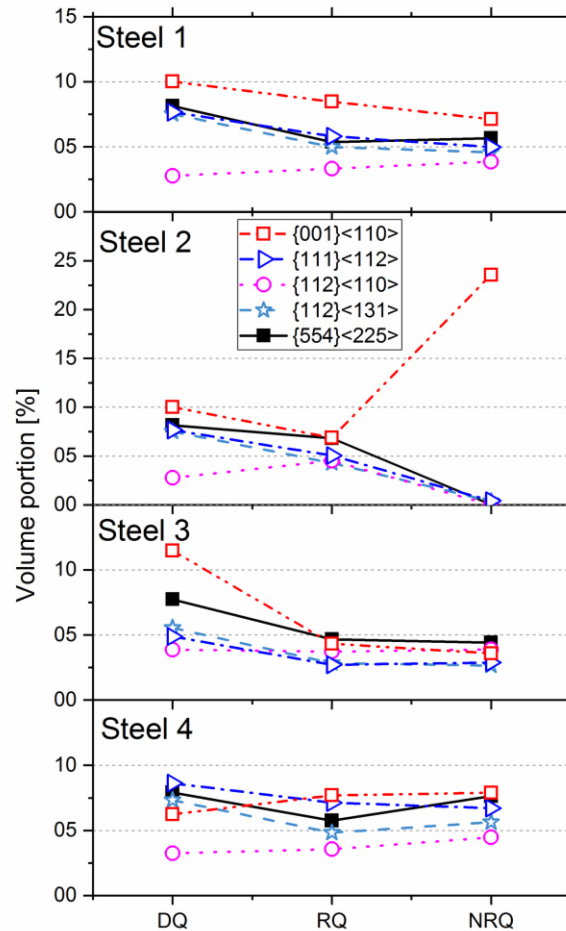


Figure 6: Effect of the different hardening procedures on the texture components of the investigated steels calculated through MTEX based the obtained pole figures. Decreasing textures can be observed during re-austenitization of steel 1 and 3. Steel 2 shows an augmented {001}<110> texture after normalization, steel 4 exhibits texture remnants, however the proportions change after re-austenitization.



for the relevant plate position of 1.5 mm below the surface. The orientations of interest and their distributions are highlighted in Figure 5 and 6. All steels investigated contain a decisive fraction of the  $\{001\}\langle 110 \rangle$  component, especially steel 1 - 3 after DQ from the rolling heat. This orientation arises from the recrystallized austenite cube texture <sup>[50,51]</sup> and thus is sparsely present in steel 4 which is alloyed with strong recrystallization retarding elements (Nb) preventing a recrystallization prior to transformation. The  $\{001\}\langle 110 \rangle$  texture is unfavorable for impact toughness, provokes delamination and crack propagation <sup>[50,52]</sup>, which can be observed in the  $A_v/T$  diagram in Figure 3. With the presence of a strong  $\{001\}\langle 110 \rangle$  texture (Figure 6), the Charpy impact toughness of steel 2 decreases after NRQ and already at a temperature of 0° C below 50 J. These values are even lower than the values measured for steel 3, although a higher toughness is expected for steel 4 according to the diametrical trend of strength and ductility. The prevailing components in steel 3 after DQ are  $\{111\}\langle 112 \rangle$ ,  $\{112\}\langle 110 \rangle$  and  $\{112\}\langle 131 \rangle$  which emerge from a deformed austenite <sup>[29]</sup>. The latter ranks as a very stable orientation for higher toughness towards the rolling direction <sup>[31,33,50-52]</sup>. Furthermore all steels contain significant fractions of  $\{554\}\langle 225 \rangle$  arising as well from a strongly deformed  $\gamma$  grain <sup>[20,50]</sup>. This component is inherited to RQ and even present after NRQ. The relatively high proportions of the  $\{001\}$  in-sheet plane component in the DQ condition of steel 1 - 3 might explain differences between L and T. This is confirmed by the fact, that a reduction of the  $\{001\}\langle 110 \rangle$  partitions reduce the impact toughness anisotropy after RQ. However, the question remains, why an almost levelled-out texture distribution as it exists in steel 3 after re-austenitization (Figure 5 and 6) still possesses small but present differences between L and T. And in opposite to that, steel 4, which exhibits a significant amount of defined texture components even after HRQ exhibits excellent Charpy impact values in each condition (DQ and RQ) with a relatively small anisotropy. Consequently, a clear link between a remaining anisotropy and prevailing textures thus cannot be made with certainty. Furthermore, a strict distinction, whether a mechanical anisotropy can be attributed to an elongated  $\gamma$  grain, texture fractions or non-metallic inclusions <sup>[23]</sup> is not possible. In a previous publication <sup>[10]</sup> it was found, that variances in the FRT can even affect the properties of Q+T steels, contrary to the assumption, that the FRT has no effect on the properties of steels which are later re-austenitized and quenched. The present investigations confirm, that the FRT not only plays a major role during TMP but rather influences the mechanical properties through the inheritance of microstructural characteristics. Although, the usage of MAE and the reduction of the FRT provokes through a highly deformed  $\gamma$  grain a mechanical anisotropy, this does not mean simultaneously, that the microstructural cancellations of these peculiarities are the key to a mechanical isotropy.

## 5. Summary

In order to study the dependency of the mechanical anisotropy on the microstructure, four low-C UHS steels were subjected to varying austenitization conditions prior to hardening. The results described above have shown, that through thermomechanical rolling microstructural peculiarities remain in the material, which are responsible for differences between the longitudinal and transversal direction. This

mechanical anisotropy cannot be eliminated entirely through re-austenitization. The main findings are summarized in the following:

- Differences in the impact toughness between the longitudinal and transversal direction can be lowered through re-austenitization or normalization prior to quenching. However, this improvement reduces the yield strength and impact toughness significantly. The microstructural benefits which are accompanied by thermomechanical processing, such as a grain refinement through a highly deformed  $\gamma$  grain are extinguished through re-austenitization.
- The mechanical anisotropy can partially be contributed to texture components, which are promoted by hot-rolling. These preferential orientations arise either from a recrystallized austenite, such as  $\{001\}\langle 110 \rangle$  or through a deformed  $\gamma$  grain such as  $\{111\}\langle 112 \rangle$ ,  $\{112\}\langle 110 \rangle$  or  $\{112\}\langle 131 \rangle$ . The  $\{554\}\langle 225 \rangle$  component, which was also observed arises from a highly deformed austenite and is inherited to quenching after re-austenitization and even present after normalization.
- A fine  $\gamma$  grain as a result of Nb micro-alloying consolidates the aforementioned texture components and prevents their decimation after re-austenitization.
- The microstructural inheritance through thermomechanical rolling cannot be erased through re-austenitization or normalization. The effect of this inheritance is dependent on the intensity of the TM-program, in specific the usage of MAE and the reduction in the non-recrystallization regime.

### Acknowledgements

Funding of the Austrian BMVIT in the framework of the program “Production of the future”, the Austrian Federal Ministry for Digital and Economic Affairs, the National Foundation for Research, Technology and Development as well as the “BMVIT Professorship for Industry” is gratefully acknowledged. Further, we sincerely thank the voestalpine Stahl AG, who provided the steel samples for the present investigations.

### Conflict of Interest

The authors declare no conflict of interest.

### 6. References

- 1 I. Tamura, ed.: *Thermomechanical Processing of High-Strength Low-Alloy Steels*, Butterworths, London, UK, 1988.
- 2 M. Klein, R. Rauch, H. Spindler, and P. Stiaszny: *BHM Berg- Hüttenmänn. Monatshefte*, 2012, vol. 157, pp. 108–112.

- 3 M. Klein, H. Spindler, A. Luger, R. Rauch, P. Stiaszny, and M. Eigelsberger: *Mater. Sci. Forum*, 2005, vol. 500–501, pp. 543–50.
- 4 P.D. Hodgson, H. Beladi, and M.R. Barnett: *Mater. Sci. Forum*, 2005, vol. 500–501, pp. 39–48.
- 5 M.K. Banerjee, P.S. Banerjee, and S. Datta: *ISIJInt.*, 2001, vol. 41, pp. 257–261.
- 6 L.J. Cuddy: in *Thermomechanical Processing of Microalloyed Austenite*, Warrendale, PA, 1981, pp. 129–40.
- 7 C. Ouchi: *ISIJInt.*, 2001, vol. 41, pp. 542–553.
- 8 A. Kaijalainen, S. Pallaspuuro, and D.A. Porter: *Adv. Mater. Res.*, 2014, vol. 922, pp. 316–21.
- 9 A.J. Kaijalainen, P.P. Suikkanen, T.J. Linnell, L.P. Karjalainen, J.I. Kömi, and D.A. Porter: *J Alloys Compd.*, 2013, vol. 577, pp. S642–8.
- 10 R. Esterl, M. Sonnleitner, B. Gschöpf, and R. Schnitzer: *Steel Res. Int.*, 2019, DOI:10.1002/srin.201800640.
- 11 K.E. Hensger and M.L. Bernštejn: *Thermomechanische Veredlung von Stahl*, VEB Deutscher Verlag für Grundstoffindustrie, Leipzig, DDR, 1984.
- 12 L. Bracke, W. Xu, and T. Waterschoot: *Mater. Today Proc.*, 2015, vol. 2, pp. S659–62.
- 13 A. Kaijalainen, N. Vähäkuopus, M. Somani, S. Mehtonen, D. Porter, and J. Kömi: *Arch. Metall. Mater.*, 2017, vol. 62, pp. 619–626.
- 14 A.J. Kaijalainen, P.P. Suikkanen, L.P. Karjalainen, and D.A. Porter: *Mater. Sci. Eng. A*, 2016, vol. 654, pp. 151–60.
- 15 A.J. Deardo: *Int. Mater. Rev.*, 2003, vol. 48, pp. 371–402.
- 16 B. Dutta and C.M. Sellars: *Mater. Sci. Technol.*, 1986, vol. 2, pp. 146–53.
- 17 T. Swarr and G. Krauss: *Metall. Trans. A*, 1976, vol. 7, pp. 41–8.
- 18 G. Krauss and A.R. Marder: *Metall. Trans.*, 1971, vol. 2, pp. 2343–57.
- 19 R.G. Davies and C.L. Magee: *Metall. Trans.*, 1971, vol. 2, pp. 1939–1947.
- 20 A.J. Kaijalainen, P. Suikkanen, L.P. Karjalainen, and J.J. Jonas: *Metall. Mater. Trans. A*, 2014, vol. 45, pp. 1273–83.
- 21 B. Pereda, B. Lopez, and J.M. Rodriguez-Ibabe: *2007 Int. Conf. Microalloyed Steels Process. Microstruct. Prop. Perform. Proc.*, 2007, pp. 151–9.
- 22 S. Vervynckt, K. Verbeken, B. Lopez, and J.J. Jonas: *Int. Mater. Rev.*, 2012, vol. 57, pp. 187–207.
- 23 M.S. Jo, D.W. Suh, and H.K.D.H. Bhadeshia: *ISIJInt.*, 2013, vol. 53, pp. 1305–14.
- 24 A. Kaijalainen, P. Karjalainen, D. Porter, P. Suikkanen, J. Kömi, V. Kesti, and T. Saarinen: in *Proc 8th Int Conf Clean Steel*, Budapest, Hungary, 2012, p. 10.
- 25 J. Courbon, G. Lormand, G. Dudragne, P. Daguiet, and A. Vincent: *Tribol. Int.*, 2003, vol. 36, pp. 921–8.
- 26 T. Imai, Y. Nishida, and S. Kogiso: *J Mech. Work. Technol.*, 1982, vol. 7, pp. 147–61.
- 27 B.K. Sokolov and V.D. Sadovskii: *Met. Sci. Heat Treat. Met.*, 1959, vol. 1, pp. 7–14.
- 28 M. Sharma and W. Bleck: *Steel Res. Int.*, 2018, vol. 89, p. DOI: 10.1002/srin.1800107.
- 29 D. Raabe: *Steel Res. Int.*, 2003, vol. 74, pp. 327–37.
- 30 R.D.K. Misra, H. Nathani, F. Siciliano, and T. Carneiro: *Metall. Mater. Trans. A*, 2004, vol. 35, pp. 3024–9.
- 31 W. Bleck, R. Grossterlinden, U. Lotter, and C.-P. Reip: *Steel Res.*, 1991, vol. 62, pp. 580–6.
- 32 H.L. Haskel, E. Pauletti, J. de P. Martins, and A.L.M. de Carvalho: *Mater. Res.*, 2014, vol. 17, pp. 1238–50.
- 33 M.S. Jo, D. -W. Suh, J.H. Bae, N. Sanchez Mouriño, R. Petrov, L.A.I. Kestens, and H.K.D.H. Bhadeshia: *Mater. Sci. Eng. A*, 2012, vol. 556, pp. 601–6.
- 34 T. Gladman: *The Physical Metallurgy of Microalloyed Steels*, Institute of Materials, London, England, 1997.

- 35 H. Bhadeshia and R. Honeycombe: in *Steels: Microstructure and Properties (Fourth Edition)*, H. Bhadeshia and R. Honeycombe, eds., Fourth Edition., Butterworth-Heinemann, Oxford, UK, 2017, pp. 101–34.
- 36 G.E. Totten: *Steel Heat Treatment: Metallurgy and Technologies*, 2nd edition., CRC Press, Portland, Oregon, USA, 2006.
- 37 C.R. Brooks: *Principles of the Heat Treatment of Plain Carbon and Low Alloy Steels*, 1st edn., ASM International, Materials Park, OH, USA, 1996.
- 38 W.R. Babcock and Wilcox: *Mater. Manuf. Process.*, 1995, vol. 10, pp. 330–1.
- 39 H.L. Andrade, M.G. Akben, and J.J. Jonas: *Metall. Trans. A*, 1983, vol. 14, pp. 1967–1977.
- 40 R. Lagneborg, T. Siwecki, S. Zajac, and B. Hutchinson: *Scand JMet.*, 1999, vol. 28, pp. 186–241.
- 41 H. Bhadeshia and R. Honeycombe: in *Steels: Microstructure and Properties*, Fourth Edition, Butterworth-Heinemann, Oxford, UK, 2017, pp. 237–70.
- 42 G. Gottstein: *Physikalische Grundlagen der Materialkunde*, 3. Aufl., Springer, Berlin, Germany, 2007.
- 43 R. Esterl, M. Sonnleitner, and R. Schnitzer: *Steel Res. Int.*, 2019, vol. 90, pp. 382–91.
- 44 W. Österle: *Textur- und Gefügeentwicklung beim Walzen von polykristallinem alpha-Eisen*, PhD Thesis, RWTH Aachen, Germany, 1981.
- 45 F. Bachmann, R. Hielscher, and H. Schaeben: in *Texture and Anisotropy of Polycrystals III*, vol. 160, Trans Tech Publications, 2010, pp. 63–68.
- 46 S.F. Medina: *Mater. Sci. Technol.*, 1998, vol. 14, pp. 217–21.
- 47 K.-E. Thelning: *Steel and Its Heat Treatment: Bofors Handbook*, Butterworth-Heinemann, Oxford, UK 1967.
- 48 R. Esterl, M. Sonnleitner, M. Stadler, G. Wölger, and R. Schnitzer: *Pract. Metallogr.*, 2018, vol. 55, pp. 203–22.
- 49 S.I. Wright, M.M. Nowell, and J.F. Bingert: *Metall. Mater. Trans. A*, 2007, vol. 38, pp. 1845–55.
- 50 R.K. Ray, J.J. Jonas, M.P. Butrón-Guillén, and J. Savoie: *ISIJ Int.*, 1994, vol. 34, pp. 927–42.
- 51 S. Suwas and R.K. Ray: *Crystallographic Texture of Materials*, Springer, London, UK, 2014.
- 52 X.-L. Yang, Y.-B. Xu, X.-D. Tan, and D. Wu: *Mater. Sci. Eng. A*, 2015, vol. 641, pp. 96–106.